

**THE INTERACTION OF SURFACE PLASMA  
WAVES WITH ELECTRON BEAMS AND  
NANOPARTICLES**

**GAGAN KUMAR**



**DEPARTMENT OF PHYSICS  
INDIAN INSTITUTE OF TECHNOLOGY DELHI  
FEBRUARY 2008**

# **The Interaction of Surface Plasma Waves with Electron Beams and Nanoparticles**

*by*

**Gagan Kumar**

**Department of Physics**

*Submitted*

*In fulfillment of the requirements of the degree of*

**DOCTOR OF PHILOSOPHY**

*to the*



**Indian Institute of Technology Delhi**

**February 2008**

## CERTIFICATE

This is to certify that the thesis entitled “**The Interaction of Surface Plasma Waves with Electron Beams and Nanoparticles**” being submitted by *Gagan Kumar* to the *Indian Institute of Technology Delhi*, is worthy of consideration for the award of the degree of *Doctor of Philosophy* and is a record of bonafide research work carried out by him under my guidance and supervision and that the results contained in it have not been submitted in part or full to any other university or institute for award of any degree/diploma.

I certify that he has pursued the prescribed course of research. I approve the thesis for the award of the aforesaid degree.

February 2008

Prof. V. K. Tripathi,  
(Supervisor)  
Department of Physics  
Indian Institute of Technology, Delhi  
New Delhi – 110016, India

## ACKNOWLEDGEMENTS

*I express my deep gratitude and sincere thanks to my research supervisor Prof. V. K. Tripathi for his invaluable guidance, inspiring discussions, critical review, care and encouragement throughout this work. His ideas, stimulating comments, interpretations and suggestions increased my cognitive awareness and have helped considerably in the fruition of my objectives. I remain obliged to him for his help and guidance through all stages of this. Their constant inspiration and encouragement towards my efforts shall always be acknowledged.*

*I want to convey my deepest thanks to Prof. C. S. Liu, University of Maryland, for his graciousness to give me a chance to work with him during various research papers. It is a memorable experience to interact and learn from him during my visit in ICTP, Italy. I remain obliged for his inspiring discussions, constant inspiration and encouragement throughout the work.*

*Author is grateful to the Council of Scientific and Industrial Research (CSIR), Government of India for providing financial support to carry out research program. I express my sincere thanks to the faculty members of Physics Department, I. I. T. Delhi for general support and providing congenial working environment.*

*My sincere thanks are due to Dr. A. K. Sharma for his support and encouragement throughout my research work. I am thankful to Prof. R. P. Sharma, centre of Energy Studies and Dr. A. K. Shukla, Physics Department for their valuable suggestions at various stages. Dr. Amir Ahmad deserves special mention for his support and consistent discussions at various stages. Fruitful discussions with Dr. D. B. Singh are greatly acknowledged in our collaborative work. I am thankful to Prof. Shyam Kumar, Dr. Mudgil, Dr. M. S. Yadaw, Dr. Aggarwal for their support during the work.*

*I am thankful to all plasma group members Dr. Anamika Sharma, Dr. Lalita Bhasin, Dr. Hyder, Dr. Anoonu Rashid, Dr. Pawan Tiwari, Dr. Vikas Rai, Dr. Naveen Vats, Anuraj Panwar, Vishwa Bandhu, Updesh Verma, Dhamini, Sukhdeep Kaur, Vivek Sajal, Ashok Kumar, Pawan Kumar, Pitamber, Animesh Kuley, Deepak Dahiya, Asheel, Binod Pandey, Amrita Rathi, Inam and Rajender, Rohtash, Ranjeet, Khaleel, Nafis for their affection and support during my research work.*

*I pay my humble respect to my father Mr. Nihal Chand whose blessings are always with me. I further express my deep respect to my mother for their unlimited affection and care. I pay my hearty respect to brother Mr. Gulshan who always wish me success and want me to study more and more. I remember and thank my sisters Tara, Neelam, and Anita and jiju Mr. Sanjay, Mr. Deshraj, Mr. Manmohan Hans, and lovely little Shivam, Amrita, Jyoti, Parshant, Nitin for their tremendous love, affection, moral support and help. I remember and pay my regards to my High Se. Sec. physics teacher Mr. Narender Kumar whose kind personality made me deeply interested in Physics.*

*I also wish to thank my friends and seniors Vishal, Ravinder Kumar, Manish Kashyap, Nitin, Nonu, shiwani, Harsha, Monika Sharma, Shilpa, Vinod Kumar, Pardeep Rodha, Sohanpal, Ramniwas, Narender, Sandeep, Samarth, Tanu, Krishan, Suresh, Ramesh, Gaurav, Jai Parkash, Ajay, Om, Gayatri, Mukesh, Jatin, Satinder, Aashish, Vandana, Suneet, Pawan Mudgil, Ashok, Dinesh, Ankur, Yogender, Yogesh, Amit, Parshant, Ritwick, Bhargav, Rajan, Sandeep Duhan for their affection and support.*

*Debts being various, are not easy to remember, hence I convey my heartiest thanks to all those who helped me or blessed me in making this milestone. I deeply regret here for not mentioning these individuals.*

*February, 2008*

**Gagan Kumar**

## ABSTRACT

The thesis focuses on linear and non-linear effects resulting from the interaction of surface plasma waves with electron beams, nanoparticles and the surface on which they reside.

A theory has been developed for fiber optic sensor in which a guided laser undergoes mode conversion into a surface plasma wave in a metal coated optical fiber. The fiber metal interface has a ripple to assist k-matching. The laser induces oscillatory velocity on the electrons of the metal that beats with the space modulated density to produce a current, driving the surface plasma wave on the metal free space interface. When the metal has metallic particles attached to it and molecules are adsorbed on them, the surface plasma wave undergoes surface enhanced Raman scattering with them. The scattered signals propagate backward as a TM body wave and can be detected.

We propose a modified surface enhanced Raman scattering (SERS) sensor in which laser is replaced by a laser driven surface plasma wave on a planar surface. The surface plasma wave, propagating along a metal surface, embedded with regularly arranged nanoparticles, undergoes SERS from molecules adsorbed over the particles. The enhancement in the scattered signal depends on the shape and dielectric constant of the metallic particles.

A scheme of electron acceleration has been proposed that employs resonant interaction of electrons with a surface plasma wave. It employs a configuration of two parallel metal surfaces separated by a vacuum region. The configuration supports a surface plasma wave having finite axial electric field in the middle but the vanishing

transverse ponderomotive force. This scheme can be useful in accelerating electrons to higher energies with the control in their trajectories when injected at the centre of vacuum region.

We study the anomalous absorption of surface plasma waves by metal particles placed over a metal surface. A surface plasma wave excites resonant plasma oscillations in the particles at a specific frequency depending on the shape of the particles. The particles absorb energy from the wave via electrons, incurring attenuation of the surface plasma wave.

At large amplitude, a surface plasma wave is seen to undergo filamentation instability over a compensated semiconductor. A small perturbation in the amplitude of the SPW across the direction of propagation exerts a ponderomotive force on free electrons and holes, causing spatial modulation in free carrier density and hence in the effective permittivity  $\epsilon_{eff}$  of the semiconductor. The  $\epsilon_{eff}$  profile has a tendency to converge the SPW energy to regions of higher  $\epsilon_{eff}$ , leading to the growth of amplitude perturbation.

We have also studied the excitation of surface plasma wave over a plasma cylinder by a relativistic electron beam. A solid relativistic electron beam propagating inside the plasma cylinder is seen to be more efficient in exciting a surface plasma wave than an annular beam placed just outside. The interaction occurs via Cerenkov resonance.

## TABLE OF CONTENTS

<b>Certificate</b>	i
<b>Acknowledgement</b>	ii
<b>Abstract</b>	iv
<b>Table of Contents</b>	vi
<b>List of Figures</b>	x
Chapter 1: <b>Introduction</b>	1
1.1 Dispersion relation of surface plasma wave	2
1.2 Excitation of surface plasma waves	5
1.3 Scattering of surface plasma waves	8
1.4 Surface enhanced Raman scattering	9
1.5 Applications of surface plasma waves	11
1.5.1 Surface plasmon resonance sensors	11
1.5.2 Surface plasma wave assisted electron acceleration	13
1.5.3 Plasmonics	14
1.5.4 Surface plasma wave absorption and electron emission	16
1.6 Parametric instabilities of surface plasma waves	17
1.7 Plan of thesis	18
List of Publications	22
References	23

**Chapter 2: Laser mode conversion into a surface plasma wave in a metal coated optical fiber**

2.1 Introduction	28
2.2 Body Waves and Surface Waves	30
2.3. Mode Conversion	36
2.4 Surface Enhanced Raman Scattering of SPW into a Body Wave	41
2.5 Discussion	44
References	46

**Chapter 3: Surface enhanced Raman scattering of a surface plasma wave**

3.1 Introduction	48
3.2 Laser Driven Surface Plasma Wave	49
3.3 Surface Enhanced Raman Scattering	51
3.4. Discussion	58
References	59

**Chapter 4: Electron acceleration by surface plasma waves in double metal surface structure**

4.1 Introduction	61
4.2 Surface plasma wave in a double metal surface configuration	62
4.3 Electron acceleration in double surface configuration	66
4.4 Electron acceleration by SPW over a single metal surface	70
4.5 Discussion	74

References	75
------------	----

**Chapter 5: Anomalous absorption of surface plasma wave by particles adsorbed on metal surface**

5.1. Introduction	77
5.2. Surface plasma wave propagation	78
5.3. Absorption of surface plasma wave by metallic particles	80
5.4. Discussion	84
References	85

**Chapter 6: Filamentation of a surface plasma wave over a semiconductor-free space interface**

6.1 Introduction	87
6.2 Ponderomotive force and effective permittivity over s/c surface	89
6.3 Growth Rate	91
6.4 Discussion	95
References	97

**Chapter 7: Excitation of surface plasma wave over a plasma cylinder by a relativistic electron beam**

7.1 Introduction	98
7.2 Surface plasma wave propagation	99
7.3 SPW excitation by a solid beam	101

7.4 SPW excitation by an annular beam outside the cylinder	105
7.5 Discussion	107
<b>Chapter 8: Conclusions and directions for future work</b>	<b>109</b>
References	112
Appendices	113
Bio data of the author	115

## LIST OF FIGURES

### Chapter 1

**Fig. 1.1** Geometry of surface plasma wave propagation at metal-dielectric interface.

**Fig. 1.2** Dispersion curves for surface plasma wave.

**Fig. 1.3** Kretschmann configuration for SPW excitation.

**Fig. 1.4** Phase matching of Light to SPW using diffraction grating.

**Fig. 1.5** Schematic of the SPW scattering processes from topographical surface defect.

### Chapter 2

**Fig. 2.1** Schematic of a metal coated optical fiber.

**Fig 2.2** Variation of normalized frequency  $\Omega$  with normalized wave vector  $q_z$  for TM mode body wave and SPWs. The parameters are:  $a\omega_p/c = 20$ ,  $b/a = 1.01$ .

**Fig. 2.3** Variation of normalized frequency  $\Omega$  with normalized wave vector  $q_z$  for TM mode body wave and SPW . The parameters are:  $a\omega_p/c = 17$ ,  $b/a = 1.01$ .

**Fig. 2.4** Variation of normalized frequency  $\Omega$  with normalized wave vector  $q_z$  for TM mode and SPW. The parameters are:  $a\omega_p/c = 20$ ,  $b/a = 1.1$ .

**Fig. 2.5** Mode conversion of a TM mode into SPW due to rippled interface between fiber and metal coating.

**Fig. 2.6** Variation of  $|A/A_1^L|$  i.e. ratio of amplitudes of surface plasma wave to incident laser versus normalized distance  $\omega_L z/c$ .

### Chapter 3

**Fig. 3.1** Schematic of a prism coated with thin metal layer. Surface plasma wave undergoes surface enhance Raman scattering with the molecules adsorbed on the particles placed over the metal surface.

**Fig. 3.2** Variation of the angle,  $\theta_R$  (in degrees) for the scattered wave normal to the metal surface versus normalized wave number  $q \omega_R / c$  of regularly arranged particles.

**Fig. 3.3** Variation of the ratio of the intensities of the Raman scattered wave to that of the incident laser  $I_R / I_O$  versus scattering angle  $\theta_R$  (in degrees) with surface normal.

### Chapter 4

**Fig. 4.1 (a)** Schematic of two metal surface plasmon structure. The electrons are injected in the centre of the free space region.

**Fig. 4.1 (b)** The excitation of surface plasma wave in attenuated total reflection (ATR) configuration.

**Fig 4.2** Variation of the normalized frequency  $\Omega = \omega / \omega_p$  versus normalized wave number  $q = k c / \omega_p$  of the surface plasma wave in double metal surface structure.

**Fig 4.3** Variation of Kinetic energy of the accelerated electron  $(\gamma - 1)mc^2$  (in keV) versus normalized distance  $z \omega_p / c$  in double metal surface for  $\omega / \omega_p = 0.06$ .

**Fig 4.4** Variation of Kinetic energy of the accelerated electron  $(\gamma - 1)mc^2$  (in keV) versus normalized distance  $z \omega_p / c$  in double metal surface for  $\omega / \omega_p = 0.087$ .

**Fig 4.5** Variation of Kinetic energy of the accelerated electron  $(\gamma - 1)mc^2$  (in keV) versus normalized distance  $z \omega_p / c$  in double metal surface for  $\omega / \omega_p = 0.1$ .

**Fig 4.6** Variation of kinetic energy of the accelerated electron  $(\gamma-1)mc^2$  versus normalized distance  $z\omega_p/c$  over the single metal surface.

**Fig 4.7** The trajectory of electron (normalized x versus normalized z) in (a) single metal surface and (b) double metal surface configuration.

## Chapter 5

**Fig. 5.1** Schematic for the absorption of surface plasma waves by the metallic particles placed on metal surface.

**Fig. 5.2** Variation of normalized absorption constant,  $k_{ip}c/\omega_p$  versus normalized frequency  $(\omega - \omega_{pe}/\sqrt{3})/\omega_{pe}$  for the particles of radius i)  $r_c = 6.5 \text{ nm}$  and ii)  $r_c = 8 \text{ nm}$ .

## Chapter 6

**Fig. 6.1** Variation of normalized growth rate  $\Gamma_{nor}$  versus normalized transverse wavenumber  $qc/\omega_p$  for normalized SPW amplitudes  $eA_0/m\omega_p c = 1.845 \times 10^{-4}$  and  $eA_0/m\omega_p c = 1.304 \times 10^{-4}$ .

**Fig. 6.2** Variation of normalized growth rate  $\Gamma_{nor}$  versus normalized frequency  $\omega/\omega_p$ .

## Chapter 7

**Fig. 7.1** Schematic of a plasma cylinder for the excitation of SPW by solid electron beam.

**Fig. 7.2** Variation of normalized frequency  $\omega/\omega_p$  versus normalized wavenumber  $k_z c/\omega_p$  of the SPW for three different radii of plasma cylinder.

**Fig. 7.3** T The growth rate  $\omega_i (s^{-1})$  of the SPW excited by solid electron beam as a function of normalized frequency  $\omega/\omega_p$  for three different radii of plasma cylinder.

**Fig. 7.4** The wave frequency  $\omega/\omega_p$  as a function of beam velocity  $v_{0b}/c$  for three different radii of plasma cylinder.

**Fig. 7.5** The growth rate  $\omega_i (s^{-1})$  as a function of normalized frequency  $\omega/\omega_p$  for plasma cylinder of radius  $a = 300 \mu m$  in case SPW is excited by annular beam propagating outside the cylinder.

## Chapter 1

# INTRODUCTION

A surface plasma wave [1-5] (SPW) is a guided electromagnetic wave that propagates along the interface between a metal and a dielectric, often a vacuum. The amplitude of the SPW decays exponentially away from the interface in both the media. The magnetic field of the SPW is parallel to the surface and perpendicular to its direction of propagation while electric field has components parallel to the direction of propagation and perpendicular to the surface.

These waves were first observed by Wood in 1902 [6]. He noted anomalous behavior in the diffraction intensities for small angular and spectral variations from the grating of large and rapid changes. In 1907, Rayleigh gave the first theoretical explanation of these anomalies suggesting that such behavior was due to the cutoff or the appearance of a new spectral order [7]. However, more precisely Fano in 1941, theoretically suggested the excitation of surface plasma wave over the grating surface [8]. He pointed out that such wave can be excited only by TM incident wave and exists only at the interface of a dielectric and a medium with negative real part of effective relative permittivity viz. plasma and conductor. In gaseous plasmas, Trivelpiece and Gould (1959) first experimentally observed surface plasma wave over a cylindrical plasma column enclosed in a glass tube that was coaxial with a circular metallic waveguide [9].

The SPW offers a variety of applications, ranging from high sensitivity sensors to supplementary heating in a fusion reactor, coherent radiation generation, enhanced material ablation, electron emission and plasma diagnostics. The total absorption of

electromagnetic waves can be achieved via the excitation of surface plasma waves when sub-wavelength grating is placed in front of the plasma surface.

Major developments in the excitation of surface plasma waves over solid state plasmas took place in 1968 when Otto proposed the SPW excitation in attenuated total reflection configuration (ATR) [10]. Kretschmann and Raether [11] later proposed an alternative configuration of Otto's method. Agranovich studied reflection, refraction and diffraction from separation boundaries between media [12].

The SPW is confined near the metal surface and its amplitude at the surface is significantly larger than that of the laser. The enhanced field of the SPW could increase the emission rate of luminescent dyes placed near the metal surface. This enhancement can increase the efficiency and brightness of solid-state LEDs [13]. In last two decades, surface plasma wave based sensors have emerged as a powerful tool for characterizing and quantifying bimolecular interactions. Surface plasma waves are being explored for their potential in sub-wavelength optics, magneto-optic data storage and microscopy [14-16]. The properties of surface plasma waves can lead to miniaturized photonic circuits by creatively designing the structure of metal's surface.

### **1.1 Dispersion relation of the SPW**

The fields of a surface plasma wave at metal-dielectric interface are governed by Maxwell's equation in each medium and the associated boundary conditions. Boundary conditions involve the continuity of the tangential component of the electric field and magnetic fields across the interface and vanishing of these fields away from the interface.

Consider a dielectric of relative permittivity  $\epsilon_1$  for  $x > 0$  and a metal with effective relative permittivity  $\epsilon(\omega)$  in the half space  $x < 0$  (Fig. 1.1).

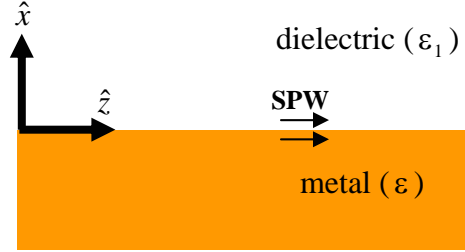


Fig. 1.1 Geometry of surface plasma wave propagation at metal-dielectric interface

When a SPW propagates at the dielectric-metal interface with  $(t, z)$  variation as  $e^{-i(\omega t - k_z z)}$ , its behavior is governed by Maxwell's equations.

$$\nabla \times \vec{E} = -\frac{1}{c} \frac{\partial \vec{H}}{\partial t}, \quad (1.1)$$

$$\nabla \times \vec{H} = \frac{\epsilon'}{c} \frac{\partial \vec{E}}{\partial t}, \quad (1.2)$$

which on taking curl of Eq. (1.1) and using Eq. (1.2) give

$$\nabla^2 \vec{E} - \frac{\epsilon'}{c^2} \frac{\partial^2 \vec{E}}{\partial t^2} = 0, \quad (1.3)$$

where  $\epsilon' = \epsilon(\omega) = \epsilon_L - \omega_p^2 / \omega^2$  for  $x < 0$  and  $\epsilon' = \epsilon_1$  for  $x > 0$ .  $\epsilon_L$  is the lattice permittivity,  $\omega_p$  is the plasma frequency. The continuity conditions on electromagnetic fields at the interface demand that the  $t$  and  $z$  variation of fields be the same in both media. Thus replacing  $\partial / \partial z$  and  $\partial / \partial t$  in Eq. (1.3) by  $ik_z$  and  $-i\omega$  respectively, we get

$$\frac{\partial^2 \vec{E}}{\partial x^2} - (k_z^2 - \frac{\omega^2}{c^2} \varepsilon) \vec{E} = 0. \quad (1.4)$$

The well behaved solutions of Eq. (1.4) are

$$\begin{aligned} \vec{E} &= \left( \hat{z} + \hat{x} \frac{ik_z}{\alpha_1} \right) A e^{-\alpha_1 x} e^{-i(\omega t - k_z z)}, & \text{for } x > 0, \\ \vec{E} &= \left( \hat{z} - \hat{x} \frac{ik_z}{\alpha_2} \right) A e^{\alpha_2 x} e^{-i(\omega t - k_z z)}, & \text{for } x < 0. \end{aligned} \quad (1.5)$$

where  $\alpha_1^2 = k_z^2 - \varepsilon_1 \omega^2 / c^2$ ,  $\alpha_2^2 = k_z^2 - \omega^2 \varepsilon(\omega) / c^2$ . The real part of  $\alpha_1, \alpha_2$  must be positive for an electromagnetic wave localized to the dielectric-metal interface at  $x = 0$ .

The continuity of  $E_z$  and  $\varepsilon' E_x$  at the interface yields  $A = B$ ,

$$\frac{\alpha_2}{\alpha_1} = -\frac{\varepsilon(\omega)}{\varepsilon_1}. \quad (1.6)$$

Squaring both sides and rearranging the terms, one obtains the explicit dispersion relation for surface plasma waves

$$k_{sp} = \frac{\omega}{c} \left[ \frac{\varepsilon_1 \varepsilon(\omega)}{\varepsilon_1 + \varepsilon(\omega)} \right]^{1/2}. \quad (1.7)$$

Further,  $\alpha_1^2 = -\frac{\omega^2}{c^2} \frac{\varepsilon_1^2}{\varepsilon_1 + \varepsilon}$ ,  $\alpha_2^2 = -\frac{\omega^2}{c^2} \frac{\varepsilon^2}{\varepsilon_1 + \varepsilon}$ . For  $\alpha_1$  and  $\alpha_2$  to be positive one needs

$\varepsilon_1 + \varepsilon < 0$  or  $\omega < \frac{\omega_p}{\sqrt{\varepsilon_L + \varepsilon_1}}$ . In case of metal-free space interface, the surface plasma

wave dispersion relation reduces to  $k_z = \frac{\omega}{c} \left( \frac{\varepsilon}{1 + \varepsilon} \right)^{1/2}$ . We have plotted the dispersion

relation at dielectric-metal and air-metal interfaces in fig. 1.2 for the parameters:

$\epsilon_1 = 2.25$ ,  $\epsilon_L = 4$ . One may note that at a given frequency the SPW wave number increases with  $\epsilon_1$ .

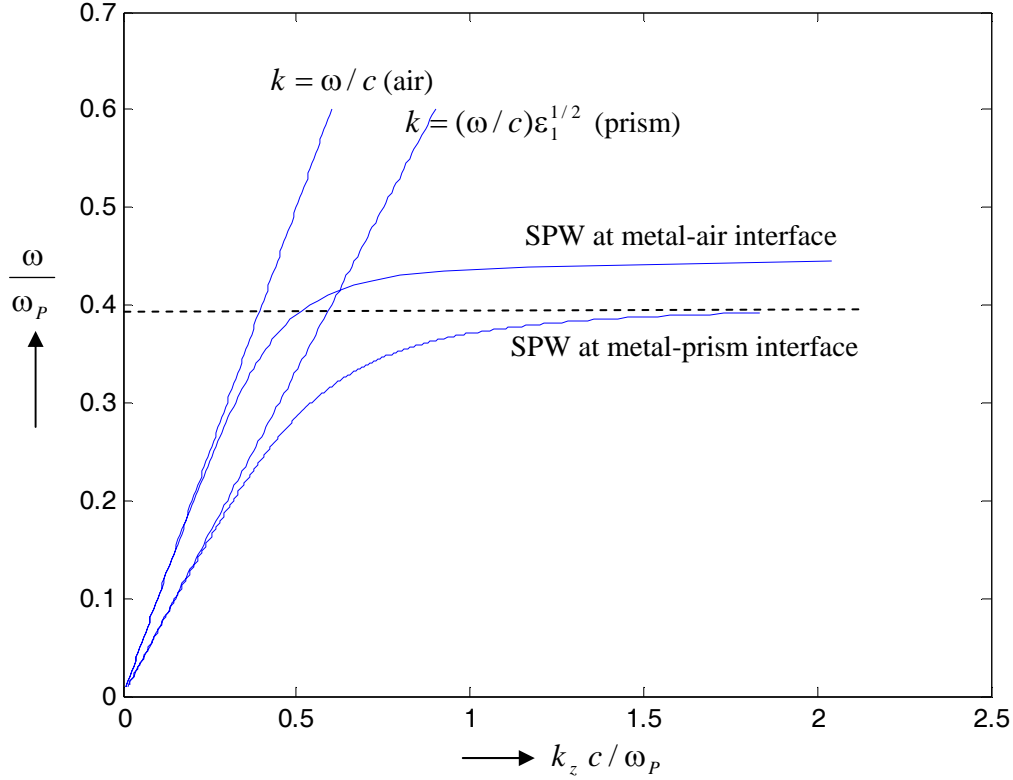


Fig. 1.2 Dispersion curves for surface plasma wave.

### 1.2 Excitation of surface plasma waves

In order to excite SPW by a p-polarized light from the adjacent dielectric medium, the frequency of the incident light should be equal to the frequency of the SPW and the component of the wave vector of the incident light along the interface,  $\sqrt{\epsilon_1} (\omega / c) \sin \theta$  where  $\theta$  is the angle of incidence, should be equal to the wavenumber of the SPW  $(\omega / c)[\epsilon_1 \epsilon(\omega) / (\epsilon(\omega) + \epsilon_1)]^{1/2}$ . But from the dispersion relation, it is clear that SPW wave number is greater than the light wave number. Therefore light shining on a metal

surface cannot directly couple to the SPW. However, light and the SPW wavenumber can be matched by some special arrangement. The most commonly used technique for the SPW excitation is Kretschmann configuration [18-19] (fig. 1.3).

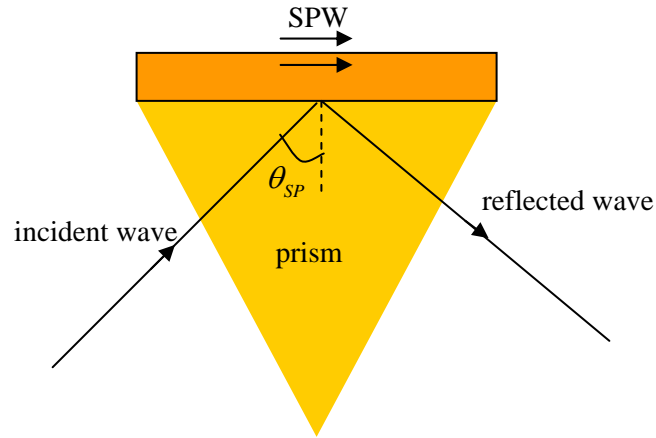


Fig. 1.3 Kretschmann configuration for SPW excitation

In this configuration, a thin metal film is deposited over the glass. The light is incident on the glass metal interface from the glass side at a specific angle of incidence where the component of the light wave along the interface becomes equal to the SPW wavenumber. Under this resonant condition a sharp minimum in the reflectivity of the light occurs and light couples to the SPW with almost 100 % efficiency. Since the SPW field is constructed close to the interface, it is significantly enhanced at the surface. When 60 nm thick silver film is illuminated with red light, more than two order of magnitude enhancement in the intensity of SPW is observed [3]. As the metal thickness is increased, the efficiency of SPW excitation decreases. In this configuration the SPW will not be excited at metal dielectric interface because the wave number of SPW at this interface is greater than the light wave number for all angle of incidence. In order to

excite SPW at this interface, one requires depositing a dielectric layer of small dielectric constant between metal and prism. The SPWs can be excited at both the interfaces by changing the angle of incidence.

The SPW at a thick metal film is excited using Otto configuration [10]. In this case prism is placed close to the metal surface and photon tunneling occurs through the air gap between the prism and the surface. The resonant conditions are similar to the one in the Kretschmann configuration.

The SPW can also be excited using a diffraction grating [3] or a ripple of suitable wave number. If a diffraction grating is created over the metal surface of wave number  $k_d$ , the SPW of wavenumber  $k$  can be excited if  $k = k_{\parallel} + nk_d$  where  $n$  is some integer and  $k_{\parallel}$  is the component of the wave vector of incident light along the metal surface (fig. 1.4). Such an excitation technique provides efficient coupling to surface plasma waves at both air-metal and substrate-metal interface if the film thickness and grating profile depth are suitably adjusted.

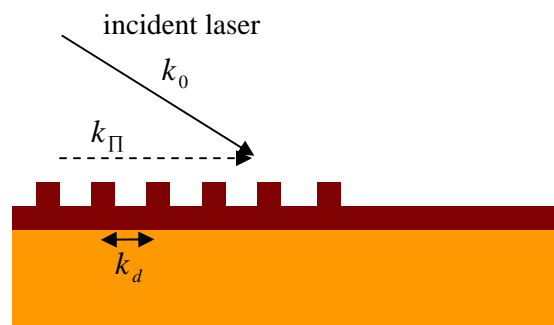


Fig. 1.4 Phase matching of Light to SPW using diffraction grating

The SPW excitation can also be achieved through the illumination of rough surfaces as well, because in the near field region diffracted component of light with all wave vectors are present [20-21]. However, this technique results in low efficiency of light to SPW coupling as this is a non-resonant excitation and there is a strong presence of the reflected exciting light close to the surface.

Denton et al. studied the plasmon excitation by charged particles moving near a solid surface [22]. The phase velocity of the SPW is smaller than the velocity of light in vacuum, hence they can be excited by a relativistic electron beams via Cerenkov interaction as in a traveling wave tube or a Smith-Purcell metal grating device [23, 24]. In this case, when the SPW passes over a surface ripple, it produces a coherent radiation.

### **1.3 Scattering of surface plasma waves**

The scattering of surface plasma wave plays an important role in determining the optical properties of rough and nano-structured surfaces. The scattering may occur any of the three ways in their interaction with surface defects viz. scattering in same direction as that of the incident SPW, scattering in another direction and scattering of SPW into light. The scanning near field optical microscopy (SNOM) has been vigorously used to study the scattering processes because of their potential to measure electromagnetic field distribution related to SPW in the near field region over a surface. The SPW scattering by different types of surface defects has been studied with SNOM [25, 26]. Surface defects for SPW scattering can be categorized into three types namely topography variations, subsurface defects and dielectric constant variation.

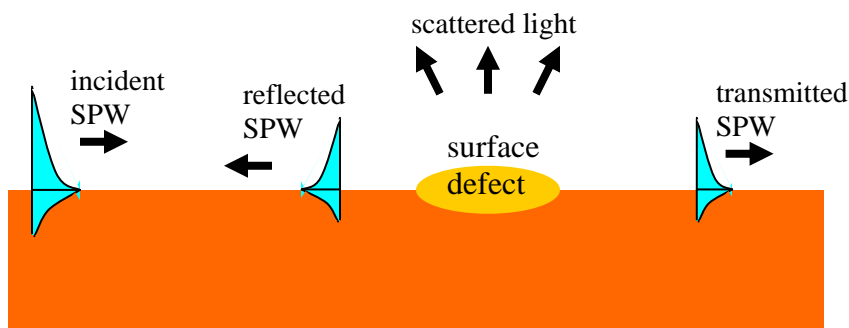


Fig. 1.5 Schematic of the SPW scattering processes from topographical surface defect

#### 1.4 Surface enhanced Raman scattering (SERS)

Raman scattering has been a subject of considerable interest because of its ability to produce well resolved spectra that provide a unique fingerprint for every Raman active substance or component. In 1974, Fleischmann et al. observed large Raman signals, as large as  $10^6$  times in intensity, from pyridine adsorbed onto electrochemically roughened silver electrodes [27]. He attributed enhanced intensity to increased surface area. Later Jeanmaire and Van Duyne in 1977 showed that Raman cross section per molecule was enhanced by million times [28]. The silver and gold electrodes are the most efficient one to obtain Raman enhanced signals.

The Raman intensities scale as the product of the incident field intensity and polarizability derivative, therefore two commonly considered mechanisms are responsible for SERS. One is the electromagnetic mechanism, which involves the electromagnetic field enhancement of the light at the surface under the conditions of surface plasmon excitation. The amplification occurs both in the incident laser field and the scattered Raman field. The enhancement factor  $F_e$  at each molecule approximately is given by

$$F_e = |F(\omega)|^2 |F(\omega')|^2 ,$$

where  $F(\omega)$  is the local field enhancement factor at the incident frequency  $\omega$  and  $F(\omega')$  is the corresponding factor at the Stokes-shifted frequency  $\omega'$ . The more rigorous expression for the electromagnetic enhancement is given by Kerker [29]. The another class of SERS mechanism is chemical enhancement. This enhancement occurs in polarizability due to chemical effects such as charge transfer excited states [30-32]. Moskovits has given the detailed description of surface enhanced processes in his review [33]. Owing to its high sensitivity and specificity, SERS has the potential for the detection of chemical and biological agents, detection of cancer genes [34], glucose sensing at physiological concentrations [35] with high sensitivity.

The detection of single molecule is a major development brought in by SERS. Earlier, the fluorescence spectroscopy was used for this purpose. However, the broad fluorescence bands, obtained under “normal” conditions at room temperature and in a liquid environment, are relatively insensitive to molecular structure. The surface enhanced Raman scattering (SERS) spectroscopy has shown new promise in the detection of selective single molecule using nanoparticles. In vibrational pumping experiments, unexpectedly large enhancement factors on the order of  $10^{14}$  corresponding to effective Raman cross sections of  $\sim 10^{-16} \text{ cm}^2$  per molecule in non-resonant SERS at near field excitation was observed. Such Raman cross sections are effective for single molecule Raman spectroscopy. To achieve effective Raman cross sections of the order of  $10^{-16} \text{ cm}^2$  per molecule, they have to be attached to aggregated colloidal silver particles in aqueous solution. Silver has been proved to be best for maximum enhancement of certain

vibrational signals of an analyte. Mandal et al. used  $\text{Au}_{\text{core}}\text{-Ag}_{\text{shell}}$  bimetallic nanoparticle for sniffing a single molecule through SERS [36].

Stokes and Vo-Dinh in 2000 developed a single mode optical fiber SERS sensor [37]. The fiber optic SERS sensors have various potential applications viz. environmental monitoring [38], remote monitoring [39], water quality monitoring [40], biochemical monitoring [41], in-situ sensing of volatile organic compounds in groundwater [42] and detection of bio-molecules in aqueous solutions [43].

## **1.5 Applications of Surface plasma waves**

The surface plasma waves are rapidly being used for various applications e.g. surface plasmon resonance (SPR) sensors, surface enhanced Raman scattering sensors, electron acceleration, surface plasmon induced electron emission, material ablation and many more. The emerging field of plasmonics is based on exploiting the coupling between light and surface plasmons. The properties of surface plasma waves may lead to ultracompact devices and ultrasensitive detectors by properly designing plasmonic structures. The discovery of novel metamaterials has boosted the interest in the field of plasmonics. The applications of surface plasma wave are discussed in subsequent sections.

### **1.5.1 Surface plasmon resonance sensors**

The potential of SPR for the characterization of thin films was realized almost 30 years ago. In 1982, the use of SPR for gas detection and biosensing was demonstrated by Nylander and Liedberg [44]. Since then SPR sensors have attracted wide attention.

SPR sensors comprise an optical system which contains a source of optical radiation, optical structure in which SPW can be excited, a transducing medium and an electronic system supporting optoelectronic components of the sensor allowing data processing. The transducing medium transforms changes in the quantity of interest into changes in the refractive index which can be determined by optically interrogating the SPR.

In order to realize surface plasmon resonance sensors, different configurations have been employed. One of the most widely used geometry in SPR sensor is using attenuated total reflection optical prism couplers. The SPW is excited at metal free space interface. The SPR condition is very sensitive to the variations in the optical properties of the dielectric adjacent to the metal layer supporting SPW. Therefore the variations in the optical parameters of the transducing medium can be detected by monitoring the interaction between the SPW and the optical wave.

Another configuration of SPR sensors can be realized using grating coupler. In this case, the metal-dielectric interface is periodically distorted and diffracted beams are observed at various angles for the incident optical wave. When the total component of the momentum of the diffracted beam is equal to that of the SPW, the optical wave may couple to the SPW. The sensitivity of the SPR sensor based on grating coupler has been found to be less than that of using ATR prism coupler.

Now days SPR sensors make use of the optical waveguides. These provide attractive features such as efficient control of properties of light, suppression of effects of stray light and small size. The SPW may be excited simply as in the case of Kretschmann configuration. Currently, optical fiber SPR sensors are mostly employed. The use of

optical fiber for SPR sensor was first proposed by Jorgenson and Yee [45]. Optical fibers allow the highest level of miniaturization of SPR devices, and chemical and biological sensing in inaccessible areas over longer distances. Slavik et al. have investigated a single mode optical fiber sensor based on the resonance excitation of a surface plasma wave [46].

### **1.5.2 Surface plasma wave assisted electron acceleration**

The acceleration of electrons by laser has been a subject of considerable interest over several decades. The schemes of laser beat wave acceleration [47, 48] and laser wake field acceleration [49, 50] have been pursued vigorously and electron acceleration approaching GeV energy is being achieved. In some applications, however, electron beams of moderately relativistic energies are required. From this point of view surface plasma waves have a promise.

Experiments have revealed that SPW is effective for low energy electron acceleration. Zawadzka et al. have experimentally demonstrated electron acceleration of 40 eV using 150 fs, 6- $\mu\text{m}$  (21 GW/cm<sup>2</sup>) laser pulses in Kretschmann configuration for SP coupling [51]. In the follow up experiment, they generated 400 eV energetic electrons with 40 TW/cm<sup>2</sup> while depositing 50 nm thin layer of silver on glass prism [52]. They generated electron bunches through the femtosecond laser excitation of surface plasmons. At higher incident intensities, a strong high frequency evanescent field ( $\sim 10^{10}$  V/cm, 375 THz) is created on the metal surface resulting in a ponderomotive potential. This causes the charged particles being pushed away from the surface. Few years later, Irvine et al. also demonstrated the generation of 0.4 keV, sub-27 fs electron pulses using low intensity

laser pulses from Ti-sapphire oscillator through the excitation of surface plasmon waves on a time scale with in plasmon lifetime [53, 54]. Similar experiments on electron acceleration by surface plasma waves have been performed by other research groups as well. Kuperzstych et al. have demonstrated 25 eV electron acceleration by 60 fs, 8 GW/cm<sup>2</sup> laser pulses employing a metallic grating for launching SP waves [55]. With the increase in electron pulse duration, electron acceleration increases. The electron acceleration of 40 eV was observed using pulse duration of 800 fs. Further investigations using 0.5 mJ (30 GW/cm<sup>2</sup>) laser pulses, reveal that energies beyond 2 keV are possible. Irvine and Elezzabi have discussed a model describing the ultrafast photoemission and acceleration simulation, which offers flexibility of acceleration geometries and electron emission processes [54].

### **1.5.3 Plasmonics**

In modern communication systems, one requires huge data transfer at high speeds. Much effort has been made to realize such systems while making use of best features of electronic and optical devices. Electronic circuits are small in size but their operation speeds are limited. Optical circuits provides high speed data transfer but their sizes are constrained by diffraction limit. This led to a new class of devices that are not constrained by such limits. The excitation of surface plasmons at metal dielectric interface with much shorter wavelength has provided the possibility of realizing such devices. The emerging field of plasmonics is based on exploiting the coupling between light and surface plasma waves over conducting materials. Harry Atwater's group in 2000 gave the name plasmonics to this emerging filed, sensing its importance in the

development of entirely new class of devices with ultracompact and ultrafast features [17]. In order to realize such devices one requires efficient light-SPW coupling. Recently Lopez-Tejiera et al. [56] have proposed efficient unidirectional nanoslit coupler for surface plasmons.

The Plasmonic materials may improve the resolution of microscopes, the efficiency of Light Emitting Diodes (LEDs) and sensitivity of chemical and biological sensors. In medical applications, plasmon resonance absorption may be used to kill cancerous tissues. Surface plasma waves with much shorter wavelength as the outside electromagnetic waves can be generated by creatively designing the metal dielectric interface. This could allow plasmons to travel along nanoscale wires called interconnects. Plasmonic interconnects could be very useful in transmitting data quickly across the chip. The striking ability of shrinking the wavelength may open the path to nanoscale plasmonic structures that could replace electronic circuits containing wires and transistors. Researchers are making efforts to make a plasmonsters switch with transistor like properties.

The field of plasmonics has received boost with the discovery of novel metamaterials [57]. Metamaterials are artificially made microscopic structures that have unusual electromagnetic properties, e.g. negative index of refraction which means they refract light in a totally new way. The refractive index is given as  $n = \pm\sqrt{\epsilon\mu}$ , where  $\epsilon$  and  $\mu$  are the electric permittivity and magnetic permeability respectively. In order to have refractive index negative,  $\epsilon$  and  $\mu$  must take the negative sign. Veselago in 1968 was the first to investigate theoretically the electrodynamics of such materials [58]. He predicted that wave vector of a wave propagating through a left-handed substance is

antiparallel to its Poynting-vector. In 2001, metamaterials were finally demonstrated experimentally which exhibits a frequency band in the microwave regime with negative index of refraction. Sir Pendry has developed the concept of superlenses while making use of metamaterials [59].

#### **1.5.4 Surface plasma wave absorption and electron emission**

In order to construct the tabletop sources of energetic electrons, ions, and photons, one requires the efficient coupling of incident laser light with matter. Therefore the absorption of electromagnetic radiation by matter has been of much interest over several years. The planar metal surfaces have been found to be poor absorbers of light because their high electron density re-emits light back into the surrounding. Clusters and metallic particles have proved to be very efficient absorbers of light. For rare gas clusters [60], almost 100% absorption of laser light has been observed in experiments. In metallic particles, when light interacts with them, it excites resonant plasma oscillations in the particle. The local field enhancement occurs inside or near the metallic particle at plasma resonance. The resonant absorption takes place via electron collision inside the particle.

The absorption of electromagnetic waves can be enhanced via the excitation of surface plasma waves. Recently Bliokh et al. have experimentally observed total absorption of an electromagnetic wave by an overdense plasma when a sub-wavelength diffraction grating is placed in front of the plasma surface [61]. The absorption takes place via the resonant excitation of surface plasma waves. The SPWs are excited by the evanescent component of the diffracted electromagnetic field. Vorobyev and Guo studied the femtosecond laser ablation of gold while increasing the number of shots [62].

They measured the change in absorptance due to structural modifications. For lower number of laser shots (<10), absorption takes place due to the nanostructuring of the gold surface. For higher number of laser shots, microstructure formation results in the absorption of electromagnetic energy via the excitation of surface plasma waves.

The electron emission can be greatly enhanced by the excitation of the SPW. The electron emission occurs via two processes viz. photoelectric effect and the heating of metal electrons resulting in thermionic emission. The two processes compete with each other on the basis of intensity and length of laser pulses. Anisimov et al. [63] have shown that thermionic emission is predominant for absorbed flux density above  $10^9$ - $10^{10}$  W/cm<sup>2</sup>. In femtosecond regime, the dividing line between the two processes falls within the flux range of 0.7-1.1 mJ/cm<sup>2</sup>.

## **1.6 Parametric instabilities of surface plasma waves**

The surface plasma waves are known to excite parametric instabilities. Atanassov et al. [64] have considered a nonlinear interaction of three high-frequency electrostatic surface waves, producing a low-frequency density perturbation. Aliev and Brodin [65] investigated the excitation of a surface plasma wave and a volume plasma wave in an inhomogeneous plasma by p-polarized pump wave. Brodin and Lindberg [66] considered the same problem including thermal effects. Lindgren et al. [67] developed a general theory of three wave interactions in plasmas with sharp boundaries by using the diffuse charge distribution model. Lee and Mun [68] investigated the parametric decay instability where a p-polarized light wave decays into another light wave and a transverse magnetic mode. Lee and Cho [69] investigated parametric decay of a p-polarized wave into two

surface plasma waves in semi-infinite plasma formulating the nonlinear boundary conditions in terms of space charge and volume currents. Lee and Kim [70] studied the oscillating two stream instability of electrostatic plasma surface waves excited by an oscillating pump electric field theoretically. They solve the coupled mode equations describing parametric interactions of the electrostatic plasma surface wave, the pump wave and the both Stoke and anti-Stoke side bands. The purely growing nonlinear surface wave modes were excited more easily than that of volume wave purely growing mode. They calculated the growth rate evaluating the rippling effect on the parametric interactions. Sergueychev [71] has shown that parametrically excited SPW in bounded gaseous plasma can efficiently heat plasma ions. Yasumoto [72] investigated the decay instability of high frequency light wave into a SPW and a low frequency ion-acoustic wave. In another study, decay instability of two high frequency SPWs in semi-infinite plasma was considered. At large amplitude, SPW can onset other nonlinear effect such as filamentation instability. This is an important nonlinear process in the interaction of sub-millimeter waves with semiconductors.

## **1.7 Plan of the thesis**

The present thesis focuses on Raman scattering of SPW at conductor-free space interface and its applications in fiber optic sensors. We also study absorption of SPW by nanoparticles and two major nonlinear effects of SPW at high amplitudes, viz. electron acceleration and filamentation. We also bring out a compact scheme of exciting SPW by solid and annular beams in a plasma cylinder. Work in the proposed thesis is distributed over eight chapters. A chapter wise summary of the thesis is as follows.

**Chapter 2** discusses laser mode conversion into a surface plasma wave in a metal coated optical fiber suitable for surface enhanced Raman scattering (SERS) sensor. An optical fiber, coated with thin metal film, supports two distinct kinds of waves *viz.*, body waves that propagate through the fiber as TM (transverse magnetic) and TE (transverse electric) modes, and surface plasma waves (SPW) that propagate on metal free space interface. When the metal has a ripple of suitable wave number  $q$ , a body wave of frequency  $\omega$  and propagation constant  $k_z$  induces a current at  $\omega, k_z + q$  in the ripple region that resonantly derives a surface plasma wave. When the metal surface has metallic particles attached to it and molecules are adsorbed on them, the surface plasma wave undergoes surface enhanced Raman scattering with them. The scattered signals propagate backward as a TM body wave and can be detected.

In **chapter 3**, we explore the possibility of replacing laser by a laser driven surface plasma wave in a surface enhanced Raman scattering sensor. A surface plasma wave, propagating along a metal surface, embedded with regularly arranged nanoparticles, undergoes surface enhanced Raman scattering from molecules adsorbed over the particles. The SPW polarizes the particles, resonantly enhancing the local field. The field polarizes the molecules adsorbed on particles. The scattered field produced by the adsorbed molecules gets enhanced by the same plasmon effect again. The enhancement in the scattered signal depends on the shape and dielectric constant of the metallic particles. The scattered signal can be detected above the metal surface as a space wave if the particles have a periodic arrangement with wave number  $q$  such that  $\omega_R > (k_S - q)c$  where  $\omega_R$  is the frequency of the scattered signal and  $k_S$  is the wave number of surface plasma wave.

In **chapter 4**, we discuss electron acceleration employing resonant interaction of electrons with a surface plasma wave. Two parallel metal sheets, separated by a thin vacuum region, support a surface plasma wave (SPW) whose amplitude is maximum on the two parallel interfaces and minimum in the middle. This mode can be excited by a laser using a glass prism. An electron beam launched into the middle region, experiences a longitudinal ponderomotive force due to the surface plasma wave and gets accelerated to velocities of the order of phase velocity of the surface wave. The scheme is viable to achieve beams of tens of keV energy with the control in their trajectory. In the case of a surface plasma wave excited on a single metal-vacuum interface, the field gradient normal to the interface pushes the electrons away from the high field region, limiting the acceleration process. The acceleration energy thus achieved is in agreement with the experimental observations.

In **chapter 5**, we study the anomalous absorption of surface plasma waves by metal particles placed over a metal surface. A surface plasma wave (SPW) propagating on a metal surface excites resonant plasma oscillations in the particles. The particles absorb energy from the wave via electrons, incurring attenuation of the surface plasma wave. For spherical metallic particles with plasma frequency  $\omega_{pe}$ , the resonant plasma oscillations occurs at  $\omega = \omega_{pe} / \sqrt{3}$ , where  $\omega$  is the frequency of incident laser. In the vicinity of this frequency, a sharp increase in the absorption of surface plasma wave by the metallic particles, depending upon its size occurs.

In **chapter 6**, we study the filamentation instability of a surface plasma wave over a semiconductor-free space interface. A large amplitude surface plasma wave (SPW), propagating over a semiconductor-free space interface, is susceptible to filamentation

instability. A small perturbation in the amplitude of the SPW across the direction of propagation exerts a ponderomotive force on free electrons and holes, causing spatial modulation in free carrier density and hence the effective permittivity  $\epsilon_{eff}$  of the semiconductor. The regions with higher  $\epsilon_{eff}$  attract more power from the neighborhood, leading to the growth of the perturbation. The growth rate increases with the intensity of the surface wave. It decreases with the frequency of the SPW.

In **chapter 7**, we study the excitation of surface plasma wave over a plasma cylinder by a relativistic electron beam. A relativistic electron beam propagating in a plasma cylinder excites a surface plasma wave via Cerenkov interaction. The wave frequency decreases with beam velocity. The growth rate, however, initially increases with frequency  $\omega$ , attains a maximum and then falls off. For typical parameters, optimal growth occurs at  $\omega/\omega_p \approx 0.36$ , where  $\omega_p$  is the plasma frequency. With the increase in the radius of plasma, the optimum growth rate increases in magnitude.

In **chapter 8**, we summarize our work and future directions of our thesis.

## List of Publications

### Published

1. C. S. Liu, **Gagan Kumar**, V. K. Tripathi, “Laser mode conversion into a surface plasma wave in a metal coated optical fiber”, *J. Appl. Phys.* **100**, 013304 (2006).
2. **Gagan Kumar**, D. B. Singh, V. K. Tripathi, “Surface enhanced Raman scattering of a surface plasma wave”, *J. Phys. D: Appl. Phys.* **39** (2006) 4436–4439.  
The Corrigendum of this paper published in *J. Phys. D: Appl. Phys.* **39** (2006) 4738.
3. D. B. Singh, **Gagan Kumar**, and V K Tripathi, “Probing of a surface plasma wave by an obliquely incident laser on the metal surface”, *J. Appl. Phys.* **101**, 043306 (2007). (Selected in Virtual Journal of Ultrafast Science).
4. C. S. Liu, **Gagan Kumar**, D. B. Singh and V. K. Tripathi, “Electron acceleration by surface plasma waves in double metal surface structure,” *J. Appl. Phys* **102**, 113301 (2007).
5. **Gagan Kumar** and V. K. Tripathi, “Anomalous absorption of surface plasma wave by particles adsorbed on metal surface”, *Appl. Phys. Lett.* **91**, 161503 (2007).
6. **Gagan Kumar** and V. K. Tripathi, “Filamentation of a surface plasma wave over a semiconductor free space interface”, *J. Appl. Phys.* **102**, 123301 (2007).
7. D. B. Singh, **Gagan Kumar**, and V K Tripathi, “Surface plasmon induced heating and emission of electrons from metallic targets”, *Phys. Plasmas.* **14**, 102108 (2007).

### Communicated

1. **Gagan Kumar** and V. K. Tripathi, “Excitation of surface plasma wave over plasma cylinder by a relativistic electron beam”, Communicated to *Phys. Plasmas*.

## References

1. E. Burstein, in: *Polaritons* (E. Burstein and F. de Martini, eds.) (Pergamon, New York, 1974) p. 1.
2. F. Abels, “Surface plasmon (SEW) phenomena” in *Electromagnetic Surface Excitations*, edited by R. F. Fallis and G. I. Stegeman (Springer-Verlag, New York, 1986), p. 8.
3. H. Raether, Surface plasmons on smooth and rough surfaces and on gratings, in Springer Tracts in Modern Physics, vol. 111( Springer-Verlag, New York, 1988).
4. A. D. Boardman, in: *Electromagnetic Surface Modes* (A. D. Boardman, ed.) (John Wiley & Sons Ltd., New York, 1982) p. 1.
5. A. A. Zayats, I. I. Smolyaninov, and A. A. Maradudin, *Phys. Reports* **408**, 131 (2005).
6. R. W. Wood, *Philos. Mag.* **6**,396 (1902).
7. L. Rayleigh, *Philos. Mag.* **14**, 60 (1907).
8. U. Fano, *J. Opt. Soc. Amer.* **31**, 213 (1941).
9. A. W. Trivelpiece and R. W. Gould, *J. Appl. Phys.* **30**,1784 (1959).
10. A. Otto, *Z. Physik* **216**, 398 (1968).
11. E. Kretschmann and H. Raether, *Z. Naturforsch*, **23**, 2135 (1968).
12. V. M. Agranovich, *Zh. Eksp. Teor. Fiz* **77**, 1124 (1979).
13. K. Okamoto, I. Niki, A. Shvartser, Y. Narukawa, T. Mukai, and A. Scherer, *Nature* **3**, 601 (2004).
14. W. L. Barnes, Alain Dereux, and T. W. Ebbesen, *Nature* **424**, 824 (2003).

15. C. Genet and T. W. Ebbesen, *Nature* **445**, 39 (2007)
16. V. V. Klimov, M. Ducloy, and V. S. Letokhov, *Chem. Phys. Lett.* **358**, 192 (2002).
17. H. Atwater, "Promises of plasmonics", *Sci. Am.*, March 2007.
18. H. J. Simon, C. Huang, J. C. Quail, and Z. Chen, *Phys. Rev. B* **38**, 7408 (1988).
19. H.-E. Ponath, G.I. Stegeman (Eds.), *Nonlinear Surface Electromagnetic Phenomena*, North-Holland, Amsterdam, 1991.
20. V. M. Agranovich, D. L. Mills (Eds.), *Surface Polaritons*, North-Holland, Amsterdam, 1982.
21. L. Salomon, G. Bassou, J. P. Dufour, F. de Fornel, A. V. Zayats, *Phys. Rev. B* **65**, 125409 (2002)
22. C. Denton, J. L. Gervasoni, R. O. Barrachina, and N. R. Arista, *Phys. Rev. A* **57**, 4498 (1998).
23. K. J. Woods, J. E. Walsh, R. E. Stoner, H. G. Kirk, and R. C. Fernow, *Phys. Rev. Lett.* **74**, 388 (1995).
24. J. Urata, M. Goldstein, M. F. Kimmitt, A. Naumov, C. Platt, and J. E. Walsh, *Phys. Rev. Lett.* **80**, 516 (1998).
25. S.I. Bozhevolnyi, I.I. Smolyaninov, A.V. Zayats, *Phys. Rev. B* **51**, 17916 (1995).
26. B. Hecht, H. Bielefeldt, L. Novotny, Y. Inouye, D.W. Pohl, *Phys. Rev. Lett.* **77**, 1889 (1996).
27. M. Fleischmann, P. J. Hendra, and A. J. McQuillan, *Chem. Phys. Lett* **26**, 163 (1974).
28. D. L. Jeanmaire and R. P. Van Duyne, *J. Electroanal. Chem.* **84**, 1 (1977).

29. M. Kerker, *J. Colloid Interf. Sci* **118**, 417 (1987).
30. J. Gersten, A. Nitzan, *J. Chem. Phys.* **73**, 3023 (1980).
31. M. Moskovits, *Solid State Commun.* **32**, 59 (1979).
32. M. Moskovits, *J. Chem. Phys.* **69**, 4159 (1978).
33. M. Moskovits, *Rev. Mod. Phys.* **57**, 783 (1985).
34. T. Vo-Dinh, Leonardo R. Allain, and David L. Stokes, *J. Raman Spectrosc.* **33**, 511 (2002).
35. C. R. Yonzon, C. L. Haynes, X. Zhang, J. T. J. Walsh, and R. P. Van Duyne, *Anal. Chem.* **76**, 78 (2004).
36. M. Mandal, S. Kundu, S. K. Ghosh, N. R. Jana, M. Panigrahi and T. Pal, *Current Science* **86**, 556 (2004).
37. David L. Stokes, Tuan Vo-Dinh, *Sens. Actuators B* **69**, 28-36 (2000).
38. D. L. stokes, J. P. Alarie, V. Ananthanarayanan, and T. Vo-Dinh, *Proc. SPIE Int. Soc. Opt. Eng.* **3534**, 647 (1997).
39. D. L. Stokes, J. P. Alarie, and T. Vo-Dinh, *Proc. SPIE Int. Soc. Opt. Eng.* **2504**, 552 (1995).
40. B. Mizaikoff, *Water Sci. Technol.* **47**, 35-42 (2003).
41. J. F. Masson, K. Hamersky, S. Beaudoin, and K. S. Booksh, *Proc. SPIE* **5261**, 123-134 (2004).
42. H. Steiner, M. Jakusch, M. Kraft, M. Karlowatz, T. Baumann et al., *Appl. Spectrosc.* **57**, 607-613 (2003).
43. J.B. Jensen, L.H. Pedersen, P.E. Hoiby, L.B. Nielsen, T.P. Hansen, J.R. Folkenberg et al., *Opt. Lett.* **29**, 1974-1976 (2004).

44. B. Liedberg, C. Nylander, I. Landstrom, *Sensors and Actuators* 4, 299 (1983).
45. R. C. Jorgenson, S. S. Yee, *Sensors and Actuators B* **12**, 213 (1993).
46. R. Slavik, J. Homola and J. Ctyroky, *Sens. Actuators B* **54**, 74 (1999).
47. S. Ya. Tochitsky, R. Narang, C. V. Filip, P. Musumeci, C. E. Clayton et al., *Phys. Rev. Lett.* **92**, 095004 (2004).
48. B. Hafizi, A. Ting, E. Esarey, P. Sprangle, and J. Krall, *Phys. Rev. E* **55**, 5924 (1997).
49. V. Malka, S. Fritzler, E. Lefebvre, M.-M. Aleonard, F. Burgy et al., **98** *Science*, 1596 (2002).
50. M. I. K. Santala, Z. Najmudin, E. L. Clark, M. Tatarakis, K. Krushelnick, *Phys. Rev. Lett.* **86**, 1227 (2001).
51. J. Zawadzka et al. *Nucl. Instrum. Methods Phys. Res. Sect. A* **445**, 324 (2000).
52. J. Zawadzka, D. Jaroszynski, J. J. Carey, and K. Wynne, *Appl. Phys. Lett.* **79**, 2130 (2001).
53. S. E. Irvine and A. Y. Elezzabi, *Appl. Phys. Lett.* **86**, 264102, (2005).
54. S. E. Irvine and A. Y. Elezzabi, *Phys. Rev. A* **73**, 013815 (2006).
55. J. Kupersztych, M. Raynaud, and C. Riconda, *Phys. Plasmas* **11**, 1669 (2004).
56. F. Lopez-Tejeira et al., *Nature Physics* 3, 324 (2007).
57. D. R. Smith, W. J. Padilla, D. C. Vier, S. C. Nemat-Nasser, and S. Schultz, *Phys. Rev. Lett.* **84**, 4184 (2000).
58. V. G. Veselago, *Sov. Phys. Usp.* **10**, 509 (1968)
59. J. B. Pendry, *Phys. Rev. Lett.* **85**, 3966 (2000).
60. T. Ditmire et al., *Phys. Rev. Lett.* **78**, 3121 (1997).

61. Y. P. Bliokh, J. Felsteiner, and Y. Z. Slutsker, Phys. Rev. Lett. **95**, 165003 (2005).
62. A. Y. Vorobyev and C. Guo, Phys. Rev. B **72**, 195422 (2005).
63. S. I. Anisimov, B. L. Kapelovich, and T. L. Perel'man, Sov. Phys. JETP **39**, 375 (1974).
64. V. Atanassov, E. Mateev and I. Zhelyazkov, J. Plasma Phys. **26**, 217 (1981).
65. Y. M. Aliev and G. Brodin, Phys Rev. A **42**, 2374 (1990).
66. G. Brodin and J. Lundberg, J. Plasma Phys. **46**, 299 (1991).
67. T. Lindgren, J. Larsson, and L. Stenflo, Plasma Phys. **24**, 1177 (1982).
68. H. J. Lee and B. S. Mun, J. Plasma Phys. **62**, 35 (1999).
69. H. J. Lee and S. H. Cho, Phys. Rev. E **59**, 3503 (1999).
70. H. J. Lee and J. I. Kin, Plasma Phys. Control. Fusion **42**, 99 (2000).
71. K. F. Sergueychev, Sov. Phys. JETP **31**, 620 (1970).
72. K. Yasumoto, J. Appl. Phys. **52**, 3238 (1982).

## Chapter 2

# LASER MODE CONVERSION INTO A SURFACE PLASMA WAVE IN A METAL COATED OPTICAL FIBER

### 2.1 Introduction

Surface plasma waves (SPW) are being used widely for the development of high sensitivity sensors. A conventional SPW sensor employs attenuate total reflection (ATR) geometry [1] in which a thin film is deposited on a prism and laser is made incident on a bright face of the prism. The transmitted light suffers reflection from the glass metal interface and comes out from the other bright face of the prism. As one varies angle of incidence of the laser, the reflectivity varies mildly. However, at some specific angle the reflectivity is drastically reduced. This angle, called surface plasmon resonant angle depends on the dielectric constant of the medium above the metal film. Hence a measurement of surface plasmon resonant angle gives information about the material above the film. The reduction in reflectivity is caused by the diversion of laser energy into a surface plasma wave over the metal free space boundary. The electric field of the SPW is an order of magnitude higher than the laser field [2]. The presence of nanoparticles or traces of bio-materials on metal surface bring noticeable change in resonant angle of incident,  $\theta_r$  reflectivity and phase of reflected light, from which information about the material can be deduced [3].

Alternatively, one may employ surface enhanced Raman scattering (SERS). In SERS sensors, molecules adsorbed on rough metal surface [4, 5] produce up to six orders of magnitude enhancement [6] in Raman signal as compared to naked molecules, due to

plasmon resonance. A laser incident on a rough metal surface or nano-particles induces a huge field on particle surface strongly polarizing the atoms of the molecules adsorbed. As the atoms of a molecule vibrate about their centre of mass, the induced dipole moment oscillates at laser frequency and the sidebands, Raman shifted by the vibration frequency are produced. The Raman shifted atomic dipole induces a strong, plasmon enhanced, field inside the particle, and the latter behaves as a radiating dipole, producing highly enhanced Raman signal [7-13]. SERS has various potential applications. Recent applications of SERS have included detection of cancer genes [14], glucose sensing at physiological concentrations [15] and detection of chemical and biological agents [16].

Currently there is very significant interest in developing fiber SERS sensors. A roughened optical fiber coated with silver is employed for SERS detection [17]. Stokes and Vo-Dinh have developed an integrated single-fiber SERS sensor in which excitation and collection of Raman signal is done by the same fiber [18].

In this chapter we examine the mode conversion of a laser in a metal coated fiber, from TM mode to surface plasma wave. The fiber metal interface has a ripple to assist k-matching. We model the ripple as an electron density modulation at wave number  $k_w$ . When a laser propagates through the fiber it induces oscillatory velocity on electrons of the metal. The oscillatory velocity beats with the space modulated density to produce a current driving the surface plasma wave on the metal free space interface. The SPW field polarizes the metal particles present on metal surface, resonantly enhancing local fields. The fields polarize the molecules adsorbed on particles. The scattered field produced by the adsorbed molecules gets enhanced again by the same plasma effect as stated above,

discussed by Liao et. al. [19]. Finally we have calculated the ratio of the amplitude of body wave going back into the fiber to that of amplitude of incident laser.

In section 2.2, we derive dispersion relation for body and surface plasma waves of a metal coated optical fiber. In section 2.3, we study the mode conversion of a body wave due to a ripple at fiber metal interface. In section 2.4, we study the SERS of a surface plasma wave. In section 2.5, we discuss the results.

## 2.2 Body waves and surface waves

Consider an optical fiber of radius ‘a’ and permittivity  $\varepsilon_g$ , coated with metal ( $a < r < b$ ) of effective permittivity  $\varepsilon_m$  (Fig. 2.1). A laser propagates through this structure in azimuthally symmetric TM mode ( $E_z$  and  $E_r$  are finite) with  $t-z$  variation as  $\exp[-i(\omega t - k_z z)]$ . The fields are governed by Maxwell’s equations.

$$\nabla \times \vec{E} = -\frac{1}{c} \frac{\partial \vec{H}}{\partial t}, \quad (2.1)$$

$$\nabla \times \vec{H} = \frac{\varepsilon'}{c} \frac{\partial \vec{E}}{\partial t}. \quad (2.2)$$

where  $\varepsilon' = \varepsilon_g$  for  $r < a$ ,  $\varepsilon' = \varepsilon_m = \varepsilon_L - \omega_p^2 / \omega(\omega + i\nu)$  for  $a < r < b$ , and  $\varepsilon' = 1$  for  $r > b$  (free space).  $\varepsilon_L$  is the lattice permittivity of the metal,  $\omega_p$  is the plasma frequency of free electrons inside the metal and  $\nu$  is the electron collision frequency. Taking curl of Eq. (2.1) and using Eq. (2.2), we get

$$\nabla^2 \vec{E} - \frac{\varepsilon'}{c^2} \frac{\partial^2 \vec{E}}{\partial t^2} = 0$$

Replacing  $\partial / \partial t$  by  $-i\omega$  and  $\partial / \partial z$  by  $ik_z$ , one obtains

$$\frac{\partial^2 E_z}{\partial r^2} + \frac{1}{r} \frac{\partial E_z}{\partial r} + \left( \frac{\omega^2}{c^2} \epsilon' - k_z^2 \right) E_z = 0, \quad (2.3)$$

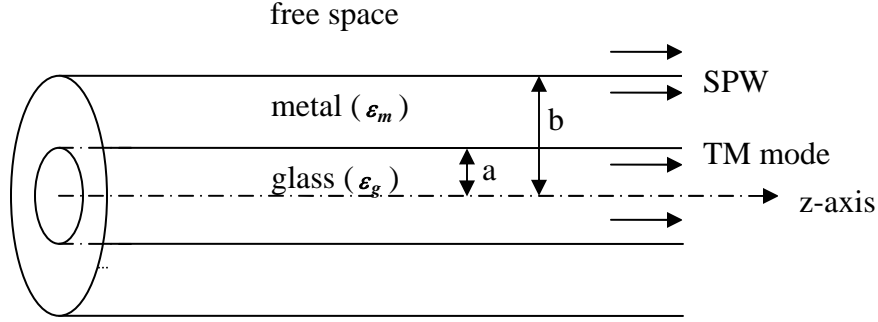


Fig. 2.1 Schematic of a metal coated optical fiber. TM mode propagates primarily through the glass, and surface plasma wave propagates on the metal-free space interface.

The solutions of Eq. (2.3) in different media can be written as

$$\vec{E} = A_1 \left[ J_0(k_{\perp} r) \hat{z} + \frac{i k_z}{k_{\perp}} J_0'(k_{\perp} r) \hat{r} \right] e^{-i(\omega t - k_z z)}, \quad 0 < r < a,$$

$$\vec{E} = \left[ (A_{21} I_0(\alpha_2 r) + A_{22} K_0(\alpha_2 r)) \hat{z} - \left( \frac{i k_z}{\alpha_2} \right) (A_{21} I_0'(\alpha_2 r) + A_{22} K_0'(\alpha_2 r)) \hat{r} \right] e^{-i(\omega t - k_z z)},$$

$$a < r < b,$$

$$\vec{E} = A_3 \left[ K_0(\alpha_3 r) \hat{z} - \left( \frac{i k_z}{\alpha_3} \right) K_0'(\alpha_3 r) \hat{r} \right] e^{-i(\omega t - k_z z)}, \quad r > b, \quad (2.4)$$

where  $k_{\perp} = \left( \frac{\omega^2 \epsilon_g}{c^2} - k_z^2 \right)^{1/2}$ ,  $\alpha_2 = \left( k_z^2 - \frac{\omega^2 \epsilon_m}{c^2} \right)^{1/2}$ ,  $\alpha_3 = \left( k_z^2 - \frac{\omega^2}{c^2} \right)^{1/2}$  and the prime

denotes differentiation w. r. t. argument. Here we have employed the  $\phi$  component of

Eq. (2.1) and r-component of Eq. (2.2) to write the radial component of electric fields.

Continuity of  $E_z$  and  $\varepsilon' E_r$  at  $r = a, b$  demands

$$A_{21} I_0(\alpha_2 a) + A_{22} K_0(\alpha_2 a) = A_1 J_0(k_\perp a),$$

$$A_{21} I_0'(\alpha_2 a) + A_{22} K_0'(\alpha_2 a) = -\left(\frac{\varepsilon_g \alpha_2}{\varepsilon_m k_\perp}\right) A_1 J_0'(k_\perp a),$$

$$A_{21} I_0(\alpha_2 b) + A_{22} K_0(\alpha_2 b) = A_3 K_0(\alpha_3 b),$$

$$A_{21} I_0'(\alpha_2 b) + A_{22} K_0'(\alpha_2 b) = \left(\frac{\alpha_2 A_3}{\varepsilon_m \alpha_3}\right) K_0'(\alpha_3 b). \quad (2.5)$$

leading to the dispersion relation

$$\left[ J_0(k_\perp a) + \left(\frac{\alpha_2 \varepsilon_g}{k_\perp \varepsilon_m}\right) \left(\frac{J_0'(k_\perp a)}{K_0'(\alpha_2 a)}\right) K_0(\alpha_2 a) \right] \left[ I_0(\alpha_2 b) - \left(\frac{\alpha_3 \varepsilon_m}{\alpha_2}\right) \left(\frac{I_0'(\alpha_2 b)}{K_0'(\alpha_3 b)}\right) K_0(\alpha_3 b) \right] = Q, \quad (2.6)$$

where,

$$Q = \frac{I_0'(\alpha_2 a)}{K_0'(\alpha_2 a)} \left[ J_0(k_\perp a) + \frac{\alpha_2 \varepsilon_g}{k_\perp \varepsilon_m} \frac{J_0'(k_\perp a)}{I_0'(\alpha_2 a)} I_0(\alpha_2 a) \right] \left[ K_0(\alpha_2 b) - \frac{\alpha_3 \varepsilon_m}{\alpha_2} \frac{K_0'(\alpha_2 b)}{K_0'(\alpha_3 b)} K_0(\alpha_3 b) \right]$$

In the limit  $b \rightarrow \infty$  or  $a \rightarrow 0$ ,  $Q=0$ . In the former, the first factor in Eq. (2.6) equated to zero gives the body wave (TM mode)

$$J_0(k_\perp a) = -\frac{\alpha_2 \varepsilon_g}{k_\perp \varepsilon_m} \frac{J_0'(k_\perp a)}{K_0'(\alpha_2 a)} K_0(\alpha_2 a). \quad (2.7)$$

For  $a \rightarrow 0$ , the second factor in Eq. (2.6) equated to zero gives the surface plasma wave

$$I_0(\alpha_2 b) = \frac{\alpha_3 \varepsilon_m}{\alpha_2} \frac{I_0'(\alpha_2 b)}{K_0'(\alpha_3 b)} K_0(\alpha_3 b). \quad (2.8)$$

In the limit  $b \rightarrow \infty$ , Eq. (2.8) reduces to  $\varepsilon_m = -\alpha_2/\alpha_3$ , giving the usual dispersion relation for SPW over a planar surface

$$k_z^2 = \frac{\omega^2}{c^2} \frac{\epsilon_m}{\epsilon_m + 1}. \quad (2.9)$$

In the general case when  $a$  and  $b$  are finite the modes are significantly modified by finite  $Q$ . In the case of much interest,  $\alpha_2 b \gg 1$ ,  $Q$  is small and the coupling between the two factors on the left of Eq. (2.6) is weak.

Eq. (2.6) admits another surface plasma wave that propagates along the glass-metal interface with dispersion relation

$$K_o(\alpha_2 a) \cong -\frac{\epsilon_m}{\epsilon_g} \frac{k_\perp}{\alpha_2} \frac{K_o'(k_\perp a)}{J_o'(k_\perp a)} J_o(k_\perp a), \quad (2.10)$$

In the limit  $a \rightarrow \infty$ , it takes the form  $k_z^2 = (\omega^2 / c^2) \epsilon_m \epsilon_g / (\epsilon_m + \epsilon_g)$ . We have solved Eq. (2.6) numerically and plotted normalized frequency  $\Omega = \omega / \omega_p$  versus normalized wave number  $q_z = k_z c / \omega_p$  in Fig. 2.2 and 2.3 for  $\epsilon_g = 2.13$ ,  $\epsilon_L = 10$ ,  $a = 4 \mu m$ ,  $b = 4.04 \mu m$ .

In Fig. 2.2 and 2.3, one may note that the frequency for the TM mode begins with a cutoff and rises as  $q_z$  increases. The surface plasma wave has linear variation of  $\Omega$  with  $q_z$  initially, however at large value of  $q_z$ ,  $\Omega$  tends to a saturation value. At a given  $\Omega$ , the difference in  $q_z$  value for the TM mode and SPW represents the wave number mismatch or the wave number required for resonant mode conversion. At  $a \omega_p / c = 20$ , we see that a minimum of  $q_z$  is required for  $\Omega = 0.2453$ , and this minimum value is  $q_z = 0.0184$ . It is only in a narrow range of  $\Omega$ , we can convert body wave into SPW with a ripple of small  $q_z$ . Outside this range we need a ripple of very high  $q_z$ , which is quite difficult to obtain.

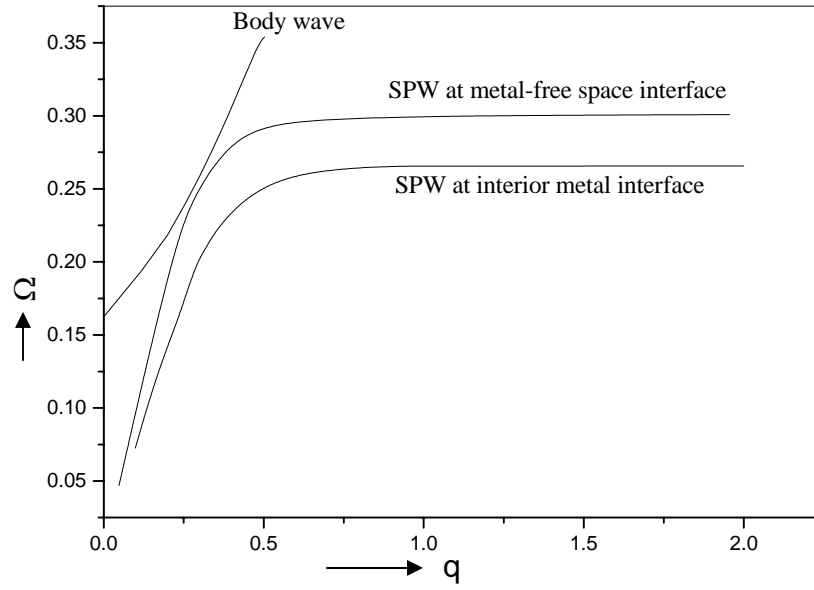


Fig. 2.2 Variation of normalized frequency,  $\Omega$  with normalized wave vector,  $q_z$  for TM mode body wave and SPWs. The parameters are:  $a\omega_p/c = 20$ ,  $\varepsilon_g = 2.13$ ,  $\varepsilon_L = 10$ ,  $b/a = 1.01$ .

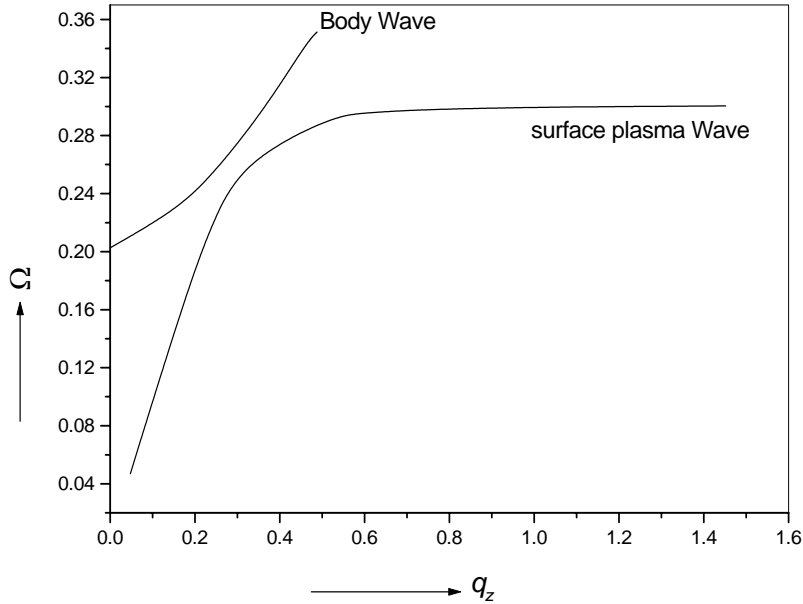


Fig. 2.3 Variation of normalized frequency,  $\Omega$  with normalized wave vector,  $q_z$  for TM mode and SPW. The parameters are:  $a\omega_p/c = 17$ ,  $\varepsilon_g = 2.13$ ,  $\varepsilon_L = 10$ ,  $b/a = 1.01$ .

In Fig. 2.2, we note that surface plasma waves at metal-free space and glass-metal interfaces have significantly different wave numbers at a given frequency. Therefore one cannot excite both the surface plasma waves simultaneously by the same laser body wave using a same ripple. Only the surface plasmon mode at the metal-free space interface has the relevance in SERS sensors, therefore we will be choosing ripple wave number such that it couples this surface plasma wave to the TM mode. Hence we ignore the surface wave on glass-metal interface.

In Fig. 2.4, we have plotted  $\Omega$  Vs  $q_z$  for  $a\omega_p/c = 20$  with  $b/a = 1.1$  i.e. increased metal thickness to  $400nm$ . In this case the surface plasma wave and body wave dispersion curve touch each other at a certain frequency. If we need to convert a body wave into a SPW of this frequency then it does not require a ripple.

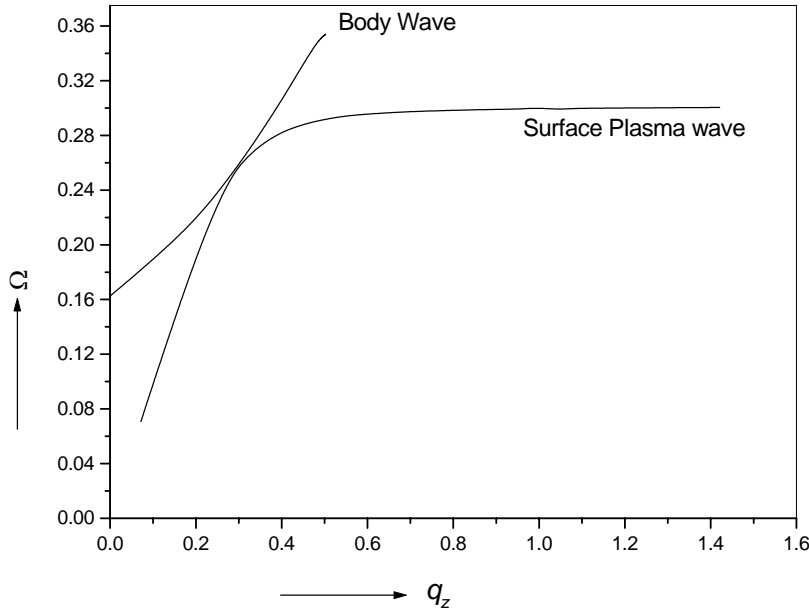


Fig. 2.4 Variation of normalized frequency,  $\Omega$  with normalized wave vector,  $q_z$  for TM mode and SPW. The parameters are:  $a\omega_p/c = 20$ ,  $\epsilon_g = 2.13$ ,  $\epsilon_L = 10$ ,  $b/a = 1.1$ .

### 2.3 Mode conversion

Consider the fiber metal interface to be rippled (Fig. 2.5),  $r = a + h \cos(k_w z)$ . On the outer side of the ripple, the electron density in the metal is  $n_0$ . In the ripple region ( $a - h < r < a + h$ ), it is periodic function of  $z$ ,  $n(z) = n(z + \lambda_w)$ , where  $\lambda_w = 2\pi / k_w$ .

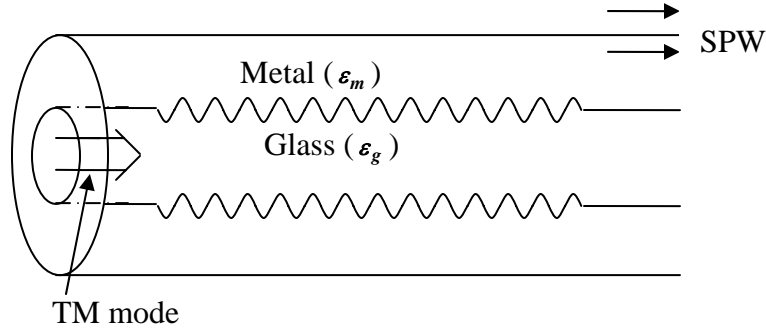


Fig. 2.5 Mode conversion of a TM mode into SPW due to rippled interface between fiber and metal coating.

Following Liu and Tripathi [20], we model the ripple by an electron density modulation,

$$n = \frac{n_0}{2} (1 + \sin(k_w z)), \quad \text{for } a - h < r < a + h. \quad (2.11)$$

A laser of frequency  $\omega_L$  and parallel wave number  $k_z = k_L$  propagates through the fiber in TM mode. Its field in different regions is given by Eq. (2.4) with  $A'_s$ ,  $k_\perp$ ,  $\alpha_2$ ,  $\alpha_3$  having a superfix L, designating laser. From Eq. (2.5),  $A_{21}^L$ ,  $A_{22}^L$ ,  $A_3^L$  are expressed in terms of  $A_1^L$ . Thus we may write the laser field as  $\vec{E} = A_1^L \vec{\psi}_L(r) \exp(-i(\omega_L t - k_L z))$ .

This field imparts oscillatory velocity to electrons,  $\vec{v} = e\vec{E}/mi\omega_L$ , where  $-e$  and  $m$  are the electronic charge and mass. Within the ripple region,  $\vec{v}$  beats with  $n$  to produce a nonlinear current density at frequency  $\omega_L$  and wave number  $k_s = k_L + k_w$ ,

$$\vec{J}_s^{NL} = -\frac{n_0 e^2 A_1^L}{4mi\omega} \vec{\psi}_L \exp(-i(\omega_L t - k_s z)). \quad (2.12)$$

$\vec{J}_s^{NL}$  is localized in the ripple region and can be taken to be a delta function of  $r$  with  $\vec{\psi}_L(r)$  replaced by  $h\vec{\psi}_L(a)$ .  $\omega_L, k_s$  satisfy the dispersion relation for SPW, hence  $\vec{J}_s^{NL}$  derive the surface plasma wave. The relevant Maxwell's equations for the SPW are

$$\begin{aligned} \nabla \times \vec{E}_s &= \left(\frac{i\omega_L}{c}\right) \vec{H}_s, \\ \nabla \times \vec{H}_s &= -\left(\frac{i\omega_L}{c}\right) \epsilon' \vec{E}_s + \left(\frac{4\pi}{c}\right) \vec{J}_s^{NL}. \end{aligned} \quad (2.13)$$

Let the solution of these equations when  $\vec{J}_s^{NL} = 0$  be  $\vec{E}_{so}$  and  $\vec{H}_{so}$ , i. e.

$$\begin{aligned} \nabla \times \vec{E}_{so} &= \left(\frac{i\omega_L}{c}\right) \vec{H}_{so}, \\ \nabla \times \vec{H}_{so} &= -\left(\frac{i\omega_L}{c}\right) \epsilon' \vec{E}_{so}. \end{aligned} \quad (2.14)$$

$\vec{E}_{so}$  is given by Eq. (2.4) with all  $A$ 's,  $\alpha_2, \alpha_3$  having superscript  $s$ , denoting SPW.

Using Eq. (2.5),  $A_{21}^s, A_{22}^s, A_3^s$  are expressible in terms of  $A_1^s$ . When  $\vec{J}_s^{NL}$  is retained,

let the fields, following Liu and Tripathi [20] be

$$\vec{E}_s = A(z) \vec{E}_{so}(r, z, t), \quad \vec{H}_s = B(z) \vec{H}_{so}(r, z, t). \quad (2.15)$$

Using these in Eq. (2.13) and employing Eq. (2.14), we obtain

$$\frac{\partial A}{\partial z} \hat{z} \times \vec{E}_{so} = \frac{i\omega_L}{c} (B - A) \vec{H}_{so}, \quad (2.16)$$

$$\frac{\partial B}{\partial z} \hat{z} \times \vec{H}_{so} = \frac{i\omega_L}{c} \varepsilon' (B - A) \vec{E}_{so} + \frac{4\pi}{c} \vec{J}_s^{NL}. \quad (2.17)$$

Multiplying Eq. (2.16) by  $\vec{H}_{so}^* r dr$ , Eq. (2.17) by  $\vec{E}_{so}^* r dr$  and integrating over  $r$  from 0 to  $\infty$ , we get

$$\frac{\partial A}{\partial z} = + \frac{i\omega_L}{c} (B - A) \frac{P_2}{P_3^*}, \quad (2.18)$$

$$\frac{\partial B}{\partial z} = - \frac{i\omega_L}{c} (B - A) \frac{P_1}{P_3} + R A_1^L, \quad (2.19)$$

where  $R = \frac{\pi n_0 e^2 h a}{c P_3 m i \omega_L} \vec{\psi}_L(a) \cdot \vec{\psi}_S^*(a)$ ,  $\vec{E}_{so} = \vec{\psi}_s \exp[-i(\omega_L t - k_S z)]$ ,

$$\vec{\psi}_L(a) = J_0(k_\perp a) \hat{z} + \frac{i k_z}{k_\perp} J_0'(k_\perp a) \hat{r}, \quad \vec{\psi}_S(a) = I_0(\alpha_2 a) \hat{z} - \frac{i k_z}{\alpha_2} I_0'(\alpha_2 a) \hat{r},$$

$$P_1 = \varepsilon' \int_0^\infty \vec{E}_{so} \cdot \vec{E}_{so}^* r dr, \quad P_2 = \int_0^\infty \vec{H}_{so} \cdot \vec{H}_{so}^* r dr, \quad P_3 = \int_0^\infty (\vec{E}_{so}^* \times \vec{H}_{so})_z r dr.$$

\* denotes the complex conjugate. Eqs. (2.18) and (2.19), with initial conditions at  $z = 0$ ,

$A = B = 0$  give

$$\frac{A}{A_1^L} = \frac{R}{(1 + P_1 P_3^* / P_2 P_3)} \left( z + (e^{-i\gamma z} - 1) / i\gamma \right), \quad (2.20)$$

where  $\gamma = (\omega_L / c) (P_1 P_3^* / P_2 P_3)$ . This treatment is valid as long as  $z < k_{si}^{-1}$ , where  $k_{si}^{-1}$  is

the absorption coefficient of the SPW given by

$$k_{si} = \text{Im} \left[ \frac{\omega_L}{c} \left( \frac{\varepsilon_m}{1 + \varepsilon_m} \right)^{1/2} \right]. \quad (2.21)$$

Substituting  $\varepsilon_m = \varepsilon_L - \omega_p^2 / \omega_L (\omega_L + i\nu)$  in Eq. (2.21) we get

$$k_{si} = k_{SPW} \left( \frac{\omega_p^2 \nu}{2\omega_L^3} \right) \frac{1}{[\omega_p^2 / \omega_L^2 - (\varepsilon_L + 1)][\omega_p^2 / \omega_L^2 - \varepsilon_L]}, \quad (2.22)$$

where  $k_{SPW} = (\omega_L / c) \left[ (\omega_p^2 / \omega_L^2 - \varepsilon_L) / (\omega_p^2 / \omega_L^2 - (\varepsilon_L + 1)) \right]^{1/2}$ . For  $\nu \approx 10^{12} \text{ s}^{-1}$ ,  $\varepsilon_L = 10$ ,  $\omega_L / \omega_p = 0.2453$ ,  $\omega_L = 3.1970 \times 10^{15} \text{ rad / sec}$ , then we obtain  $z < 0.12 \text{ cm}$ .

In order to have an appreciation of  $|A|$  with  $z$ , we consider the case of frequency of the body wave, for a given  $a\omega_p / c$ , for which minimum ripple wave number is required. For  $a\omega_p / c = 20$ , this frequency is  $\omega_L / \omega_p = \Omega = 0.2453$  with wave number  $k_z c / \omega_p = q_z = 0.2727$  and corresponding ripple wave number  $k_w c / \omega_p = q_w = 0.0184$ . Also we use  $\omega_L h / c \approx 0.2$ . For these values we get  $P_1 = 3.5792 \text{ cm}^2$ ,  $P_2 = 3.47176 \text{ cm}^2$ ,  $P_3 = 2.34354 \text{ cm}^2$ ,  $|R| = 47.214 \text{ cm}^{-1}$ . This give  $P_1 P_3^* / P_2 P_3 = 1.03 \cong 1$ . Substituting this value in Eq. (2.20) and taking modulus gives

$$\left| \frac{A}{A_L^1} \right| = \left[ \left( \frac{|R|^2}{(\omega_L / c)^2} \right) \left( \frac{1}{4} \left( \frac{\omega_L z}{c} - \sin \left( \frac{\omega_L z}{c} \right) \right)^2 + \sin^4 \left( \frac{\omega_L z}{2c} \right) \right) \right]^{1/2}. \quad (2.23)$$

Eq. (2.23) gives the ratio of amplitude of the surface plasma wave to the amplitude of the incident laser. We have plotted  $|A / A_L^1|$  versus  $\omega_L z / c$  i.e. normalized length of the fiber in Fig. 2.6 for  $z = 0.12 \text{ cm}$ . One can note that amplitude of surface plasma wave increases linearly with fiber length.

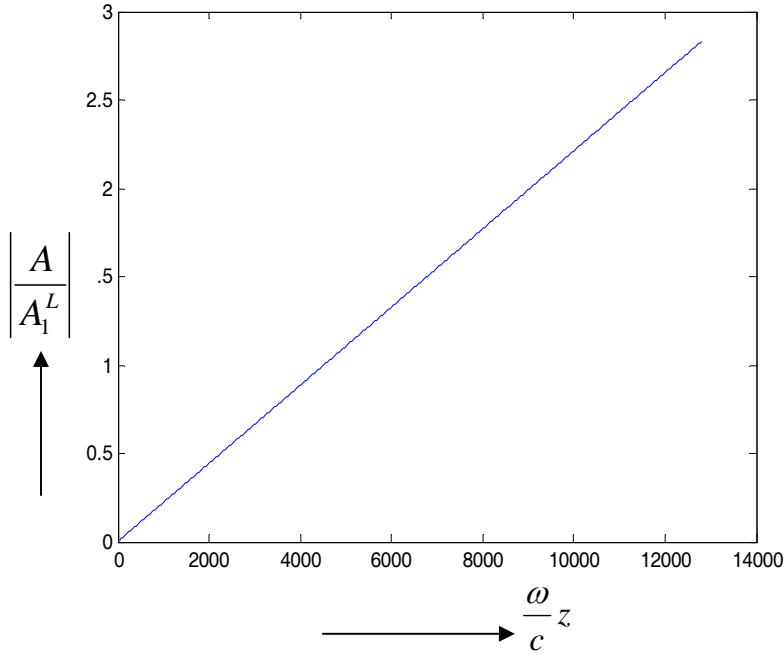


Fig. 2.6 Variation of  $\left|A/A_1^L\right|$  i.e. ratio of amplitudes of surface plasma wave to incident laser with  $\omega_L z/c$  for  $z = 0.12 \text{ cm}$ . The parameters are:  $\omega_L/\omega_p = 0.2453$ ,  $\omega_L h/c \approx 0.2$ ,  $\omega_L = 3.1970 \times 10^{15} \text{ rad/sec}$ .

It may be mentioned that an actual fiber has a cladding. Only after removing this cladding we coat it with metal. When a TM mode enters from the cladded fiber into the metal coated fiber, it encounters a change in the wave number from  $k_z'$  to  $k_z$  and a power reflection occurs, with intensity reflection co-efficient  $R_1$ , given by

$$R_1 \approx \frac{\left|k_z' - k_z\right|^2}{\left|k_z' + k_z\right|^2},$$

where  $k_z'$  and  $k_z$  are the wave number in the cladded fiber and metal coated fiber respectively.  $R_1$  may be of the order of 1 %.

## 2.4 Surface enhanced Raman scattering of SPW into a body wave

Consider spheroid shaped particles attached on the metal coated optical fiber. Some molecules are adsorbed on the particles. These molecules give rise to Raman scattering. Let  $2l_x, 2l_y, 2l_z$  be the lengths of principle axes of the spheroid along  $x, y, z$  directions. A TM mode laser of field  $\vec{E}_L$  and frequency  $\omega_L$  is launched into the fiber. This mode converts into a surface plasma wave of field  $\vec{E}_S$ . If the latter is directed along the principal axes of spheroid with a molecule also located on principle axes, then it induces a field  $\vec{E}_m$  inside the particles [21], given as

$$E_m = [1 + (\varepsilon(\omega_L) - 1)A]^{-1} E_S(\omega_L), \quad (2.24)$$

where  $\varepsilon(\omega) = \varepsilon_1(\omega) + i\varepsilon_2(\omega) = \varepsilon_L - \omega_p^2 / \omega(\omega + i\nu)$ , and  $A$  is a depolarization factor depending on particle shape. Induced field polarizes the spheroid particle. This gives equivalent point dipole of magnitude  $P_E(\omega_L) = \alpha_E(\omega_L)E_S(\omega_L)$  at the particle centre with

$$\alpha_E(\omega_L) = \frac{V}{4\pi} \frac{\varepsilon(\omega_L) - 1}{1 + [\varepsilon(\omega_L) - 1]A}, \quad (2.25)$$

where  $\alpha_E(\omega_L)$  is particle susceptibility tensor and  $V$  is the particle volume. At resonance induced dipolar field of the spheroid is large and produces a large Raman polarization and molecular dipole moment,  $\mu_m$  oscillating at stokes frequency ( $\omega_S$ ),  $\mu_m(\omega_S) = 2\alpha_R \alpha_E(\omega_L) / d^3$ . Here  $\alpha_R$  is the molecular polarizability and  $d$  is the distance from the centre of spheroid to the molecule. The field of molecular dipole in turn polarizes the spheroid to produce a spheroid dipole at the stokes frequency,  $\mu_E(\omega_S) = 2\alpha_E(\omega_S) \mu_m(\omega_S) / d^3$  which is larger than usual Raman molecular dipole by the factor<sup>19</sup>

$$K = \left( \frac{V}{2\pi d^3} \right)^2 \left[ \frac{\varepsilon(\omega_s) - 1}{1 + [\varepsilon(\omega_s) - 1]A} \right] \left[ \frac{\varepsilon(\omega_L) - 1}{1 + [\varepsilon(\omega_L) - 1]A} \right]. \quad (2.26)$$

For a sphere,  $A=1/3$ ; for a 3:1 prolate spheroid,  $A=0.1087$ . Eq. (2.26) shows a resonance at  $\varepsilon(\omega) = (1 - 1/A)$ . For sphere, this resonance occur if  $\varepsilon \approx -2$ ; a 3:1 prolate spheroid is resonant if  $\varepsilon(\omega) \approx -8.1996$ . Silver can satisfy these conditions for a visible light. The imaginary part of  $\varepsilon$  is small ( $\approx 0.3$ ) while the real part decreases from -2 to -20 over the range 350 – 700nm [22].

In an optical fiber of radius ‘ $a$ ’ and permittivity  $\varepsilon_g$ , coated with metal ( $a < r < b$ ) of effective permittivity  $\varepsilon_m$ . The  $r$ - variation of the fields of surface plasma wave in the glass interior and metallic region is governed by Eq. (2.3), whereas in the space above the conductor, it is given by

$$\frac{\partial^2 E_z}{\partial r^2} + \frac{1}{r} \frac{\partial E_z}{\partial r} + \left( \frac{\omega_L^2}{c^2} \varepsilon' - k_z^2 \right) E_z = - \frac{2\omega_L^2}{c^2} \frac{N}{b} K \alpha_R |E_S|, \quad (2.27)$$

where  $\varepsilon' = \varepsilon_g$  for  $r < a$ ,  $\varepsilon' = \varepsilon_m$  for  $a < r < b$ , and  $\varepsilon' = 1$  for  $r > b$ .  $N$  is the number of particles per unit length. The well behaved solution of these equations in three different regions is given by Eq. (2.4). Applying boundary condition of continuity of  $E_z$  and  $\varepsilon' E_r$  at  $r = a$  and continuity of  $E_z$  at  $r = b$  and condition of its derivative

$$\left. \frac{\partial E_z}{\partial r} \right|_{b^+} - \left. \frac{\partial E_z}{\partial r} \right|_{b^-} = - \frac{2\omega_L^2}{c^2} \frac{N}{b} K \alpha_R |E_S|.$$

We get

$$A_{21} I_0(\alpha_2 a) + A_{22} K_0(\alpha_2 a) = A_1 J_0(k_{\perp} a),$$

$$A_{21} I_0'(\alpha_2 a) + A_{22} K_0'(\alpha_2 a) = - \left( \frac{\varepsilon_g \alpha_2}{\varepsilon_m k_\perp} \right) A_1 J_0'(k_\perp a),$$

$$A_{21} I_0(\alpha_2 b) + A_{22} K_0(\alpha_2 b) = A_3 K_0(\alpha_3 b)$$

$$A_{21} I_0'(\alpha_2 b) + A_{22} K_0'(\alpha_2 b) = \left( \frac{\alpha_3 A_3}{\alpha_2} \right) K_0'(\alpha_3 b) - \frac{2\omega_L^2}{c^2} \frac{N}{\alpha_2 b} K \alpha_R |E_S|. \quad (2.28)$$

These equations can be solved for the ratio of amplitude of the wave going back in the fiber to the amplitude of the incident laser beam and is given as

$$\frac{A_1}{A_1^L} = \frac{|E_S|}{A_1^L} \frac{\left[ \frac{2\omega_L^2}{c^2} \frac{N}{\alpha_3 b} K \alpha_R \right] \left[ \frac{K_0(\alpha_3 b)}{K_0'(\alpha_3 b)} \right] \left[ I_0(\alpha_2 a) - \left( \frac{I_0'(\alpha_2 a)}{K_0'(\alpha_2 a)} \right) K_0(\alpha_2 b) \right]}{\left[ J_0(k_\perp a) + \left( \frac{\alpha_2 \varepsilon_g}{k_\perp \varepsilon_m} \right) \left( \frac{J_0'(k_\perp a)}{K_0'(\alpha_2 a)} \right) K_0(\alpha_2 a) \right] \left[ I_0(\alpha_2 b) - \left( \frac{\alpha_2}{\alpha_3} \right) \left( \frac{I_0'(\alpha_2 b)}{K_0'(\alpha_3 b)} \right) K_0(\alpha_3 b) \right] - Q}$$

where  $Q$  is given by Eq. (2.6). In the limit  $b \rightarrow \infty$  or  $a \rightarrow 0$ ,  $Q=0$ , so neglecting  $R'$ , we have

$$\frac{A_1}{A_1^L} = \frac{|E_S|}{A_1^L} \frac{\left[ \frac{2\omega_L^2}{c^2} \frac{N}{\alpha_3 b} K \alpha_R \right] \left[ \frac{K_0(\alpha_3 b)}{K_0'(\alpha_3 b)} \right] \left[ I_0(\alpha_2 a) - \left( \frac{I_0'(\alpha_2 a)}{K_0'(\alpha_2 a)} \right) K_0(\alpha_2 a) \right]}{D}, \quad (2.29)$$

where

$$D = \left[ J_0(k_\perp a) + \left( \frac{\alpha_2 \varepsilon_g}{k_\perp \varepsilon_m} \right) \left( \frac{J_0'(k_\perp a)}{K_0'(\alpha_2 a)} \right) K_0(\alpha_2 a) \right] \left[ I_0(\alpha_2 b) - \left( \frac{\alpha_2}{\alpha_3} \right) \left( \frac{I_0'(\alpha_2 b)}{K_0'(\alpha_3 b)} \right) K_0(\alpha_3 b) \right].$$

Since  $D \approx 0$ , we have  $D \approx \frac{\partial D}{\partial k_z} \frac{1}{L} \approx \frac{\lambda}{L}$  where,  $L$  is the length of metal coated region of

the fiber for which surface plasma wave propagates.

In order to have an appreciation of the field enhancement of incident laser, we calculate  $A_1/A_1^L$  i.e. the ratio of amplitudes of TM mode going back into the fiber and

the incident laser. Enhancement factor  $K$  can be calculated using Eq. (2.26) for a particular frequency of SPW. We consider a 3:1 prolate shaped spheroid with a molecule of Nitric Oxide ( $NO$ ) adsorbed at the tip of principal axis along which SPW field is applied. If we choose incident laser field such that it give rise to SPW of wavelength  $589.6nm$ , then for the silver spheroid ( $n \approx 5.87 \times 10^{22} cm^{-3}$ ) we obtain,  $\varepsilon(\omega_L) \approx -8.26$ . If the molecule is oscillating with vibrational frequency  $2347cm^{-1}$ , it induces a dipole moment in the spheroid at stokes frequency, corresponding dielectric constant is  $\varepsilon(\omega_S) = -14.53$ , Therefore the enhancement factor comes out  $K = 1.7458 \times 10^6$ . The ratio of amplitudes of SPW and incident laser i.e.  $|E_S|/A_1^L$  can be obtained from Eq. (2.23) for a given length of propagation of SPW. For  $L = z = 0.12cm$ , we obtain  $|E_S|/A_1^L \approx 2.827$ . Also we have  $D \approx .5896 \times 10^{-3}$  for the wavelength  $589.6nm$  of SPW. The Raman polarizability of the molecule is  $\alpha_R = 1.72 \times 10^{-24} cm^3$ . Putting these values in Eq. (2.29), we obtain  $|A_1/A_1^L| = 0.13$  for the spheroid of size  $16nm$ .

## 2.5 Discussion

The mode conversion of a TM mode into SPW in a metal coated optical fiber is facilitated by a surface ripple of suitable wave number. TM mode has a sharp frequency cutoff, beyond which its frequency monotonically increases with wave number. The frequency of surface plasma wave rises from a low value at low wave number to higher values as wave number rises. As wave number  $k \rightarrow \infty$ , wave frequency saturates at  $\omega = \omega_p / (1 + \varepsilon_L)^{1/2}$ . There is always a wave number mismatch between the TM mode and

the SPW in an optical fiber depending upon its radius. This wave number mismatch corresponds to the required ripple wave number for resonant mode conversion. When normalized fiber radius  $a\omega_p/c$  increases, the cutoff value of body wave decreases and the ripple wave number required for mode conversion decreases. Once surface plasma wave is excited, it undergoes surface enhanced Raman scattering with the molecules adsorbed on metallic particles deposited on the metal surface of the fiber. The enhancement factor depends upon depolarization factor, which in turn depends upon shape of particle. For different shapes of particles, resonant condition for enhancement is satisfied for different values of their dielectric constant. Required dielectric constant can be obtained by varying the frequency of incident wave. Hence if we choose laser light of certain wavelength depending on the shape of the particles, enhancement in the scattered signal can be obtained. For a typical metal coated optical fiber with  $\epsilon_g = 2.13$ ,  $\omega h/c = 0.2$ ,  $\omega/\omega_p = 0.2453$ ,  $\epsilon_L = 10$ , we obtain the ratio of amplitudes of the SPW and the TM mode  $\approx 2.87$  for  $L = z = 0.12 \text{ cm}$ . When the SPW of wavelength  $589.6 \text{ nm}$  undergoes SERS with *NO* molecules adsorbed on 3:1 prolate shaped silver spheroids of size  $16 \text{ nm}$  and molecules are oscillating with vibrational frequency  $2347 \text{ cm}^{-1}$ , then the ratio of amplitudes of the TM mode going back in the fiber to the incident laser comes out to be  $\approx 0.13$ .

## References

1. I. Smolyaninov, D. L. Mazzoni, and C. C. Davis, *Phys. Rev. Lett.* **77**, 3877 (1996).
2. C. S. Liu and V. K. Tripathi, *IEEE Trans. Plasma Sci.* **28**, 353-358 (2000).
3. C. L. Lei, C. C. Wei, M. C. Chen, S. Y. Ou, W. H. Li, K. C. Lee, *Mater. Sci. Eng. B* **32**, 39 (1995).
4. J. C. Tsang, J. R. Kirtley, and J. A. Bradley, *Phys. Rev. Lett.* **43**, 772 (1979).
5. J. E. Rowe, C. V. Shank, D. A. Zwemer, and C. A. Murray, *Phys. Rev. Lett.* **44**, 1770 (1980).
6. M. Moskovits, *Rev. Mod. Phys.* **57**, 783 (1985).
7. M. Moskovits, *J. Chem. Phys.* **69**, 4159 (1978).
8. E. Burstein, Y. J. Chen, and S. Lundquist, *Bull. Am. Phys. Soc.* **23**, 130 (1978).
9. S. L. McCall, P. M. Platzman, and P. A. Wolff, *Phys. Lett. A* **77**, 381(1980).
10. M. Kerker, D. S. Wang, and H. Chew, *Appl. Opt.* **19**, 4159 (1980).
11. J. I. Gertsen and A. Nitzan, *J. Chem. Phys.* **73**, 3023 (1980).
12. F. J. Adrian, *Chem. Phys. Lett.* **78**, 45 (1981).
13. D. S. Wang and M. Kerker, *Phys. Rev. B* **24**, 1777 (1981).
14. Tuan Vo-Dinh, Leonardo R. Allain, and David L. Stokes, *J. Raman Spectrosc.* **33**, 511 (2002).
15. C. R. Yonzon, C. L. Haynes, X. Zhang, J. T. J. Walsh, and R. P. Van Duyne, *Anal. Chem.* **76**, 78 (2004).
16. Fei Yan, Musundi B. Wabuyele, Guy Griffin, Arpad A. Vass, and Tuan Vo- Dinh, *IEEE Sensors J.* **5**, 665 (2005).
17. Daniel J. White and Paul R. Stoddart, *Opt. Lett.* **30**, 598 (2005).

18. David L. Stokes, Tuan Vo-Dinh, *Sens. Actuators B* **69**, 28-36 (2000).
19. P. L. Liao, J. G. Bergman, D. S. Chemla, A. Wokaun, J. Melngailis, A. M. Hawryluk, and N. P. Economou, *Chem. Phys. Lett.* **82**, 355 (1981).
20. C. S. Liu and V. K. Tripathi, *IEEE J. Quantum Electron.* **34**, 1503-1507 (1998).
21. C. J. F. Bottcher, "Theory of Electric Polarization," *Am. Elsevier* **1**, 79 (1973).
22. P. B. Johnson and R. W. Christy, *Phys. Rev. B* **6**, 4370 (1972).

## Chapter 3

# SURFACE ENHANCED RAMAN SCATTERING OF A SURFACE PLASMA WAVE

### 3.1 Introduction

Surface enhanced Raman scattering (SERS) [1] is a phenomenon vigorously employed for developing sensors and other applications. It occurs when a laser illuminates a rough metal surface or a smooth metal surface with metallic particles attached on it. When the laser frequency equals the natural frequency of plasmon oscillations of particles, the laser induces a huge field in the metallic particles, making them strong dipole oscillators at laser frequency. The molecules adsorbed on particles thus see a strong field. The Raman shifted molecular dipoles induce strong, plasmon enhanced, field inside the particles and the latter behave as radiating dipoles producing highly enhanced Raman signal [2]. Detection of cancer genes [3], glucose sensing at physiological concentrations [4] and detection of chemical and biological agents [5], detection of signal molecules [6] are among useful and recent applications of SERS. Stokes and Vo-Dinh [7] have developed an integrated single-fiber SERS sensor. It is suitable for water quality monitoring [8], detection of biomolecules and biochemical monitoring [9].

In this chapter, we explore the possibility of replacing laser by a laser driven surface plasma wave in a surface enhanced Raman scattering sensor. An ATR configuration, with thin metallic layer deposited on the hypotenuse base of a right angled prism, would convert a p-polarized laser, incident from the glass medium on the glass

metal interface at SPR angle of incidence into a surface plasma wave at the metal-free space interface. The surface plasma wave undergoes surface enhanced Raman scattering from the molecules adsorbed on metallic particles attached on the metal surface. The SPW polarizes the particles, resonantly enhancing the local field. The field polarizes the molecules adsorbed on particles. The scattered field produced by the adsorbed molecules gets enhanced by the same plasmon effect again. When the particles have periodic arrangement with certain wave number, then scattered signal can be detected as a space wave.

In section 3.2, we discuss the laser coupling to a surface plasma wave. In section 3.3, we study the surface enhanced Raman scattering of a surface plasma wave. The results are discussed in section 3.4.

### 3.2 Laser Driven Surface Plasma Wave

Consider a thin metal film (e.g., Ag or Au) of thickness ‘a’ deposited on a glass prism of refractive index  $n_g$  in the attenuated total reflection configuration (cf. Fig. 3.1). The region above the metal film ( $x > 0$ ) is free space. The effective permittivity of the metal at frequency  $\omega$  is

$$\varepsilon = \left( \varepsilon_L - \frac{\omega_p^2}{\omega^2} \right) + i \frac{\nu}{\omega} \frac{\omega_p^2}{\omega^2}, \quad (3.1)$$

where  $\varepsilon_L$  is the lattice permittivity,  $\omega_p$  is the plasma frequency and  $\nu$  is the electron phonon collision frequency.

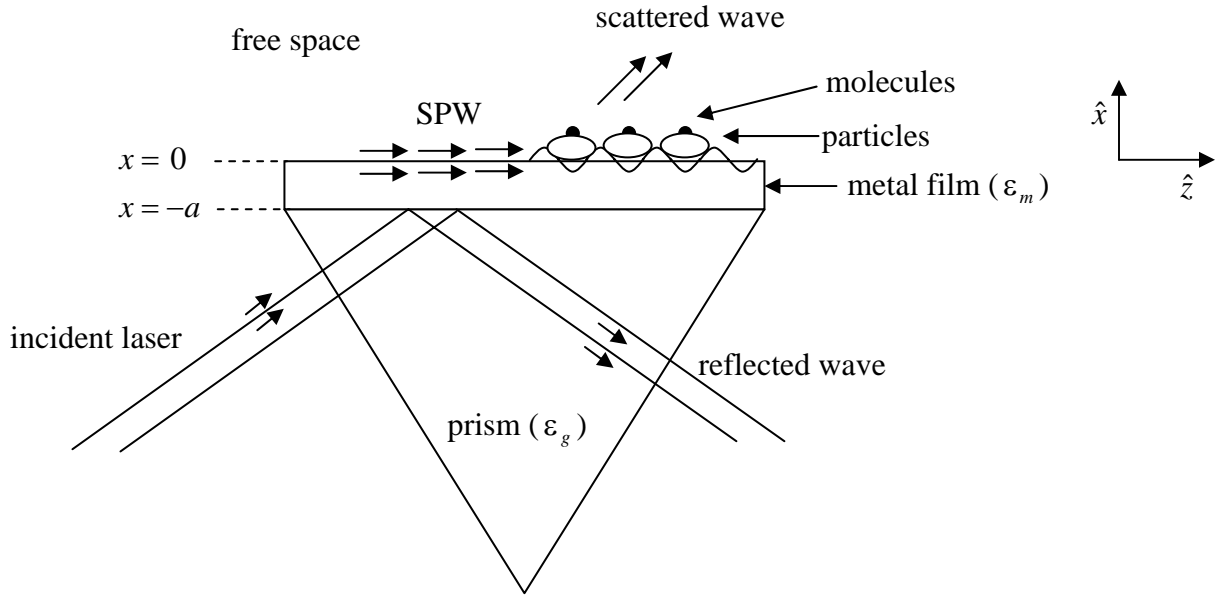


Fig. 3.1 Schematic of a prism coated with thin metal layer. The particles are attached on the metal surface. Surface plasma wave undergoes surface enhanced Raman scattering with molecules adsorbed on the particles. Scattered wave can be detected above the metal surface as a space wave.

A laser is incident on the glass metal interface at an angle of incidence  $\theta_i$ . Its electric field is uniform in  $y$  and has Gaussian amplitude profile of half width  $b'$  in the other transverse direction. The propagation vector lies in the  $x$ - $z$  plane. At  $x = -a$ , the  $z$ -component of the incident laser field is

$$E_z = A_o e^{-z^2/b^2} e^{-i(\omega t - k_z z)}, \quad (3.2)$$

where  $A_o = E_{oz}$ ,  $b = b' \sec \theta_i$ ,  $k_z = (\omega/c) \eta_g \sin \theta_i$ . The laser excites a surface plasma wave at the metal free space boundary. The field of the surface plasma wave in free space and metal region is

$$\vec{E}_s = \vec{A}_s(x) e^{-i(\omega t - k_s z)}, \quad (3.3)$$

$$\begin{aligned} \vec{A}_s &= A_{SO} \left( \hat{z} + \frac{ik_s}{\alpha_{1S}} \hat{x} \right) e^{-\alpha_{1S} x}, & \text{for } x > 0, \\ &= A_{SO} \left( \hat{z} - \frac{ik_s}{\alpha_{2S}} \hat{x} \right) e^{\alpha_{2S} x}, & \text{for } 0 > x > -a, \end{aligned}$$

where  $\alpha_{1S} = (k_z^2 - \omega^2/c^2)^{1/2}$ ,  $\alpha_{2S} = (k_z^2 - \omega^2 \varepsilon/c^2)^{1/2}$  and we have assumed  $\alpha_{2S} a > 1$ . Following Liu and Tripathi [10], the ratio of  $A_{SO}$  of the surface plasma wave to the amplitude of the incident laser is given by

$$\frac{A_{SO}}{A_o} = \frac{1}{2\sqrt{\pi}} T_{oo} (\sigma_1 + i\sigma_2) I, \quad (3.4)$$

where  $T_{oo} = T_o(x=0)$ ;  $T_o(x) = \frac{2i\psi_1}{1+i\psi_1} e^{\alpha_{2S} a} e^{-ik_s x}$ ;  $\psi_1 = n_g / \left| 1 + \varepsilon(1 - 1/n_g^2) \right|^{1/2}$ ;

$$I = \int_{-\infty}^{\infty} \frac{e^{-p^2} (p - \sigma_1 b/2 + i\sigma_2 b/2)}{(p - \sigma_1 b/2)^2 + \sigma_2^2 b^2/4} dp; \quad \psi_2 = \frac{2(1+i\psi_1)}{(1-i\psi_1)} \frac{\omega |\varepsilon|^{3/2} / c}{|1 + \varepsilon|^{1/2} (\varepsilon^2 - 1)}$$

$$p = (k_z - k_s) b/2; \quad \sigma_1 + i\sigma_2 = \psi_2 \exp(-2\alpha_{2S} a); \quad k_s = (\omega/c)(\varepsilon/(1 + \varepsilon))^{1/2}.$$

At  $x = 0$ ;  $z = 0$ , for  $\varepsilon = -4$ ,  $a\omega/c = 1$ ,  $b\omega/c = 100$ , we obtain  $|A_{SO}/A| = 6.456$ .

### 3.3 Surface Enhanced Raman Scattering

Consider spheroidal shaped particles, with molecules adsorbed on them, to be attached on the metal surface with  $2l_x, 2l_y, 2l_z$  as the lengths of the principal axes of the spheroid along the  $\hat{x}, \hat{y}, \hat{z}$  directions.

A SPW propagates along the surface with electric field in the x - z plane. It induces a field  $\vec{E}_{in}$  inside the particle [11],

$$E_{in,\beta} = \left[1 + (\varepsilon_p(\omega) - 1)A_\beta\right]^{-1} E_{S,\beta}(\omega), \quad \beta = x, y, z, \quad (3.5)$$

where,  $\varepsilon_p$  is the effective relative permittivity of the material of the particle given by Eq (3.1).  $A_\beta$  is a depolarization factor which depends on the shape of the particle. For different shaped particles, depolarization constant is different e.g. for a sphere,  $A_\beta = 1/3$ ,  $\beta = x, y, z$ ; for a prolate spheroid with  $x:y = 3:1$ ,  $A_x = 0.1087$ ;  $A_y = 0.4456$ . The induced field polarizes the particle. The magnitude of the dipole moment of the particle is  $p_{E,\beta}(\omega) = V \alpha_{E,\beta\beta}(\omega) E_{S,\beta}(\omega)$  where  $V$  is the particle volume,  $\alpha_E(\omega)$  is its susceptibility tensor,

$$\alpha_{E,\beta\beta}(\omega) = \frac{1}{4\pi} \frac{\varepsilon_p(\omega) - 1}{1 + [\varepsilon_p(\omega) - 1]A_\beta}. \quad (3.6)$$

The polarized particle induces a field at the molecule adsorbed on the tip of the spheroid,  $E_{ad,\beta}(\omega) = 2 p_{E,\beta}(\omega) / d_\beta^3$ , where  $d_\beta$  is the distance from the centre of particle to the molecule. This field polarizes the molecule with dipole moment,  $\mu_{mol,\beta} = \alpha_{R,\beta\beta} E_{ad,\beta}(\omega)$ , where  $\alpha_{R,\beta\beta}$  is the Raman molecular effective polarizability,

which gets modulated by the vibrational motion of nuclei. Thus the induced dipole moment contains a component oscillating at Stokes frequency  $\omega_R$ ,

$$\mu_{mol,\beta}(\omega_R) = 2V \alpha_{R,\beta\beta} \alpha_{E,\beta\beta}(\omega) E_{S,\beta} / d_\beta^3. \quad (3.7)$$

The molecular dipole moment induces a Raman shifted field in the spheroid,

$$E_{1,\beta}(\omega_R) = 2 \mu_{mol,\beta}(\omega_R) / d_\beta^3, \text{ giving rise to a dipole moment of the particle [12],}$$

$$p_\beta(\omega_R) = K \alpha_{R,\beta\beta} E_{S,\beta},$$

$$K_\beta = \left( \frac{V}{2\pi d_\beta^3} \right)^2 \left[ \frac{\varepsilon_P(\omega_R) - 1}{1 + [\varepsilon_P(\omega_R) - 1]A_\beta} \right] \left[ \frac{\varepsilon_P(\omega) - 1}{1 + [\varepsilon_P(\omega) - 1]A_\beta} \right]. \quad (3.8)$$

One may note that the resonance condition depends upon the value of depolarization constant,  $A_\beta$  and hence is different for particles of different shapes. For a sphere ( $A_\beta = 1/3$ ), this resonance occurs for  $\varepsilon_P \approx -2$  while for a 3:1 prolate spheroid it occurs at  $\varepsilon_P(\omega) \approx -8.1996$ . Silver can satisfy these conditions for a visible light. The imaginary part of  $\varepsilon$  is small, while the real part decreases from -2 to -20 over the range 350 – 700nm [13].

In order to obtain coherent Raman scattering we presume the particle surface density [14]

$$n = (N/2)(1 + \cos qz).$$

Hence the induced Raman shifted polarization is

$$\vec{P} = \frac{N}{2} (1 + \cos qz) \delta(x) (p_x \hat{x} + p_y \hat{y} + p_z \hat{z}), \quad (3.9)$$

where  $q$  is the ripple wave number of the regularly arranged particles.  $N$  is the number of particles per unit area.  $\vec{p}$  is the dipole moment of the particle. For a specific shape of particles and at a given laser frequency  $p_z$  may be taken to be much bigger than  $p_x, p_y$ .

The electric and magnetic fields of the Raman scattered wave  $\vec{E}_R$  and  $\vec{H}_R$  are governed by the Maxwell's equations,

$$\nabla \times \vec{E}_R = \frac{i\omega_R}{c} \vec{H}_R, \quad (3.10)$$

$$\nabla \times \vec{H}_R = \frac{4\pi}{c} \vec{J} - \frac{i\omega_R}{c} (\vec{E}_R + 4\pi \vec{P}). \quad (3.11)$$

Taking the curl of Eq. (3.10) and using Eq. (3.11), we obtain

$$\nabla^2 \vec{E}_R - \nabla(\nabla \cdot \vec{E}_R) + \frac{\omega_R^2}{c^2} \epsilon' \vec{E}_R = -\frac{\omega_R^2}{c^2} 4\pi \vec{P}, \quad (3.12)$$

where  $\omega_R$  is the Raman frequency of the signal,  $\vec{P}$  is the induced Raman shifted polarization, and  $\epsilon'=1$  in free space and  $\epsilon'=\epsilon$  in the metal.

From Eq. (3.12), x-variation of field  $E_z$  can be written as

$$\frac{\partial^2 E_{R,z}}{\partial x^2} + \frac{\omega_R^2}{c^2} \epsilon' E_{R,z} - ik_R \frac{\partial E_{R,x}}{\partial x} = -\frac{2\pi N\omega_R^2}{c^2} \delta(x) p_z(\omega_R), \quad (3.13)$$

where  $k_R = k_S - q$ ,  $\omega_R = \omega - \omega_m$ , and  $\omega_m$  is the vibrational frequency of the molecule.

Also, the same equation is valid for x-component with RHS equal to zero. The solutions of Eq. (3.13) in metal and free space regions are

$$\vec{E}_R = A_{R1} \left[ \hat{z} - \hat{x} \left( \frac{k_R}{k_{R1}} \right) \right] e^{ik_{R1}x} e^{-i(\omega_R t - k_R z)}, \quad x > 0,$$

$$\vec{E}_R = A_{R1} \left( \hat{z} - \hat{x} \frac{i k_R}{k_{R2}} \right) e^{k_{R2} x} e^{-i(\omega_R t - k_R z)}, \quad x < 0, \quad (3.14)$$

where  $k_{R1} = (\omega_R^2 / c^2 - k_R^2)^{1/2}$ ;  $k_{R2} = (k_R^2 - \varepsilon \omega_R^2 / c^2)^{1/2}$  and we have used the continuity of  $E_{R,z}$  across the metal-vacuum interface. For  $\omega_R^2 / c^2 > k_R^2$ , the scattered signal can be detected as space wave. For  $\varepsilon = -4$ , this provides  $q > 0.155 \omega_R / c$ .

The angle  $\theta_R$  which the Raman scattered wave makes with the surface normal is given by

$$\cot \theta_R = \frac{k_{R1}}{k_R},$$

$$= \left[ \frac{(1 - (k_S c / \omega_R - q c / \omega_R))^{1/2}}{(k_S c / \omega_R - q c / \omega_R)} \right]. \quad (3.15)$$

We have plotted  $\theta_R$  versus normalized wave number,  $q c / \omega_R$  for  $\varepsilon = -4$  in Fig. 3.2. One may note that  $\theta_R$  decreases monotonically with the particle periodicity wave number. When the wave number  $q$  becomes equal to SPW wave number, scattering is in perpendicular direction from the metal surface.

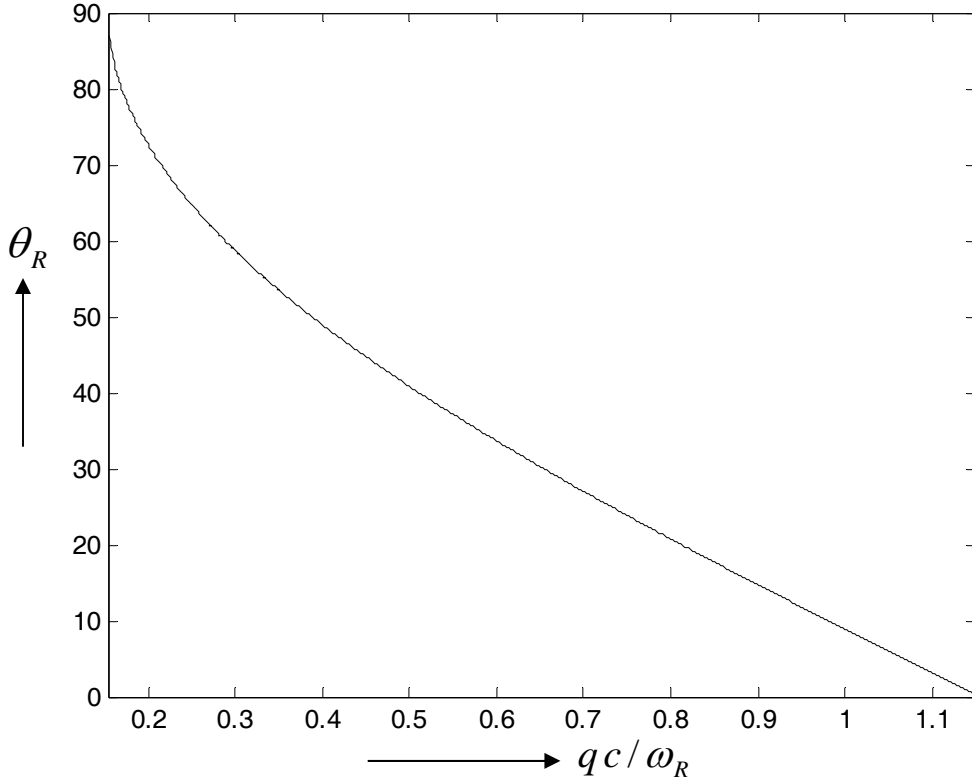


Fig. 3.2 Variation of the angle,  $\theta_R$  (in degrees), which the scattered wave makes with the surface normal versus normalized wave number  $q\omega_R/c$  of regularly arranged particles for  $\varepsilon = -4$ .

The boundary conditions on the derivative of field  $E_{R,z}$  at  $x=0$  may be obtained by integrating equation (3.13) from  $0^-$  to  $0^+$

$$\left. \frac{\partial E_{R,z}}{\partial x} \right|_{0^-}^{0^+} - ik_R E_{R,x} \Big|_{0^-}^{0^+} = -2\pi N \frac{\omega_R^2}{c^2} p_z(\omega_R), \quad (3.16)$$

$$A_{R1} = -2\pi N \frac{2\pi N p_z}{i/k_{R1} - \varepsilon/k_{R2}}. \quad (3.17)$$

The intensity of the Raman shifted signal is

$$I_R = \frac{c}{8\pi} |A_{R1}|^2 \frac{1}{\cos^2 \theta_R}. \quad (3.18)$$

The ratio of radiated Raman intensity to the incident laser intensity is

$$\frac{I_R}{I_o} = \frac{|A_{R1}|^2 \cos^2 \theta_i}{|A_o|^2 \cos^2 \theta_R}. \quad (3.19)$$

The field enhancement is strongly influenced by the enhancement factor  $K$ , which can be determined from Eq. (3.8). We consider isolated spheroidal shaped particles of size  $16\text{ nm}$  with Fullerine  $C_{60}$  molecules adsorbed at the tip of the axis along which SPW field is applied. For isolated Fullerine molecule, effective polarizability is  $\alpha_R = 77.5 \times 10^{-24} \text{ cm}^3$  and the highest mode of vibration appears at [15, 16]  $45 \text{ cm}^{-1}$ . If we choose incident laser to give rise to a surface plasma wave of wavelength  $588.7 \text{ nm}$ , then for a silver sphere ( $n \approx 5.87 \times 10^{22} \text{ cm}^{-3}$ ), enhancement factor  $|K_z|$  comes out to be  $4.02 \times 10^4$ . The ratio of amplitude of surface plasma wave to the incident laser can be obtained from Eq. (3.4). For  $a\omega/c=1$ ,  $b\omega/c=100$  and  $\varepsilon=-4$ , we have  $|A_{so}/A_o|=6.456$ .  $N$  depends upon particle size and should be less than  $1/4r^2$  for isolated spheroid to be attached on metal surface, where  $r$  is the particle size. We have taken  $N=8 \times 10^{10} \text{ cm}^{-2}$ . For these parameters, we have plotted the ratio of Raman scattered intensity to incident laser intensity as a function of angle  $\theta_R$  in Fig 3.3. The scattered power increases monotonically as the scattering direction approaches the surface. For a fixed value of the Raman scattering angle  $\theta_R = 45^\circ$ ,  $I_R/I_O$  comes out to be 0.835.

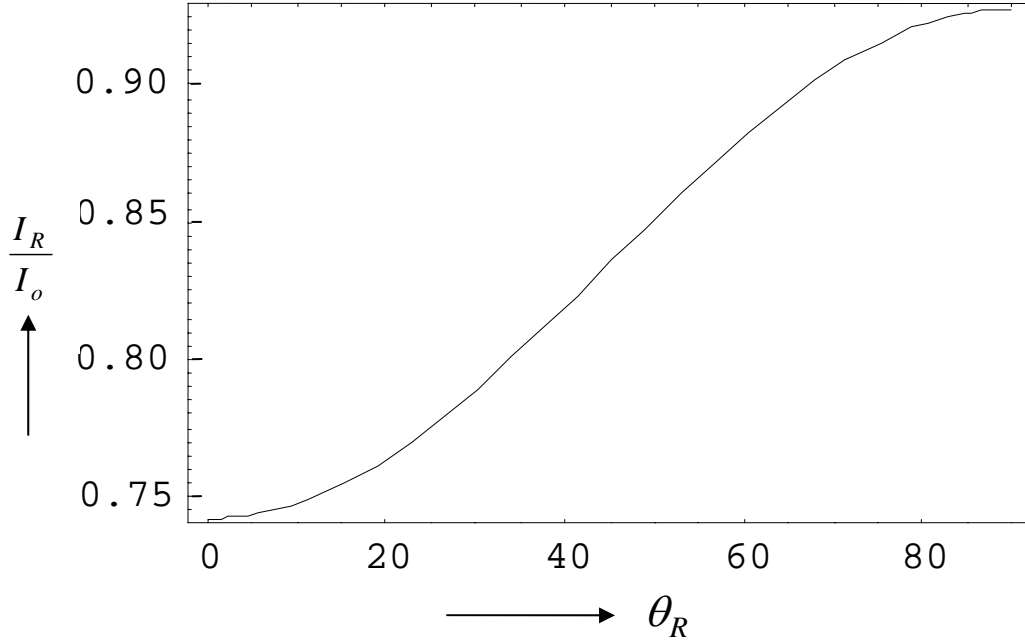


Fig. 3.3 Variation of ratio of intensities of the Raman scattered wave to that of the incident laser  $I_R / I_o$  as a function of scattering angle  $\theta_R$  (in degrees) with respect to surface normal. The parameters are:  $\alpha_R = 77.5 \times 10^{-24} \text{ cm}^3$ ,  $\omega_o = 3.2011 \times 10^{15} \text{ rad/s}$ ,  $N_o = 8 \times 10^{10} \text{ cm}^{-2}$ ,  $\omega_m = 8.4823 \times 10^{12} \text{ rad/sec}$ ,  $a\omega/c = 1$ ,  $b\omega/c = 100$ ,  $\varepsilon = -4$ .

### 3.4 Discussion

Surface enhanced Raman scattering of a surface plasma wave, with molecules adsorbed on metallic particles, is facilitated by the resonant field enhancement, caused by the collective behavior of free electrons of metallic particles. Enhancement factor depends upon the shape, free electron density and dielectric constant of the particles, besides the frequency of the incident laser. If the particles have a distribution in shape, then for a given laser wavelength only resonantly particles of a particular shape will resonantly contribute for which  $A_\beta = 1/(1 - \varepsilon_P(\omega))$ , hence the SERS enhancement factor would be reduced. Surface enhanced Raman scattering from laser driven surface plasma

wave has an additional advantage over the conventional SERS, as SPW field is one order of magnitude higher than the laser field, hence the overall enhancement in SERS is bigger.

When metallic particles are periodically arranged, with wave number  $q$  such that  $\omega_R > (k_S - q)c$ , where  $\omega_R$  is the frequency of the scattered signal and  $k_S$  is the wave number of surface plasma wave, the scattered wave can be detected as a space wave. The direction of propagation of scattered signal  $\theta_R$  with respect to surface normal depends on wave number  $q$ . Also intensity of Raman scattered signal varies with  $\theta_R$ .  $\theta_R$  decreases monotonically with  $q$ , whereas  $I_R/I_O$  increases with  $\theta_R$ . For a fixed value of the Raman scattering angle  $\theta_R = 45^\circ$ , we have calculated the ratio of intensities of the Raman scattered wave to that of the incident laser  $I_R/I_O$  for metallic particles of size  $16\text{ nm}$  with isolated Fullerene molecule adsorbed at its tip ( $\alpha_R = 77.5 \times 10^{-24} \text{ cm}^3$ ,  $\omega_o = 3.2011 \times 10^{15} \text{ rad/s}$ ,  $N = 8 \times 10^{10} \text{ cm}^{-2}$ ,  $\omega_m = 8.4823 \times 10^{12} \text{ rad/sec}$ ,  $a\omega/c = 1$ ,  $b\omega/c = 100$ ,  $\varepsilon = -4$ ). This comes out to be 0.835.

## References

1. M. Moskovits, *Rev. Mod. Phys.* **57**, 783 (1985).
2. M. Moskovits, *J. Chem. Phys.* **69**, 4159 (1978).
3. Tuan Vo-Dinh, Leonardo R. Allain, and David L. Stokes, *J. Raman Spectrosc.* **33**, 511 (2002).
4. C. R. Yonzon, C. L. Haynes, X. Zhang, J. T. J. Walsh, and R. P. Van Duyne, *Anal. Chem.* **76**, 78 (2004).
5. Fei Yan, Musundi B. Wabuyele, Guy Griffin, Arpad A. Vass, and Tuan Vo-Dinh, *IEEE Sensors J.* **5**, 665 (2005).
6. K. Kneipp, Y. Wang, H. Kneipp, L. T. Perelman, I. Itzkan, R. Dasari, M. S. Feld, *Phys. Rev. Lett.* **78**, 1667 (1997).
7. David L. Stokes, Tuan Vo-Dinh, *Sens. Actuators B* **69**, 28 (2000).
8. B. Mizaikoff, *Water Sci. Technol.* **47**, 35 (2003).
9. J.-F. Masson, K. Hamersky, S. Beaudoin, and K.S. Booksh, Brian M. Cullum ed., *Proc. SPIE 5261*, 123-134 (2004).
10. C. S. Liu, V. K. Tripathi, *IEEE Trans. Plasma Sci.* **28**, 353 (2000).
11. C. J. F. Bottcher, "Theory of Electric Polarization," *Am. Elsevier* **1**, 79 (1973).
12. P. L. Liao, J. G. Bergman, D. S. Chemla, A. Wokaun, J. Melngailis, A. M. Hawryluk, and N. P. Economou, *Chem. Phys. Lett.* **82**, 355 (1981).
13. P. B. Johnson and R. W. Christy, *Phys. Rev. B* **6**, 4370 (1972).
14. C. S. Liu and V. K. Tripathi, *IEEE J. Quantum Electron.* **34**, 1503 (1998).
15. X.-P. Li, J. P. Lu, R. M. Martin, *Phys. Rev. B* **46**, 4301 (1992).

16. Lasse Jensen, Per-Olof Astrand, Anders Osted, Jacob Kongsted, and Kurt V. Mikkelsen, *J. Chem. Phys.* **116**, 4001 (2002).

## Chapter 4

# ELECTRON ACCELERATION BY SURFACE PLASMA WAVES IN A DOUBLE METAL SURFACE STRUCTURE

### 4.1 Introduction

The acceleration of electrons by waves has been a subject of considerable interest because of its numerous applications. Laser based acceleration [1-7] schemes have been vigorously used to obtain electron energies approaching a GeV. Many applications require electron beams of moderately relativistic energies. In last few years, significant work has been reported on electron acceleration by surface plasma waves [8-13]. Surface plasma waves are localized to metal-free space interface and can be excited using a p-polarized laser [14-19]. Experiments show that the surface plasma waves are effective for accelerating electrons of low energy. Using the Kretschmann configuration [20, 21] for the SPW coupling, Zawadzka *et al.* [8, 9] have observed energetic electrons of energies  $\sim 400$  eV for laser intensity of  $10^{13}$  W/cm<sup>2</sup>. Irvine *et al.* [12, 13] have also demonstrated similar acceleration in their experiments. The acceleration energies are comparable to ponderomotive energies due to the surface plasma wave and electrons move much slower than the phase velocity of the surface wave. Kalmykov *et al.* [22] have studied SPW excitation on two parallel plane silicon carbide films separated by a vacuum region and discussed its potential for electron acceleration. Steinhauer *et al.* [23] have developed an elegant analytical formalism for surface wave propagation over two parallel conducting planes and on the inner boundary of a hollow cylinder. They have discussed its potential

for electron acceleration. However detailed analytical treatments of electron acceleration have not been given.

In this chapter, we propose a scheme of electron acceleration that employs resonant interaction of electrons with a surface plasma wave. This scheme can be useful in accelerating electrons to higher energies with the control in their trajectories. We employ a configuration of two parallel surfaces separated by a vacuum region. The configuration supports a surface plasma wave that propagates parallel to the metal surfaces with amplitude maxima on the two surfaces and a minimum in the middle. The surface wave has a finite axial electric field in the middle but the transverse ponderomotive force due to it vanishes, hence electrons placed in the middle can stay there for a long distance. When their axial velocities are comparable to the phase velocity of the surface wave they can gain large energies from the wave. We also develop formalism for electron acceleration by a SPW on a single metal surface and explain the experimental results of Zawadzka et al. [8].

In section 4.2, we derive the dispersion relation of a surface plasma wave in a double metal surface configuration. In section 4.3, we study electron acceleration by such a surface plasma wave. In section 4.4, electron acceleration by a surface plasma wave over a single metal surface is studied. The results are discussed in section 4.5.

## **4.2 Surface plasma wave in a double metal surface configuration**

Consider two parallel metal half spaces  $x < -a/2$  and  $x > a/2$ , separated by a thin vacuum region  $(-a/2 < x < a/2)$  (Fig. 4.1). The effective permittivity of metal at frequency  $\omega$  is

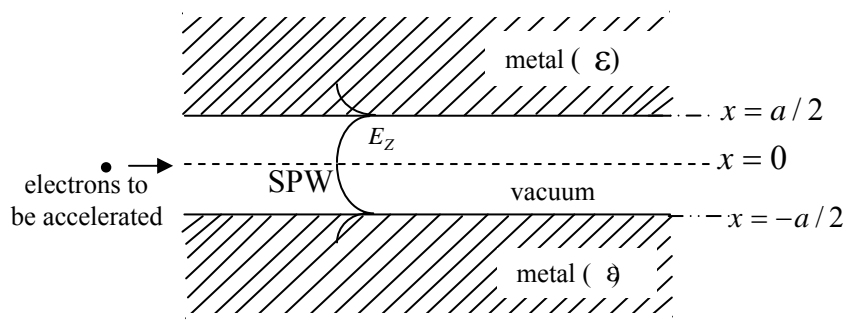


Fig. 4.1(a) Schematic of two metal surface plasmon structure. Two parallel metal surfaces at  $x = -a/2$  and  $x = a/2$  are separated by free space. The electrons are injected in the centre of the free space region. The continuous surface plasma wave field accelerates them without diverging.

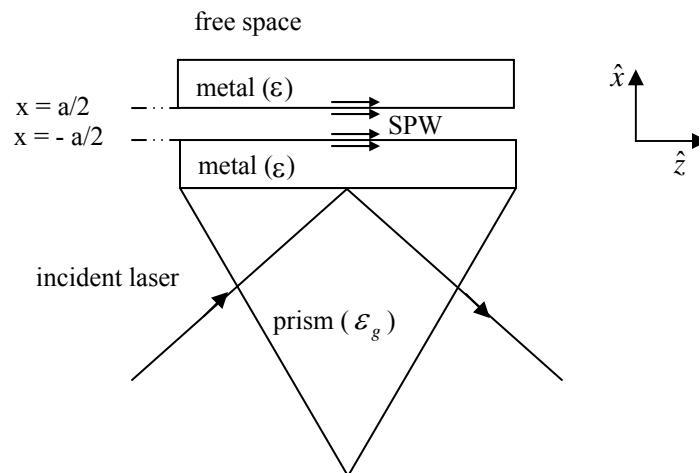


Fig. 4.1(b) The excitation of surface plasma wave in attenuated total reflection (ATR) configuration.

$$\varepsilon = \left( \varepsilon_L - \frac{\omega_p^2}{\omega^2} \right), \quad (4.1)$$

where  $\varepsilon_L$  is the lattice permittivity and  $\omega_p$  is the plasma frequency. A surface plasma wave propagates through the configuration with  $t, z$  variation as  $\exp[-i(\omega t - k_z z)]$ . The field variations are governed by Maxwell's third and fourth equations,

$$\nabla \times \vec{E} = -\frac{1}{c} \frac{\partial \vec{H}}{\partial t},$$

$$\nabla \times \vec{H} = \frac{\varepsilon'}{c} \frac{\partial \vec{E}}{\partial t},$$

where  $\varepsilon' = 1$  for  $-a/2 < x < a/2$ ,

$$= \varepsilon \text{ for } x > a/2 \text{ and } x < -a/2.$$

Taking curl of Maxwell's third equation and using fourth, we obtain wave equation. The wave equation governing  $E_z$  in three media is given by

$$\frac{\partial^2 E_z}{\partial x^2} - \left( k_z^2 - \frac{\omega^2}{c^2} \varepsilon' \right) E_z = 0, \quad (4.2)$$

The well behaved solution of Eq. (4.2), satisfying  $\nabla \cdot \vec{E} = 0$  in each region is

$$\begin{aligned} \vec{E} &= A \left( \hat{z} + \hat{x} \frac{ik_z}{\alpha_1} \right) e^{-\alpha_1 x}, & x > a/2, \\ &= \left[ A_1 \left( \hat{z} - \hat{x} \frac{ik_z}{\alpha_2} \right) e^{\alpha_2 x} + A_2 \left( \hat{z} + \hat{x} \frac{ik_z}{\alpha_2} \right) e^{-\alpha_2 x} \right], & -a/2 < x < a/2, \\ &= A_3 \left( \hat{z} - \hat{x} \frac{ik_z}{\alpha_1} \right) e^{\alpha_1 x}, & x < -a/2, \end{aligned} \quad (4.3)$$

where  $\alpha_1 = (k_z^2 - \omega^2 \varepsilon / c^2)^{1/2}$ ,  $\alpha_2 = (k_z^2 - \omega^2 / c^2)^{1/2}$ . Applying conditions of continuity of  $E_z$  and  $\varepsilon' E_x$  at  $x = a/2$  and  $x = -a/2$ , we get

$$A_1 e^{\alpha_2 a/2} + A_2 e^{-\alpha_2 a/2} = A e^{-\alpha_1 a/2}, \quad (4.4)$$

$$A_1 e^{\alpha_2 a/2} - A_2 e^{-\alpha_2 a/2} = -A \left( \frac{\varepsilon \alpha_2}{\alpha_1} \right) e^{-\alpha_1 a/2}, \quad (4.5)$$

$$A_1 e^{-\alpha_2 a/2} + A_2 e^{\alpha_2 a/2} = A_3 e^{-\alpha_1 a/2}, \quad (4.6)$$

$$A_1 e^{-\alpha_2 a/2} - A_2 e^{\alpha_2 a/2} = A_3 \left( \frac{\varepsilon \alpha_2}{\alpha_1} \right) e^{-\alpha_1 a/2}. \quad (4.7)$$

Solving these equations, we obtain the dispersion relation

$$\frac{\alpha_2^2}{\alpha_1^2} = \left| \frac{1 - e^{\alpha_2 a}}{1 + e^{\alpha_2 a}} \right|^2 \frac{1}{|\varepsilon|^2}. \quad (4.8)$$

Using dimensionless quantities:  $q = k_z c / \omega_p$ ,  $\Omega = \omega / \omega_p$ ,  $a' = a \omega_p / c$ , we normalize Eq. (4.8) and plot normalized frequency  $\Omega$  versus normalized wavenumber  $q$  in Fig. 4.2 for the mode that has  $E_x$  symmetric about the  $x = 0$  ( $A_1 = -A_2$ ). The parameters are:  $\varepsilon_L = 1$ ,  $a \omega_p / c = 100$ .

One may note that as the wave number increases, frequency increases and then saturates at higher wave numbers. For higher value of wave number  $q$ , the behavior of the curve is same as that of single metal surface structure. However in double metal surface, at lower value of wave number phase velocity is smaller and is easy to achieve wave-electron synchronism at low electron energies. The  $E_z$  field of the SPW has minimum at  $x = 0$  but its amplitude is not very significantly different from the one at  $x = a/2, -a/2$  when  $\alpha_2 a < 1$ .

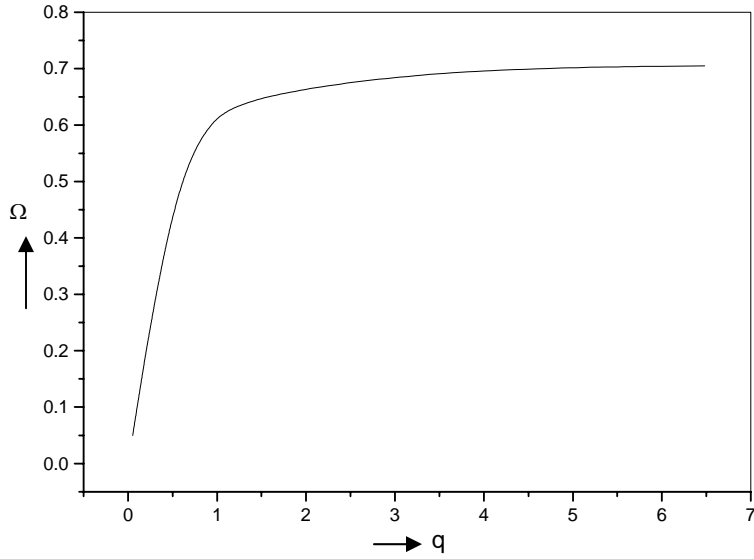


Fig. 4.2 Variation of the normalized frequency  $\Omega = \omega / \omega_p$  versus normalized wave number  $q = kc / \omega_p$  of the surface plasma wave in double metal surface structure. The parameters are:  $\varepsilon_L = 1$ ,  $a\omega_p / c = 100$ .

### 4.3 Electron acceleration in double surface configuration

Let an electron be injected into the middle of the vacuum region bounded by two metal surfaces (Fig. 4.1), in the presence of large amplitude surface plasma wave. The electron response is governed by the equation of motion

$$\frac{d\vec{p}}{dt} = -e(\vec{E} + \vec{v} \times \vec{B}), \quad (4.9)$$

where  $-e$ ,  $m$  are the electronic charge and mass and  $\vec{B} = (\nabla \times \vec{E}) / i\omega$ . Expressing  $d/dt = v_z d/dz$ , the x and z components of Eq. (4.9) can be written as

$$\frac{dp_x}{dz} = \left[ \frac{em\gamma}{p_z} \left( \frac{k_z}{\alpha_2} \right) + \frac{e}{\omega} \left( \alpha_2 - \frac{k_z^2}{\alpha_2} \right) \right] (e^{\alpha_2 x} + e^{-\alpha_2 x}) A_1' \sin(\omega t - kz + \phi), \quad (4.10)$$

$$\frac{dp_z}{dz} = \left[ -\frac{em\gamma}{p_z} (e^{\alpha_2 x} - e^{-\alpha_2 x}) \cos(\omega t - kz + \phi) + \frac{e}{\omega} \frac{p_x}{p_z} \left( -\alpha_2 + \frac{k_z^2}{\alpha_2} \right) (e^{\alpha_2 x} + e^{-\alpha_2 x}) \sin(\omega t - kz + \phi) \right] A_1', \quad (4.11)$$

where  $A_1' = A_1 e^{-(t-z/v_g)^2/2\tau_L^2}$ ,  $\gamma = (1 + p^2/m^2c^2)^{1/2}$ ,  $v_g$  is the group velocity of the surface plasma wave,  $\phi$  is the initial phase of the wave and we have considered a Gaussian temporal profile of the SPW amplitude with  $\tau_L$  pulse width. These equations are supplemented with

$$\frac{dx}{dz} = \frac{p_x}{p_z}, \quad (4.12)$$

$$\frac{dt}{dz} = \frac{\gamma m}{p_z}. \quad (4.13)$$

We introduce dimensionless quantities:  $A_1'' \rightarrow eA_1'/m\omega_p c$ ,  $X \rightarrow \omega_p x/c$ ,  $Z \rightarrow \omega_p z/c$ ,  $P_x \rightarrow p_x/(mc)$ ,  $P_z \rightarrow p_z/(mc)$ ,  $T \rightarrow \omega_p t$ ,  $\Omega = \omega/\omega_p$ ,  $q = k_z c/\omega_p$ ,  $v_g' = v_g/c$ . In terms of these, Eqs. (4.10)-(4.13) can be written as

$$\frac{\partial P_x}{\partial Z} = \left[ \frac{\gamma}{P_z} \left( \frac{q}{\alpha_2'} \right) + \frac{1}{\Omega} \left( \alpha_2' - \frac{q^2}{\alpha_2'} \right) \right] (e^{\alpha_2' X} + e^{-\alpha_2' X}) A_1'' \sin(\Omega T - qZ + \phi), \quad (4.14)$$

$$\frac{\partial P_z}{\partial Z} = \left[ -\frac{\gamma}{P_z} (e^{\alpha_2' X} - e^{-\alpha_2' X}) \cos(\Omega T - qZ + \phi) + \frac{1}{\Omega} \frac{P_x}{P_z} \left( -\alpha_2' + \frac{q^2}{\alpha_2'} \right) (e^{\alpha_2' X} + e^{-\alpha_2' X}) \sin(\Omega T - qZ + \phi) \right] A_1'', \quad (4.15)$$

$$\frac{dX}{dZ} = \frac{P_x}{P_z}, \quad (4.16)$$

$$\frac{dT}{dZ} = \frac{\gamma}{P_z}. \quad (4.17)$$

We solve Eqs. (4.14)-(4.17) numerically for electron trajectory and energy gain. In Figs. 4.3, 4.4 and 4.5, we have plotted kinetic energy (in keV) gained by the electrons versus normalized distance  $z\omega_p/c$  for different values of laser frequency, for the parameters:  $P_x(0) = 0.0$ ,  $P_z(0) = 0.09$ ,  $x(0) = 0.0$ ,  $t(0) = 0.0$ ,  $\tau_L\omega_p = 200$ ,  $\varepsilon_L = 1$ ,  $\phi = \pi/2$ ,  $E_{sp} = 1.2 \times 10^{11} \text{ V/m}$ ,  $\omega_p = 1.3 \times 10^{16} \text{ rad/sec}$ . Here we have taken width of vacuum gap  $a\omega_p/c = 100$  i.e.  $a = 231 \mu\text{m}$ . In Fig. 4.3, we obtain electron acceleration of 12.7 for laser frequency  $\omega/\omega_p = 0.06$  while in Fig. 4.4 and 4.5, we obtain the electron acceleration of 8.8 keV, 4.48 keV for  $\omega/\omega_p = 0.087$  and  $\omega/\omega_p = 0.1$  respectively. We note that with the increase in the frequency of the incident laser, electron acceleration decreases. This appears due to the decrease in the phase velocity of the SPW with decreasing  $|\varepsilon|$ . The SPW can accelerate electrons to the velocities of the order of phase velocity.

The trajectory of the accelerated electron, launched in the centre of vacuum region has been shown by the curve (b) in Fig. 4.7. It turns out to be a straight line for  $x = -a/2$ , i.e., the electron moves in z-direction without deviation from its path. The upper curve i.e. (a) is the trajectory for the accelerated electron in case of single metal surface discussed in next section.

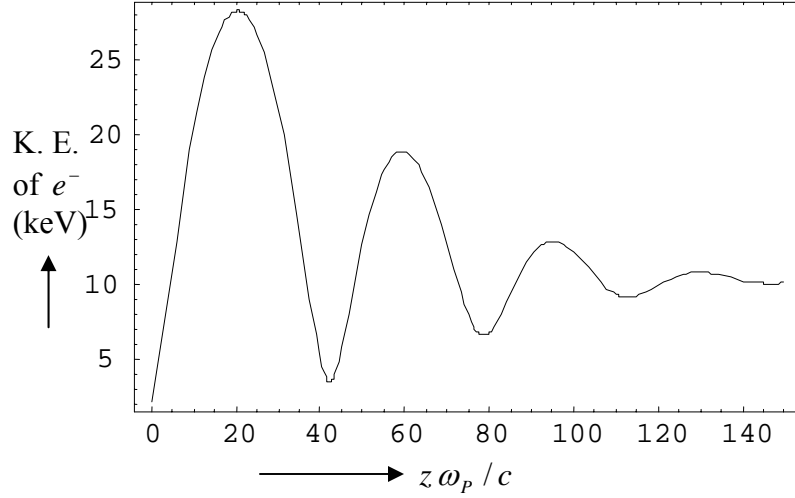


Fig 4.3 Variation of kinetic energy of the accelerated electron  $(\gamma - 1)mc^2$  (in keV) versus normalized distance  $z\omega_p/c$  in double metal surface. The parameters are:  $P_x(0) = 0.0$ ,  $P_z(0) = 0.09$ ,  $x(0) = 0.0$ ,  $t(0) = 0.0$ ,  $\tau_L\omega_p = 200$ ,  $\varepsilon_L = 1$ ,  $\phi = \pi/2$ ,  $E_{sp} = 1.2 \times 10^{11} V/m$ ,  $\omega_p = 1.3 \times 10^{16} rad/sec$  and  $\omega/\omega_p = 0.06$ ,  $a\omega_p/c = 100$ .

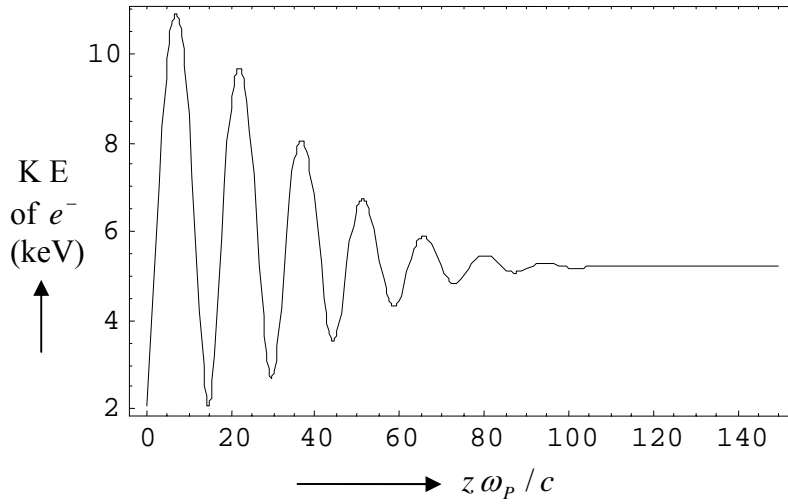


Fig 4.4 Variation of Kinetic energy of the accelerated electron  $(\gamma - 1)mc^2$  (in keV) versus normalized distance  $z\omega_p/c$  in double metal surface. The parameters are:  $P_x(0) = 0.0$ ,  $P_z(0) = 0.09$ ,  $x(0) = 0.0$ ,  $t(0) = 0.0$ ,  $\tau_L\omega_p = 200$ ,  $\varepsilon_L = 1$ ,  $\phi = \pi/2$ ,  $E_{sp} = 1.2 \times 10^{11} V/m$ ,  $\omega_p = 1.3 \times 10^{16} rad/sec$  and  $\omega/\omega_p = 0.087$ ,  $a\omega_p/c = 100$ .

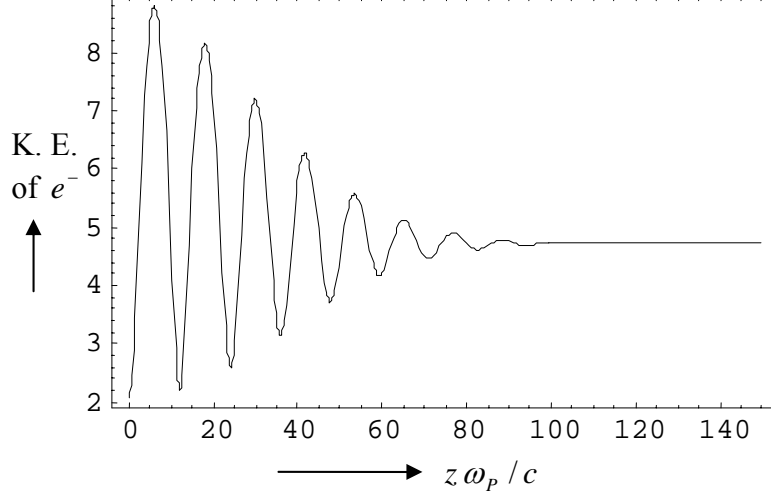


Fig 4.5 Variation of Kinetic energy of the accelerated electron  $(\gamma - 1)mc^2$  (in keV) versus normalized distance  $z\omega_p/c$  in double metal surface. The parameters are:  $P_x(0) = 0.0$ ,  $P_z(0) = 0.09$ ,  $x(0) = 0.0$ ,  $t(0) = 0.0$ ,  $\tau_L\omega_p = 200$ ,  $\epsilon_L = 1$ ,  $\phi = \pi/2$ ,  $E_{Sp} = 1.2 \times 10^{11} \text{ V/m}$ ,  $\omega_p = 1.3 \times 10^{16} \text{ rad/sec}$  and  $\omega/\omega_p = 0.1$ ,  $a\omega_p/c = 100$ .

#### 4.4 Electron acceleration by a surface plasma wave over a single metal surface

Consider an interface separating free space ( $x > 0$ ) and a metal ( $x < 0$ ). The effective permittivity of the metal is given by Eq. (4.1). A surface plasma wave propagates over the surface with [15]

$$\vec{E} = \left( \hat{z} + \hat{x} \frac{ik_z}{\alpha_1} \right) A e^{-\alpha_1 x} e^{-i(\omega t - k_z z)}, \quad \text{for } x > 0,$$

$$\vec{E} = \left( \hat{z} - \hat{x} \frac{ik_z}{\alpha_1} \right) A e^{+\alpha_2 x} e^{-i(\omega t - k_z z)}, \quad \text{for } x < 0.$$

$$k_z^2 = \frac{\omega^2}{c^2} \frac{\epsilon}{1 + \epsilon}, \quad (4.18)$$

where  $\alpha_1 = (k_z^2 - \omega_L^2 / c^2)^{1/2}$ ,  $\alpha_2 = (k_z^2 - \omega_L^2 \epsilon / c^2)^{1/2}$ , so chosen that  $\nabla \cdot \vec{E} = 0$  for both  $x < 0$  and  $x > 0$ . The magnetic field of the wave can be obtained as  $\vec{B} = (\nabla \times \vec{E}) / i\omega$ .

We launch an electron beam parallel to the surface with initial velocity  $\vec{v}_0$ . Its response to the surface plasma wave is governed by the equation of motion

$$\frac{d\vec{p}}{dt} = -e(\vec{E} + \vec{v} \times \vec{B}), \quad (4.19)$$

where  $-e$ ,  $m$  are the electronic charge and mass and  $\vec{B} = (\nabla \times \vec{E}) / i\omega$ . Expressing  $d/dt = v_z d/dz$ , the x and z components alongwith supplementary equations can be written as

$$\frac{\partial p_x}{\partial z} = A \left[ -\frac{\gamma m e}{p_z} \left( \frac{k_z}{\alpha_1} \right) \sin(\omega t - k_z z + \phi) + \frac{e}{\omega} \left( \frac{k_z^2}{\alpha_1} - \alpha_1 \right) \sin(\omega t - k_z z + \phi) \right] e^{-\alpha_1 x}, \quad (4.20)$$

$$\frac{\partial p_z}{\partial z} = A \left[ -\frac{e m \gamma}{p_z} \cos(\omega t - k_z z + \phi) - \frac{e p_x}{\omega p_z} \left( \frac{k_z^2}{\alpha_1} - \alpha_1 \right) \sin(\omega t - k_z z + \phi) \right] e^{-\alpha_1 x}, \quad (4.21)$$

$$\frac{dx}{dz} = \frac{p_x}{p_z}, \quad (4.22)$$

$$\frac{dt}{dz} = \frac{\gamma m}{p_z}. \quad (4.23)$$

where  $\phi$  is the initial phase of the SPW. Equations (4.20)-(4.23) in dimensionless form can be written as

$$\frac{\partial P_x}{\partial Z} = A'' \left[ -\frac{\gamma}{P_z} \left( \frac{q}{\alpha_1'} \right) \sin(\Omega T - qZ + \phi) + \frac{1}{\Omega} \left( \frac{q^2}{\alpha_1'} - \alpha_1' \right) \sin(\Omega T - qZ + \phi) \right], \quad (4.24)$$

$$\frac{\partial P_z}{\partial Z} = A'' \left[ -\frac{\gamma}{P_z} \cos(\Omega T - qZ + \phi) - \frac{1}{\Omega} \frac{P_x}{P_z} \left( \frac{q^2}{\alpha_1'} - \alpha_1' \right) \sin(\Omega T - qZ + \phi) \right], \quad (4.25)$$

$$\frac{dX}{dZ} = \frac{P_X}{P_Z}, \quad (4.26)$$

$$\frac{dT}{dZ} = \frac{\gamma}{P_Z}. \quad (4.27)$$

where  $A'' = A' e^{-\alpha_1 X} e^{-(T-Z/v_g)^2/2\tau_L^2}$ , and  $X$ ,  $Z$  and  $\vec{P}$  are the same as defined above.

We have solved these equations numerically for following parameters:  $P_X(0) = 0.0$ ,  $P_Z(0) = 0.007$ ,  $X(0) = 1.0$ ,  $T(0) = 0.0$ ,  $\phi = \pi$ . We express the surface wave amplitude as  $|E_s| = \eta|E_L|$ , where  $|E_L|$  is the amplitude of the laser used to excite it in the ATR (attenuated total reflection) configuration and  $\eta$  is the field enhancement factor. Presuming laser energy conversion to the SPW as 50 %, enhancement factor comes out to be  $\eta \cong 3.2$  corresponds to the laser intensity of  $10^{13}$  W/cm<sup>2</sup>. We choose  $E_L = 2.9 \times 10^5$  V/cm. The results are displayed in Fig. 4.6 and 4.7. The maximum kinetic energy gain by the electrons comes out to be  $\sim 0.39$  KeV, which is close to the experimentally observed value of 0.4 keV by Zawadzka et al. [8]. In Fig. 4.7, curve (a) represents the electron trajectory for the above parameters. One may note that the electron move away from the metal surface as it gains energy.

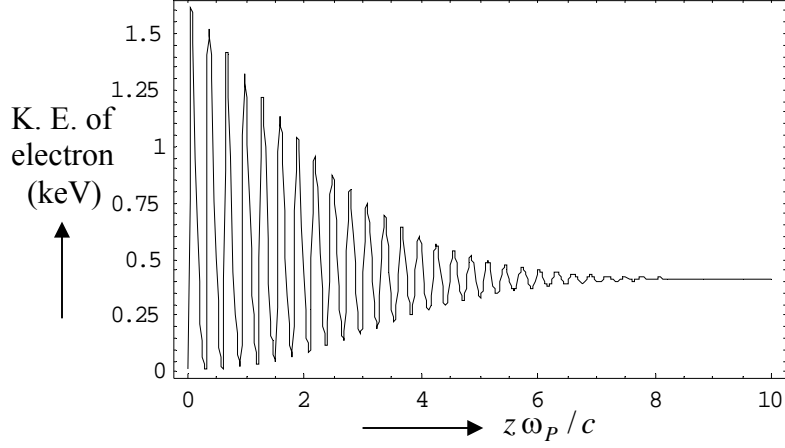


Fig 4.6 Variation of kinetic energy of the accelerated electron  $(\gamma - 1)mc^2$  versus normalized distance  $z\omega_p/c$  over the single metal surface. The parameters are:  $P_x(0) = 0.0$ ,  $P_z(0) = 0.007$ ,  $x(0) = 0.1$ ,  $t(0) = 0.0$ .  $\tau_L = 27 fs$ ,  $E_{SPW} = 10^6 V/cm$ ,  $\epsilon_L = 5$ ,  $\omega = 375 THz$ .  $\phi = \pi$ .

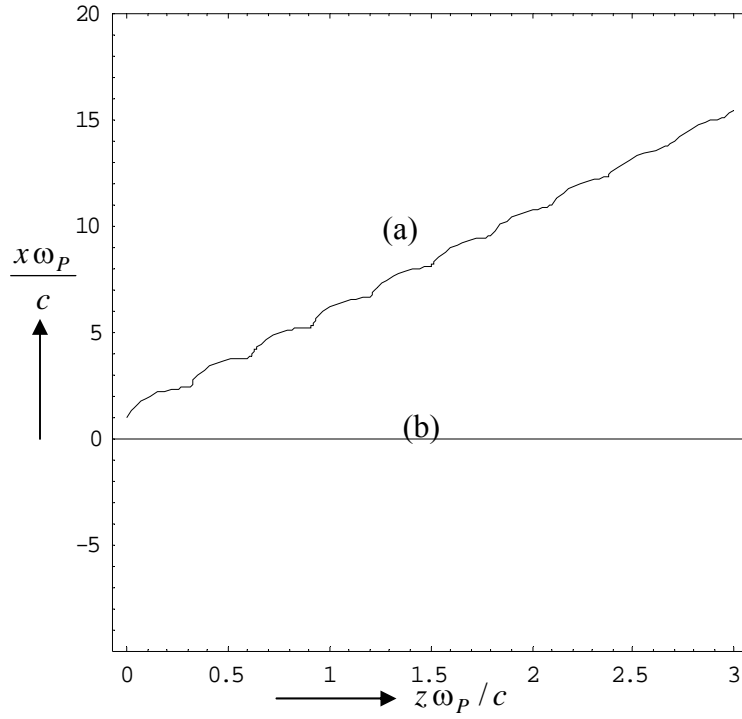


Fig 4.7 The trajectory of electron (normalized  $x$  versus normalized  $z$ ) in (a) single metal surface (for  $P_x(0) = 0.0$ ,  $P_z(0) = 0.007$ ,  $x(0) = 0.0$ ,  $t(0) = 0.0$ .  $\tau_L = 27 fs$ ,  $E_{SPW} = 10^6 V/cm$ ,  $\epsilon_L = 5$ ,  $\omega = 375 THz$ .  $\phi = \pi$ ) and (b) double metal surface configuration (for  $P_x(0) = 0.0$ ,  $P_z(0) = 0.09$ ,  $x(0) = 0.0$ ,  $t(0) = 0.0$ ,  $\tau_L\omega_p = 200$ ,  $\epsilon_L = 1$ ,  $\phi = \pi/2$ ,  $E_{SP} = 1.2 \times 10^{11} V/m$ ,  $\omega_p = 1.3 \times 10^{16} rad/sec$  and  $\omega/\omega_p = 0.1$ ,  $a\omega_p/c = 100$ ).

## 4.5 Discussion

Double metal surface configuration appears to have significant promise for accelerating electrons by a surface plasma wave upto tens of keV energy. Close to the surface wave cut-off frequency  $\omega_c \equiv \omega_p / (1 + \epsilon_L)^{1/2}$ , the phase velocity of surface plasma wave is small, hence energy gain is small. However at  $\omega \cong 0.8\omega_c - 0.9\omega_c$ , one can achieve electron energies in the 10 keV range with mildly relativistic laser intensities. For  $P_x(0) = 0.0$ ,  $P_z(0) = 0.09$ ,  $x(0) = 0.0$ ,  $t(0) = 0.0$ .  $\tau_L \omega_p = 200$ ,  $\epsilon_L = 1$ ,  $\phi = 90^\circ$ ,  $E_{sp} = 1.2 \times 10^{11} \text{ V/m}$ ,  $\omega_p = 1.3 \times 10^{16} \text{ rad/sec}$  and  $\omega/\omega_p = 0.06$  we obtain the electron acceleration of  $\sim 12.7 \text{ keV}$ .

In the case of a single metal surface, electron acceleration is limited by the transverse ponderomotive force induced displacement of electrons. Our model of ponderomotive acceleration of electrons explains the experimental results by Zawadzka et al. [8] at laser intensity of  $10^{13} \text{ W/cm}^2$ . We obtain the electron acceleration of 0.39 keV by surface plasmons excited by a laser of intensity  $10^{13} \text{ W/cm}^2$  over the single metal surface. However, in this case as the electron gains energy it moves away from the interface. When a vacuum region is bounded by two metal surfaces with surface plasma waves propagating at both the metal-vacuum interfaces then a symmetric SPW field is generated in the vacuum region. The electrons injected in the centre of vacuum region can be accelerated to higher energies with the control in their trajectory.

## References

1. S. Ya. Tochitsky, R. Narang, C. V. Filip, P. Musumeci, C. E. Clayton et al., Phys. Rev. Lett. **92**, 095004 (2004).
2. Y. Kitagawa, T. Matsumoto, T. Minamihata, K. Sawai, K. Matsuo et al., Phys. Rev. Lett. **68**, 48 (1992).
3. E. Esarey, P. Sprangle, and J. Krall, Phys. Rev. E **52**, 5443-5453 (1995).
4. B. Hafizi, A. Ting, E. Esarey, P. Sprangle, and J. Krall, Phys. Rev. E **55**, 5924 (1997).
5. T. Tajima and J. M. Dawson, Phys. Rev. Lett. **43**, 267 (1979).
6. V. Malka, S. Fritzler, E. Lefebvre, M.-M. Aleonard, F. Burgy et al., **98** Science, 1596 (2002).
7. M. I. K. Santala, Z. Najmudin, E. L. Clark, M. Tatarakis, K. Krushelnick, Phys. Rev. Lett. **86**, 1227 (2001).
8. J. Zawadzka, D. Jaroszynski, J. J. Carey, and K. Wynne, Appl. Phys. Lett. **79**, 2130 (2001).
9. J. Zawadzka, D. Jaroszynski, J. J. Carey, and K. Wynne, Nucl. Instrum. Methods Phys. Res. A **445**, 324 (2000).
10. J. Kupersztych, P. Monchicourt, and M. Raynaud, Phys. Rev. Lett. **86**, 5180 (2001).
11. J. Kupersztych, M. Raynaud, and C. Riconda, Phys. Plasmas **11**, 1669 (2004).
12. S. E. Irvine and A. Y. Elezzabi, Appl. Phys. Lett. **86**, 264102, (2005).
13. S. E. Irvine and A. Y. Elezzabi, Phys. Rev. A **73**, 013815 (2006).
14. A. Otto, Z. Phys. **216**, 398 (1968).

15. C. S. Liu and V. K. Tripathi, IEEE Trans. Plas. Sci. **28**, 353 (2000).
16. H. Raether, in Springer Tracts in Modern Physics. New York: Springer-Verlag 111 (1988).
17. D. B. Singh and V. K. Tripathi, J. Appl. Phys. **98**, 053708 (2005).
18. C. S. Liu, Gagan Kumar, and V. K. Tripathi, J. Appl. Phys. **100**, 013304 (2006).
19. A. Macchi, F. Cornolti, F. Pegoraro, T. V. Liseikina, H. Ruhl, and V. A. Vshivkov, Phys. Rev. Lett. **87**, 205004 (2001).
20. E. Kretschmann and H. Raether, Z. Naturforsch. A **23A**, 2135 (1968).
21. E. Kretschmann, Z. Phys. **241**, 313 (1971).
22. S. Kalmykov at el. Phil. Trans. R. Soc. A **364**, 725 (2006).
23. L. C. Steinhauer and W. D. Kimura, Phys Rev ST AB **6**, 061302 (2003).

## Chapter 5

# ANOMALOUS ABSORPTION OF SURFACE PLASMA WAVE BY PARTICLES ADSORBED ON METAL SURFACE

### 5.1 Introduction

Absorption of laser radiation at material surfaces has lately attracted much interest because of its relevance to material ablation [1-2] and other applications. Significant efforts have been made to achieve total absorption of electromagnetic radiation both theoretically and experimentally. The optical absorption is very poor for smooth metal surfaces because the high free electron density of metals renders effective plasma permittivity to be negative and surface re-radiates light energy in the surrounding medium. However, for the metallic particles, absorption of the electromagnetic waves could be significantly high when the wave frequency is close to the natural frequency of oscillations of the electron cloud. Infact, for metal surface having metallic particles over it, strong absorption and large enhancement in ablation yield has been reported [3]. Surface enhanced Raman scattering of light is also the consequence of this effect [4-7]. For spherical metallic nanoparticles local field enhancement factor has been observed up to 15 [8, 9]. The localized field results in strong collisional dissipation of light energy.

The total absorption of electromagnetic wave can be achieved through the excitation of surface plasma waves [10-13]. They may be excited over the metal surface either by the modification of metal surface in which periodic grating is formed over the metal surface [11] or the transformation of incident wave into evanescent wave [12, 14]. Bliokh et al. [15] have studied total absorption of microwaves by placing a sub-

wavelength grating in front of plasma surface. The absorption occurs due to the excitation of the SPW over the plasma surface. Vorobyev and Guo [16] also have experimentally observed total absorption of femtosecond laser due to surface modifications. He reported that, with higher number of laser pulses ( $>10000$ ), the surface microscale structures formation results in nearly 40% absorption of laser energy via the generation of surface electromagnetic waves.

In this chapter, we study the anomalous absorption of surface plasma waves over a metal surface having metallic nano-particles placed on it. The SPW induces a huge localized electric field inside the particles when the frequency of the incident laser is close to the frequency of space charge oscillations of the electron cloud. These electrons dissipate their energy via collisions in the particles. We have discussed the propagation of surface plasma waves and subsequently the absorption of these waves by metallic particles over the metal surface. The mathematical formalism is similar to the problem of laser absorption under similar configuration by Ahmad and Tripathi [3], however, the natures of laser and SPW are totally different.

In section 5.2, we have discussed the propagation of surface plasma waves. In section 5.3, we have discussed the absorption of surface plasma waves by metallic particles adsorbed over the metal surface. In section 5.4, we discuss the results.

## **5.2 Surface plasma wave propagation**

Consider a metal free-space interface ( $x=0$ ) with metal occupying half space ( $x<0$ ) and free space is  $x>0$  (cf. Fig. 5.1). The metal is having spherical particles of size  $r_c$  and aerial density  $N$  per unit surface area, are placed over it.

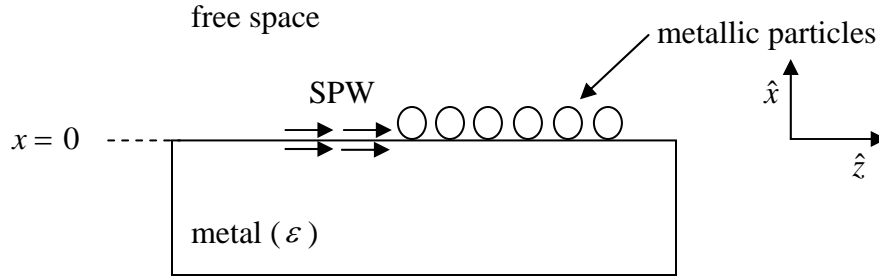


Fig. 5.1 Schematic for the absorption of surface plasma waves by the metallic particles placed on metal surface.

The effective relative permittivity  $\varepsilon$  of the metal is given as

$$\varepsilon = \left( \varepsilon_L - \frac{\omega_p^2}{\omega^2} \right) + i \frac{\nu}{\omega} \frac{\omega_p^2}{\omega^2}, \quad (5.1)$$

where  $\omega$  is the incident laser frequency.  $\varepsilon_L$  is the lattice permittivity,  $\omega_p$  is the plasma frequency and  $\nu$  is the electron phonon collision frequency in the metal film. Suppose a surface plasma wave propagates through the configuration with  $t, z$  variation as  $\exp[-i(\omega t - k_z z)]$ . The field variation of surface plasma wave in free space and metal region is given by [10]

$$\vec{E}_S = \vec{A}_S(x) e^{-i(\omega t - k_z z)}, \quad (5.2)$$

$$\text{where } \vec{A}_S = A_{SO} \left( \hat{z} + \frac{i k_z}{\alpha} \hat{x} \right) e^{-\alpha x}, \quad \text{for } x > 0,$$

$$= A_{SO} \left( \hat{z} - \frac{i k_z}{\alpha'} \hat{x} \right) e^{\alpha' x}, \quad \text{for } x < 0,$$

where  $\alpha = (k_z^2 - \omega^2 / c^2)^{1/2}$ ,  $\alpha' = (k_z^2 - \omega^2 \varepsilon / c^2)^{1/2}$ . Using boundary condition of continuity of  $\varepsilon' E_x$  at  $x = 0$ , the dispersion relation of the surface plasma wave is

$$k_z = \frac{\omega}{c} \left| \frac{\varepsilon}{1 + \varepsilon} \right|^{1/2}. \quad (5.3)$$

The SPW decays with  $z$  over a propagation length (inverse of imaginary part of  $k_z$ ),

$$L = k_{zi}^{-1} = \frac{2\omega}{v} \frac{\omega_p^2}{\omega^2} \left( \frac{\omega_p^2}{\omega^2} - \varepsilon_L - 1 \right)^{3/2} \left( \frac{\omega_p^2}{\omega^2} - \varepsilon_L \right)^{1/2}. \quad (5.4)$$

For  $\omega = 2.3 \times 10^{15} \text{ rad/sec}$ ,  $\omega_p = 4 \times 10^{15} \text{ rad/sec}$ ,  $v = 7 \times 10^{12} \text{ sec}^{-1}$ ,  $\varepsilon = -4$ , we obtain  $L = 0.0297 \text{ cm}$  which is rather long. For stronger absorption of the surface plasma wave, we examine the role of the particles placed over the metal surface.

### 5.3 Absorption of surface plasma wave by metallic particles

Consider spherical metal particles of radius  $r_c$  placed over the metal surface (cf. Fig. 5.1). When the surface plasma wave field given by Eq. (5.2) in the free space region interacts with the metal particle having internal electron density  $n_e$ , then the response of electrons of a particle is governed by equation of motion (Appendix-1)

$$m \frac{d^2 \vec{s}}{dt^2} = -e \vec{E}_s - m \nu \vec{v} - \frac{m \omega_{pe}^2 \vec{s}}{3}, \quad (5.5)$$

where,  $\vec{s}$  is the displacement of electrons of the particle from equilibrium,  $\vec{v} = d\vec{s}/dt$  is their velocity,  $m$  and  $-e$  are the electronic mass and charge,  $\omega_{pe}$  is the plasma frequency of the metal particle which is same as  $\omega_p$  when the metal particle and metal

film are of same material. Taking x-component of Eq. (5.5), the velocity of electrons in x-direction turns out to be

$$\mathbf{v}_x = \frac{e A_{SO} \omega(k/\alpha) e^{-i\omega t}}{m(\omega^2 - \omega_{pe}^2/3 + i\nu\omega)}, \quad (5.6)$$

Similarly taking z-component one obtains

$$\mathbf{v}_z = \frac{-ie A_{SO} \omega e^{-i\omega t}}{m(\omega^2 - \omega_{pe}^2/3 + i\nu\omega)}, \quad (5.7)$$

Under the influence of the SPW field, the energy absorbed by an electron per second is

$$\dot{\mathcal{E}}_{abs} = \frac{1}{2} \text{Re}[-e \vec{E}_S^* \cdot \vec{v}], \quad (5.8)$$

Where  $\vec{E}_S$  is the electric field and \* denoted the complex conjugate. Using Eq. (5.2), (5.6) and (5.7) in Eq. (5.8), we obtain

$$\dot{\mathcal{E}}_{abs} = \frac{e^2 A_{SO}^2 \omega^2 \nu(1+k^2/\alpha^2)}{2m((\omega^2 - \omega_{pe}^2/3)^2 + \nu^2 \omega^2)}, \quad (5.9)$$

If  $n_0$  is the electron density in the metal particle, then the power absorbed per second per particle is

$$\dot{\mathcal{E}}_{abs} = \frac{\omega_{pe}^2 A_{SO}^2 \omega^2 \nu(1+k^2/\alpha^2) r_c^3}{6((\omega^2 - \omega_{pe}^2/3)^2 + \nu^2 \omega^2)}. \quad (5.10)$$

When  $N$  is the number of particles per unit area on the metal surface with inter particle separation  $d = N^{-1/2} \geq r_c$ , such that

$$N = \int n_p \delta(x-a) dx,$$

then the energy absorbed in distance  $dz$  is

$$dP = -\dot{\mathcal{E}}_{abs} n_p dz,$$

$$= \frac{\omega_{pe}^2 A_{so}^2 \omega^2 v (1 + k^2 / \alpha^2) r_c \left( \frac{r_c}{d} \right)^2}{6((\omega^2 - \omega_{pe}^2 / 3)^2 + v^2 \omega^2)} dz. \quad (5.11)$$

Here  $P$  is the SPW power flow per unit y width in the vacuum region,

$$P = \frac{c}{4\pi} \int_0^\infty \text{Re} \left( \frac{\vec{E}_s \times \vec{H}_s}{2} \right)_z dx, \quad (5.12)$$

where  $\vec{E}_s$ ,  $\vec{H}_s$  are the electric field and magnetic field intensity of the surface plasma wave in the free space region. Using the third Maxwell's equation, we have

$\vec{H}_s = (c/i\omega)(\nabla \times \vec{E}_s)$ . Substituting  $\vec{E}_s$  and  $\vec{H}_s$ , we get

$$P = \frac{A_{so}^2 c^2 k}{16\pi \alpha^2 \omega} (k^2 / \alpha - \alpha), \quad (5.13)$$

From Eq. (5.11) and (5.13), we obtain

$$\int_{P_0}^P \frac{dP}{P} = - \int_0^z k_{ip} dz + C. \quad (5.14)$$

giving,  $P = P_0 e^{-k_{ip} z}$ ,

where  $P_0$  is the power at  $z = 0$ . The absorption constant  $k_{ip}$  is given as

$$k_{ip} = \frac{8\pi \alpha^2 \omega_{pe}^2 \omega^3 v (1 + k^2 / \alpha^2) r_c \left( \frac{r_c}{d} \right)^2}{3k c^2 ((\omega^2 - \omega_{pe}^2 / 3)^2 + v^2 \omega^2) (k^2 / \alpha - \alpha)}, \quad (5.15)$$

One may note that the resonant enhancement in  $k_{ip}$  occurs at  $\omega = \omega_{pe} / \sqrt{3}$ , corresponding to strong absorption of the wave. The resonant absorption depends upon the number density and the size of particles. In order to have numerical appreciation, we have plotted normalized absorption constant  $k_{ip}$  versus  $\delta / \omega_{pe} \equiv (\omega - \omega_{pe} / \sqrt{3}) / \omega_{pe}$  in

Fig. 5.2 for two different particle sizes of  $r_c = 6.5 \text{ nm}$  and  $r_c = 8 \text{ nm}$ , for the parameters:

$\omega_{pe} = 4.079 \times 10^{15} \text{ rad / sec}$ ,  $\varepsilon = -5.5$ ,  $d = 112 \text{ nm}$ ,  $\nu = 7 \times 10^{12} \text{ sec}^{-1}$ . The

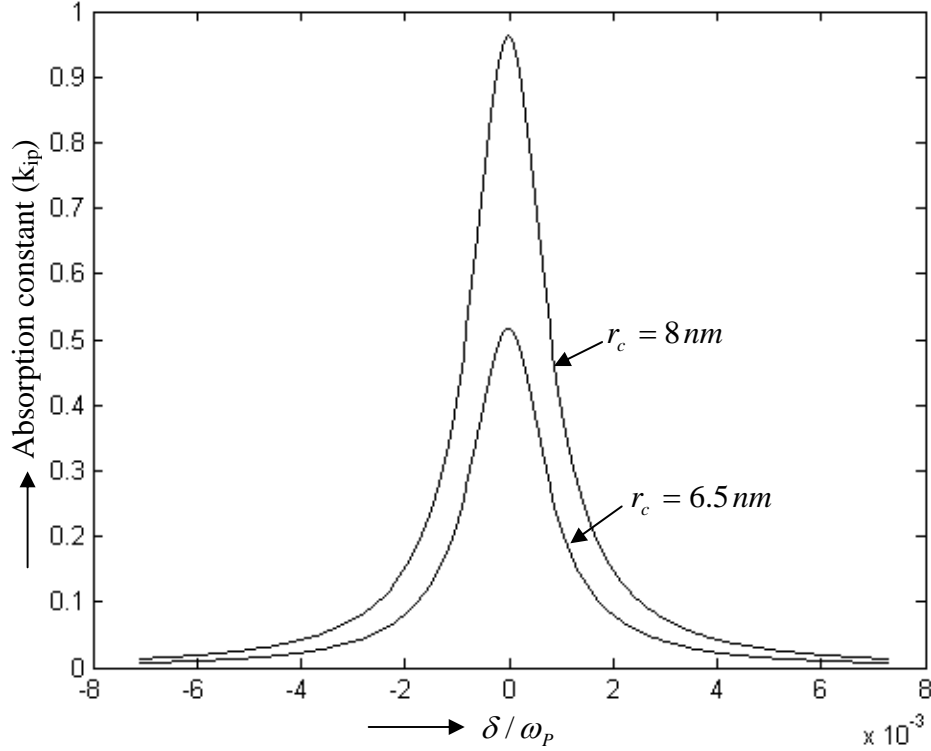


Fig. 5.2. Variation of normalized absorption constant,  $k_{ip} c / \omega_p$  versus normalized frequency  $(\omega - \omega_{pe} / \sqrt{3}) / \omega_{pe}$  for two particle of different size i)  $r_c = 6.5 \text{ nm}$  and ii)  $r_c = 8 \text{ nm}$  for the parameters:  $\varepsilon = -5.5$ ,  $\omega_{pe} = 4.079 \times 10^{15} \text{ rad / sec}$ ,  $d = 112 \text{ nm}$ ,  $\nu = 7 \times 10^{12} \text{ sec}^{-1}$ .

maximum resonance absorption constant turns out to be  $k_{ip} c / \omega_{pe} = 0.5$  and  $0.96$  respectively. Xiao-Hong Nancy Xu et al. [17] experimentally observed surface plasmon absorbance of  $0.06$  and  $0.23$  by the gold nanoparticles of sizes  $r_c = 6.5 \text{ nm}$  and  $r_c = 19 \text{ nm}$  respectively, which are close to  $0.05$  and  $0.28$  resulting out of our analysis for the same size particles. In order to obtain the specific range of the resonant incidence frequency for which absorption is significant, we calculate the full width at half

maximum (FWHM) frequency. It turns out to be  $0.00175 \omega_p$ , independent of the change in the size of particle.

#### 5.4 Discussion

The anomalous absorption of surface plasma waves by metallic nano-particles adsorbed over the metal surface is facilitated by resonant plasmon oscillations inside the particles. The surface plasma wave propagates over the metal surface and can be excited using an ATR configuration when the wave number of the incident laser along the interface becomes equal to the SPW. The resonant plasmon oscillations occurs for a specific frequency  $\omega$  of the incident wave for which plasma frequency of the particle becomes  $\sqrt{3}$  times the incident laser frequency in case of spherical particle. At resonant frequency, the absorption constant rises sharply which corresponds to the strong dissipation of the surface wave energy via collisions of the free electrons of the particle. The resonant absorption of the surface plasma wave is influenced of the size of the metallic. With the decrease in the size of particle, absorption constant decreases very rapidly.

The present treatment is limited to nano-particles of radius  $r_c \ll c/\omega$  and to low areal density of nano-particles so that the SPW field structure is not drastically modified by the particles.

## References

1. Patrick Lorazo, Laurent J. Lewis, and Michel Meunier, Phys. Rev. B **73**, 134108 (2006).
2. R. Stoian, A. Rosenfeld, D. Ashkenasi, I. V. Hertel, N. M. Bulgakova, and E. E. B. Campbell, Phys. Rev. Lett. **88**, 097603 (2002).
3. Amir Ahmad and V. K. Tripathi, Appl. Phys. Lett. **89**, 153112 (2006).
4. M. Moskovits, Rev. Mod. Phys. **57**, 783 (1985).
5. M. Moskovits, J. Chem. Phys. **69**, 4159 (1978).
6. F. J. Garcia-Vidal and J. B. Pendry, Phys. Rev. Lett. **77**, 1163 (1996).
7. K. Kneipp, H. Kneipp, Applied Spectroscopy **60**, 322A (2006).
8. T. Klar, M. Perner, S. Grosse, G. Von Plessen, W. Spirkl, and J. Feldmann, Phys. Rev. Lett. **80**, 4249 (1998).
9. B. Lamprecht, J. R. Krenn, A. Leitner, and F. R. Aussenegg, Phys. Rev. Lett. **83**, 4421 (1999).
10. H. Raether, *Surface plasmons on smooth and rough surfaces and on gratings*, in *Springer Tracts in Modern Physics*, vol. **111** (Springer-Verlag, New York, (1988).
11. C. S. Liu and V. K. Tripathi, IEEE Trans. Plasma Science **28**, 353(2001).
12. E. Kretschmann, Z. Phys. **241**, 313 (1971).
13. C. S. Liu, Gagan Kumar, and V. K. Tripathi, J. Appl. Phys. **100**, 013304 (2006).
14. A. Otto, Z. Phys. **216**, 398 (1968).
15. Yury P. Bliokh, Joshua Felsteiner, and Yokov Z. Slutsker, Phys. Rev. Lett. **95**, 165003 (2005).

16. A. Y. Vorobyev and Chunlei Guo, *Phys. Rev. B* **72**, 195422 (2005).
17. Xiao-Hong Nancy Xu, Shuang Huang, William Brownlow, Khalid Salaita, and Robert B. Jeffers, *J. Phys. Chem. B* **108**, 15543 (2004).

## Chapter 6

# FILAMENTATION OF A SURFACE PLASMA WAVE OVER A SEMICONDUCTOR FREE SPACE INTERFACE

### 6.1 Introduction

Filamentation instability is an important nonlinear process in the interaction of submillimeter waves and lasers with semiconductors [1-3]. A large amplitude electromagnetic wave propagating through a nonparabolic semiconductor, (e.g., n-InSb), for instance, heats the free electrons, raising their mass leading to increase in the refractive index of the semiconductor [4]. A small perturbation in the amplitude of the wave, across its direction of propagation, creates a spatial modulation in the refractive index with high amplitude portion having higher refractive index. The wave has a tendency to converge energy towards the regions of higher refractive index, giving rise to the growth of the perturbation. This leads to the breaking up of the wave into filaments. In the case of compensated semiconductores, with equal concentrations of electrons and holes, non uniform heating of the carriers and their ambipolar diffusion from regions of higher amplitude to lower amplitude gives rise to same effect. In gaseous plasmas filamentation may be caused by the ponderomotive force and relativistic mass nonlinearity [5-7].

Large amplitude surface plasma waves (SPW) over conductor and plasma surfaces are also a subject of strong current interest due to its applications in material ablation [8, 9], plasma diagnostics and plasma production for material processing. At large amplitude, SPW has been found to exhibit nonlinear effects. The SPW can cause

harmonic generation [10, 11]. Simon et al. [12] reported that the second harmonic generation (SHG) with SPW excitation at silver quartz grating is enhanced by 4 orders of magnitude relative to the non-resonant SHG in the quartz crystal. The surface plasma waves are susceptible to parametric instabilities. Parashar et al. [13] have studied stimulated Compton scattering of SPW over a conductor/ plasma surface. Lee et al. [14] have studied the parametric decay of a p-polarized light wave into two surface plasma waves. They formulated the nonlinear boundary conditions in terms of space charge and volume currents, and calculated the growth rate evaluating the rippling effect on the parametric interaction.

In this chapter we examine the possibility of filamentation of a large amplitude surface plasma wave over a compensated semiconductor. The physics of the process is as follows. Consider a large amplitude surface plasma wave propagating along  $\hat{z}$  on a semiconductor-free space interface ( $x = 0$ ) with amplitude decaying with  $|x|$  and uniform in  $y$ . Let the amplitude of the SPW have a small perturbation in  $y$  direction, the free electrons and holes experience a spatially periodic ponderomotive force along  $\hat{y}$ , leading to free carrier diffusion and spatial modulation of effective permittivity  $\epsilon_{eff}$ . The  $\epsilon_{eff}$  profile has a tendency to converse the SPW energy to regions of higher  $\epsilon_{eff}$ , leading to the growth of amplitude perturbation.

In section 6.2, we deduce ponderomotive force on electrons and holes and obtained the nonlinear effective permittivity to a spatially amplitude modulated SPW. In section 6.3, we solve the wave equation and obtain the growth rate of the filamentation instability. Our results are discussed in section 6.4.

## 6.2 Ponderomotive force and effective permittivity over the semiconductor surface

Consider a semiconductor-free space interface ( $x=0$ ), with semiconductor occupying half space  $x < 0$  and the free space being  $x > 0$ . The semiconductor has free electrons and holes. The density, effective mass and charge for the two species are  $n_0$ ,  $m_e$ ,  $-e$  and  $n_{0h}$ ,  $m_h$ ,  $+e$  respectively. We choose  $n_0 = n_{0h}$ . A large amplitude surface plasma wave propagates over the interface with electric and magnetic fields [15]

$$\begin{aligned}\vec{E} &= A \left( \hat{z} + \frac{ik_z}{\alpha_1} \hat{x} \right) e^{-\alpha_1 x} e^{-i(\omega t - k_z z)}, & \text{for } x > 0, \\ \vec{E} &= A \left( \hat{z} - \frac{ik_z}{\alpha_2} \hat{x} \right) e^{\alpha_2 x} e^{-i(\omega t - k_z z)}, & \text{for } x < 0,\end{aligned}\quad (6.1)$$

$$\vec{B} = (\nabla \times \vec{E}) / i\omega,$$

where  $k_z^2 = (\omega/c)^2 (\epsilon_s / (1 + \epsilon_s))$ ,  $\alpha_1 = (k_z^2 - \omega^2/c^2)^{1/2}$ ,  $\alpha_2 = (k_z^2 - \omega^2 \epsilon_s / c^2)^{1/2}$ ,  $\epsilon_s$  is the effective permittivity of the semiconductor

$$\epsilon_s = \epsilon_L - \frac{\omega_p^2}{\omega^2} - \frac{\omega_{ph}^2}{\omega^2}, \quad (6.2)$$

$\epsilon_L$  is the lattice permittivity,  $\omega_p = n_0 e^2 / m_e \epsilon_0$ ,  $\omega_{ph} = n_{0h} e^2 / m_h \epsilon_0$ .

We perturb the equilibrium by an amplitude perturbation,  $\vec{A} = \vec{A}_0 + \vec{A}_1(y, z)$ . The net field inside the semiconductor may be written as

$$\vec{E} = [A_0 + A_1(y, z)] \left( \hat{z} - \frac{ik_z}{\alpha_2} \hat{x} \right) e^{\alpha_2 x} e^{-i(\omega t - k_z z)}. \quad (6.3)$$

$A_1$ , in general, is complex while  $A_0$  is real. The SPW imparts oscillatory velocity  $\vec{v}$  to electrons and holes

$$\vec{v} = \frac{e \vec{E}}{m_e i \omega},$$

$$\vec{v}_h = -\frac{e \vec{E}}{m_h i \omega}. \quad (6.4)$$

It also exerts ponderomotive force on them [16].

$$\vec{F}_{pe} = -\frac{m_e}{2} \vec{v}^* \cdot \nabla \vec{v} - \frac{e}{2} \vec{v} \times \vec{B}^* = -\frac{e^2}{2m_e \omega^2} \nabla (\vec{E} \cdot \vec{E}^*), \quad (6.5)$$

$$\vec{F}_{ph} = -\frac{e^2}{2m_h \omega^2} \nabla (\vec{E} \cdot \vec{E}^*). \quad (6.6)$$

These forces have x and y components. The x component does not play a role in filamentation. The y component can be written as

$$F_{pey} = -\frac{e^2}{2m_e \omega^2} \frac{\partial}{\partial y} \left[ A_0 (A_1 + A_1^*) e^{2\alpha_2 x} \left( 1 + \frac{k_z^2}{\alpha_2^2} \right) \right], \quad (6.7)$$

$$F_{phy} = -\frac{e^2}{2m_h \omega^2} \frac{\partial}{\partial y} \left[ A_0 (A_1 + A_1^*) e^{2\alpha_2 x} \left( 1 + \frac{k_z^2}{\alpha_2^2} \right) \right], \quad (6.8)$$

where \* denotes the complex conjugate. The ponderomotive force expels electrons and holes away from the region of higher amplitude. In a compensated semiconductor, a steady state is realized when ponderomotive force is balanced by the pressure gradient force,

$$F_{pey} + F_{phy} - \frac{T}{n} \frac{\partial n}{\partial y} = 0, \quad (6.9)$$

where  $T$  is free carrier temperature and  $n$  is the modified free carrier density. Writing  $n = n_0 + \Delta n$ , Eq. (6.9) yields

$$\Delta n = -\alpha' n_0 e^{2\alpha_2 x} A_0 (A_1 + A_1^*), \quad (6.10)$$

where  $\alpha' = \frac{-e^2(1+k_z^2/\alpha_2^2)}{2T\omega^2} \left( \frac{1}{m_e} + \frac{1}{m_h} \right)$ . The effective permittivity of the semiconductor

may now be written as

$$\begin{aligned} \varepsilon_{eff} &= \varepsilon_L - \frac{\omega_{p0}^2(1+\Delta n/n_0)}{\omega^2} - \frac{\omega_{ph0}^2(1+\Delta n/n_{0h})}{\omega^2}, \\ &= \varepsilon_{00} + \varepsilon_2, \end{aligned} \quad (6.11)$$

where  $\varepsilon_{00} = \varepsilon_L - \omega_{p0}^2/\omega^2 - \omega_{ph0}^2/\omega^2$ ,  $\varepsilon_2 = -\varepsilon_2' \psi(x) A_0(A_1 + A_1^*)$ ,  $\psi(x) = e^{2\alpha_2 x}$ ,

$$\varepsilon_2' = \alpha'(\omega_{p0}^2/\omega^2 + \omega_{ph0}^2/\omega^2).$$

### 6.3 Growth Rate

The wave equation governing the propagation of perturbed surface plasma wave field is

$$\nabla^2 \vec{E}_1 - \nabla(\nabla \cdot \vec{E}_1) + \frac{\omega^2}{c^2}(\varepsilon_{00} \vec{E}_1 + \varepsilon_2 \vec{E}_0) = 0. \quad (6.12)$$

Employing  $\nabla \cdot \vec{D} = 0$ ,  $\partial A / \partial z \ll k A$  (WKB) approximation, we get the equation for  $A_1$

$$\frac{\partial^2 A_1}{\partial y^2} + 2ik_z \frac{\partial A_1}{\partial z} + \frac{\omega^2}{c^2} \varepsilon_2' \psi(x) A_0^2 (A_1 + A_1^*) = 0, \quad \text{for } x < 0, \quad (6.13)$$

$$\frac{\partial^2 A_1}{\partial y^2} + 2ik_z \frac{\partial A_1}{\partial z} = 0, \quad \text{for } x > 0, \quad (6.14)$$

where we have replaced  $\partial/\partial z = ik_z$  and used  $\alpha_2^2 = (k_z^2 - \omega^2 \varepsilon_{00}/c^2)$ . Multiplying Eq. (6.13) by  $e^{\alpha_2 x}$  and integrating from  $-\infty$  to 0, and Eq. (6.14) by  $e^{-\alpha_2 x}$  and integrating from 0 to  $\infty$  and then adding, we obtain

$$\left[ \frac{\partial^2 A_1}{\partial y^2} + 2ik_z \frac{\partial A_1}{\partial z} \right] \left( \frac{1}{\alpha_1} + \frac{1}{\alpha_2} \right) + \frac{\omega^2 \varepsilon_2'}{3\alpha_2 c^2} A_0^2 (A_1 + A_1^*) = 0, \quad (6.15)$$

Expressing  $A_1 = A_{1r} + iA_{1i}$  and separating real and imaginary parts,

$$\left[ \frac{\partial^2 A_{1r}}{\partial y^2} - 2k_z \frac{\partial A_{1i}}{\partial z} \right] \left( \frac{1}{\alpha_1} + \frac{1}{\alpha_2} \right) + \frac{2\omega^2}{3c^2} \frac{\varepsilon_2'}{\alpha_2} A_0^2 A_{1r} = 0, \quad (6.16)$$

$$\left[ \frac{\partial^2 A_{1i}}{\partial y^2} + 2k_z \frac{\partial A_{1r}}{\partial z} \right] \left( \frac{1}{\alpha_1} + \frac{1}{\alpha_2} \right) = 0. \quad (6.17)$$

Considering  $A_{1r}, A_{1i} \sim a_r, a_i e^{iqy} e^{\gamma z}$ , we obtain

$$\left[ -q^2 a_r - 2\gamma k_z a_i \right] \left( \frac{1}{\alpha_1} + \frac{1}{\alpha_2} \right) + \frac{2\omega^2}{3c^2} \frac{\varepsilon_2'}{\alpha_2} A_0^2 a_r = 0, \quad (6.18)$$

$$\left[ -q^2 a_i + 2\gamma k_z a_r \right] \left( \frac{1}{\alpha_1} + \frac{1}{\alpha_2} \right) = 0. \quad (6.19)$$

Eliminating  $a_i$  and  $a_r$  from Eq. (6.18) and (6.19), we obtain the dispersion relation,

$$\left( \frac{1}{\alpha_1} + \frac{1}{\alpha_2} \right) \left[ -q^2 - \frac{4\gamma^2 k_z^2}{q^2} \right] + \frac{2\omega^2}{3c^2} \frac{\varepsilon_2'}{\alpha_2} A_0^2 = 0. \quad (6.20)$$

Solving Eq. (6.20), we obtain the growth rate

$$\gamma = \frac{q}{2k_z} \left[ \frac{2\omega^2}{3c^2} \frac{e^2 A_0^2 (1+k_z^2/\alpha^2)}{2T\omega^2(1+\alpha_2/\alpha_1)} \left( \frac{1}{m_e} + \frac{1}{m_h} \right) \left( \frac{\omega_{p0}^2}{\omega^2} + \frac{\omega_{ph0}^2}{\omega^2} \right) - q^2 \right]^{1/2}. \quad (6.21)$$

The instability occurs when  $q^2 < \frac{2\omega^2}{3c^2} \frac{e^2 A_0^2 (1+k_z^2/\alpha^2)}{2T\omega^2(1+\alpha_2/\alpha_1)} \left( \frac{1}{m_e} + \frac{1}{m_h} \right) \left( \frac{\omega_{p0}^2}{\omega^2} + \frac{\omega_{ph0}^2}{\omega^2} \right)$ .

The maximum growth  $\gamma_{\max}$  occurs for  $q = q_{opt}$ ,

$$q_{opt}^2 = \frac{1\omega^2}{3c^2} \frac{e^2 A_0^2 (1+k_z^2/\alpha^2)}{2T\omega^2(1+\alpha_2/\alpha_1)} \left( \frac{1}{m_e} + \frac{1}{m_h} \right) \left( \frac{\omega_{p0}^2}{\omega^2} + \frac{\omega_{ph0}^2}{\omega^2} \right). \quad (6.22)$$

The maximum growth rate is given as

$$\gamma_{\max} = \frac{1}{2k_z} \left[ \frac{2}{3} \frac{\omega^2}{c^2} \frac{e^2 A_0^2 (1+k_z^2/\alpha^2)}{2T \omega^2 (1+\alpha_2/\alpha_1)} \left( \frac{1}{m_e} + \frac{1}{m_h} \right) \left( \frac{\omega_{p0}^2}{\omega^2} + \frac{\omega_{ph0}^2}{\omega^2} \right) \right]^{3/2}. \quad (6.23)$$

In order to have a numerical appreciation of the growth rate, we have plotted normalized growth rate  $\Gamma_{nor} = \gamma c / \omega_p$  (given by Eq. (6.21)) versus normalized wave number of perturbation  $q c / \omega_p$  in fig. 6.1 for two different SPW amplitudes. The solid line corresponds to  $e A_0 / m \omega_p c = 1.8 \times 10^{-4}$ , while the dotted line is for  $e A_0 / m \omega_p c = 1.3 \times 10^{-4}$ . We note that the growth rate initially with the wave number, attains, a maximum and thereafter decreases. The maximum growth occurs for an optimum value of the transverse wave number  $q = q_{opt}$  (given by Eq. (6.22)). One may note that, as the filamentation instability grows, the intensity in the SPW filaments increases, while electron hole density decreases. Once all free carriers have been moved out, a stable condition is reached when no further evacuation is possible. In compensated semiconductor Ge:  $\epsilon_L = 16$  at  $77^\circ K$ ,  $q c / \omega_p = 0.1056$ ,  $n_0 = 10^{17} / cm^3$ ,  $c_s = 10^8 cm/sec$ ,  $\omega / \omega_p = 0.1773 rad/sec$ , the maximum growth rate comes out  $\gamma_{\max} c / \omega_p = 0.030$  at  $q_{opt} = 0.106$  for SPW amplitude  $\sim e A_0 / m \omega_p c = 1.8 \times 10^{-4}$ . With the decrease in the SPW amplitude, growth rate decreases. For  $e A_0 / m \omega_p c = 1.3 \times 10^{-4}$ , it turns out to be  $\Gamma_{nor} = 0.015$  at  $q_{opt} = 0.074$ .

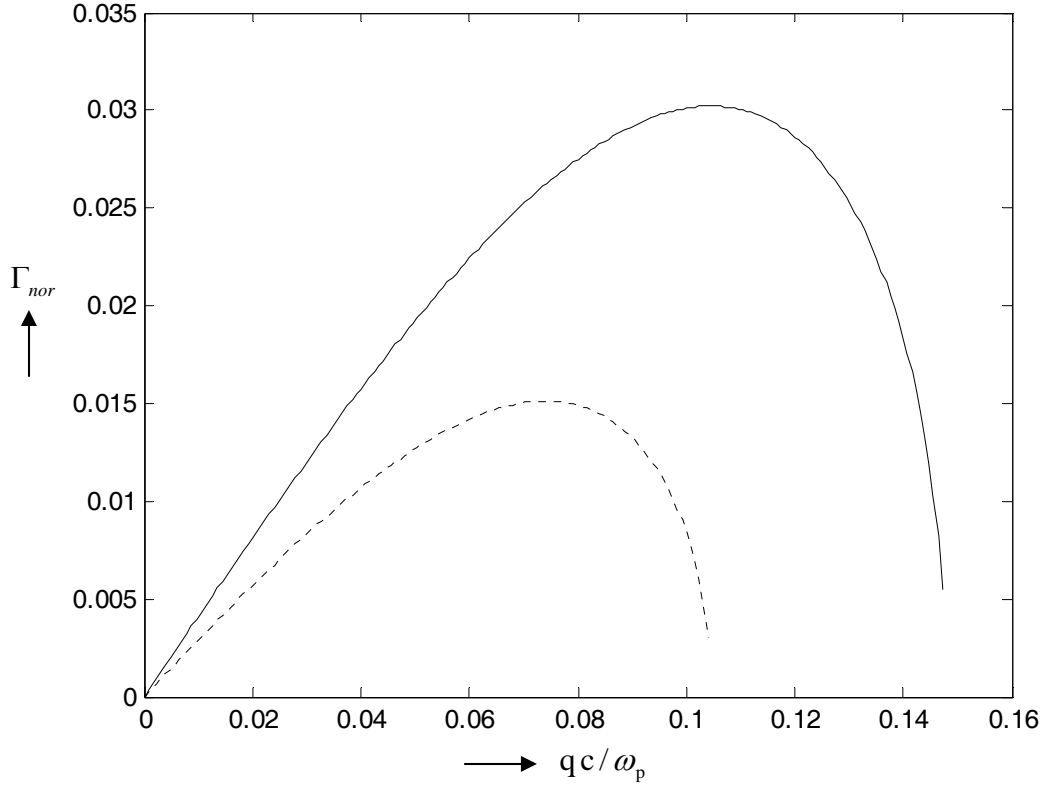


Fig. 6.1. Variation of normalized growth rate  $\Gamma_{nor}$  versus normalized transverse wavenumber  $qc/\omega_p$ . The parameters are:  $\epsilon_L = 16$  at  $77^\circ K$ ,  $c_s = 10^8$  cm/sec,  $\omega/\omega_p = 0.1773$  rad/sec,  $n_0 = 10^{17}$  /cm<sup>3</sup>,  $m_e = 0.1m$ ,  $m_h = 0.3m$  for normalized SPW amplitudes  $eA_0/m\omega_p c = 1.8 \times 10^{-4}$  ( — ) and  $eA_0/m\omega_p c = 1.3 \times 10^{-4}$  (-----).

In fig. 6.2, we have plotted normalized growth rate  $\Gamma_{nor} = \gamma c/\omega_p$  versus normalized frequency  $\omega/\omega_p$  of the surface plasma wave. It decreases monotonically with the frequency. The low-frequency electromagnetic wave turns out to be efficient for filamentation stability.

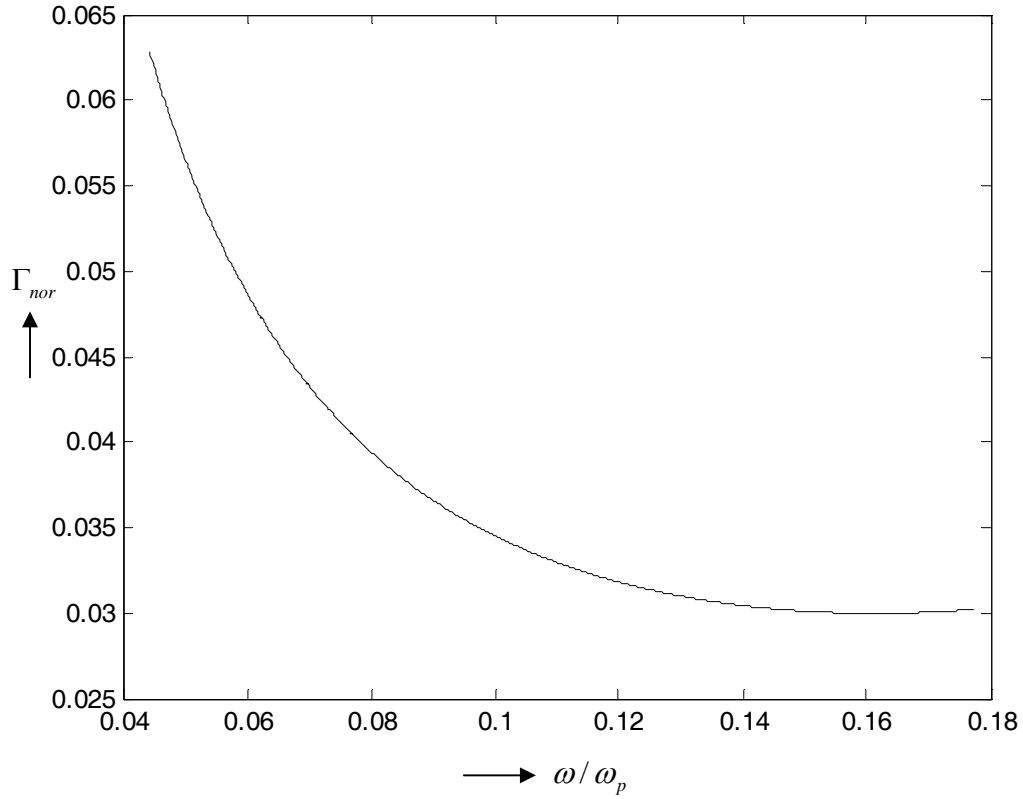


Fig. 6.2. Variation of normalized growth rate  $\Gamma_{nor}$  versus normalized frequency  $\omega/\omega_p$ . The parameters are:  $\varepsilon_L = 16$  at  $77^\circ K$ ,  $c_s = 10^8$  cm/sec,  $qc/\omega_p = 0.106$ ,  $n_0 = 10^{17}/cm^3$ ,  $m_e = 0.1m$ ,  $m_h = 0.3m$  for the SPW amplitude  $eA_0/m\omega_p c = 1.8 \times 10^{-4}$ .

#### 6.4 Discussion

A surface plasma wave over a compensated semi-conductor vacuum interface is susceptible to filamentation instability at modest powers. Both the electrons and holes play a role in the nonlinear coupling. The nonlinearity arises through the ponderomotive force driven electrons and holes redistribution inside the semiconductor. The growth rate initially increases with the wave number of the perturbation, attaining a maximum and then falls off. It decreases monotonically with the frequency of the incident wave. For a

compensated Ge at typical parameters, the spatial growth rate turns out to be  $\sim \gamma_{\max} = 0.030 \omega_p / c$  for normalized SPW amplitude  $e A_0 / m \omega_p c = 1.8 \times 10^{-4}$ . The filamentation instability appears relevant to SPW excitation in ATR (attenuated reflection configuration) configuration. The present study with semiconductors could be important in view of electron acceleration. The high field gradient of the localized SPW may cause enhanced electron acceleration.

## References

1. L. Stenflo and P. K. Shukla, Phys. Rev. B **39**, 12941 (1989).
2. M. Salimullah, M. A. Hossain, M. N. Alam, and M. Salahuddin, Phys. Rev. B **35**, 2303 (1987).
3. J. E. Economou and H. N. Spector, Phys. Rev. B **18**, 5578 (1978)
4. P. A. Wolff and G. A. Pearson, Phys. Rev. Lett. **17**, 1015 (1966).
5. P. K. Kaw, G. Schmidt and T. Wilcox, Phys. Fluids **16**, 1522 (1973).
6. C. S. Liu and V. K. Tripathi, Phys. Fluids **29**, 4188(1986).
7. P. K. Shukla and L. Stenflo, Phys. Fluids B **1**, 1926 (1989).
8. M. A. Ezaki, H. Kumagai, K. Toyoda, and M. Obara, IEEE J. Select. Topics Quant. Electron. **1**, 841 (1995).
9. S. A. Akhmanov, V. I. Emel'yanov, N. I. Koroteev, and V. N. Seminogov, Sov. Phys. Usp. **28**, 1084 (1985).
10. C. Hubert, L. Billot, P.M. Adam, R. Bachelot, and P. Royer, J. Grand, D. Gindre, K. D. Dorkenoo, and A. Fort, Appl. Phys. Lett. **90**, 181105 (2007).
11. Lina Cao, N. C. Panoiu and R. M. Osgood, Phys. Rev. B **75**, 205401 (2007).
12. H. J. Simon, C. Huang, J. C. Quail, and Z. Chen, Phys. Rev. B **38**, 7408 (1988).
13. J. Parashar, H. D. Pandey, V. K. Tripathi, J. Plasma Phys. **59**, 97 (1998).
14. Hee J. Lee and Sang-Hoon Cho, Phys. Rev. E **59**, 3503 (1999).
15. C. S. Liu and V. K. Tripathi, IEEE Trans. Plasma Sci. **28**, 353 (2000).
16. C. S. Liu and V. K. Tripathi, *Interaction of Electromagnetic Waves with Electron Beams and Plasmas* (World Scientific, Singapore, 1994).

## Chapter 7

# EXCITATION OF SURFACE PLASMA WAVE OVER A PLASMA CYLINDER BY A RELATIVISTIC ELECTRON BEAM

### 7.1 Introduction

In the previous chapters we have studied the surface plasma waves [1-2] excited by laser beams. There is yet another efficient route to SPW excitation, viz., through the employment of electron beams. The SPWs have phase velocity less than the velocity of light in free space, and possess a longitudinal component of electric field, hence can efficiently exchange energy via Cerenkov interaction. Denton et al. [3] have studied the process of SPW excitation over metal surface by charged particles. The scheme is seen to provide important information on the structure of the energy spectrum of the electron Fermi-fluid in metals. Liu and Tripathi [4] have developed an analytical formalism of SPW excitation over a planar metal surface by an electron beam propagating parallel to the interface in free space, in close proximity of the metal.

In this chapter, we study the excitation of surface plasma wave over a thin plasma cylinder by a relativistic electron beam via Cerenkov interaction. The electron beam can propagate outside the plasma cylinder or inside it as the SPW field extends to outside as well as to the axial region when plasma radius is small. One may mention that SPWs over plasma cylinders have been historically a subject of great interest. Trivelpiece and Gould [5] reported the experimental observations of surface plasma waves quite early using a cylindrical plasma column enclosed in a glass tube that was co-axial with a circular metallic waveguide. Tonk [6] studied the scattering

of electromagnetic waves by plasma column resonances assuming the wavelength of incident wave much longer than the radius of column. The main resonance was observed for  $\omega \sim \omega_p / \sqrt{2}$ .

In section 7.2, we obtain mode structure of a surface plasma wave over a plasma cylinder. In section 7.3, we study the growth of the surface plasma wave by solid electron beam. In section 7.4, we study the excitation of SPW by an annular electron beam and study its growth rate. In section 7.5, we discuss our results.

## 7.2 Surface plasma wave propagation

Consider a plasma cylinder of radius ‘a’ and permittivity  $\varepsilon$  (cf. fig. 7.1). A relativistic electron beam of density  $n_{ob}$  and velocity  $v_{ob} \hat{z}$  is launched into the plasma. We perturb this equilibrium by a surface plasma wave with  $t-z$  variation as  $\exp[-i(\omega t - k_z z)]$ .

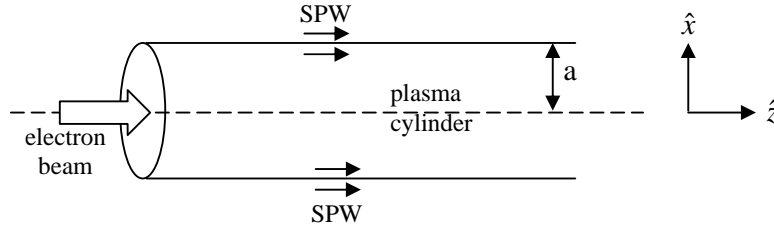


Fig. 7.1 Schematic of a plasma cylinder. An electron beam enters into the plasma leading to the excitation of surface plasma wave.

In the absence of beam, the r-variation of the axial field is governed by the wave equation

$$\frac{\partial^2 E_z}{\partial r^2} + \frac{1}{r} \frac{\partial E_z}{\partial r} + \left( \frac{\omega^2}{c^2} \varepsilon' - k_z^2 \right) E_z = 0, \quad (7.1)$$

where  $\varepsilon' = \varepsilon$  for  $r < a$ , and  $\varepsilon' = 1$  for  $r > a$  where  $\varepsilon' = \varepsilon = 1 - \omega_p^2 / \omega^2$ .  $\omega_p$  is the plasma frequency of the plasma cylinder. The well behaved solution of Eq. (7.1) in conjunction with  $\nabla \cdot \vec{E} = 0$  in plasma and free space regions, is

$$\begin{aligned}\vec{E} &= A_1 \left( \hat{z} I_0(\alpha_1 r) + \hat{r} \frac{i k_z}{\alpha_1} I_0'(\alpha_1 r) \right) e^{-i(\omega t - k z)}, & r < a, \\ &= A_2 \left( \hat{z} K_0(\alpha_2 r) + \hat{r} \frac{i k_z}{\alpha_2} K_0'(\alpha_2 r) \right) e^{-i(\omega t - k z)}, & r > a,\end{aligned}\quad (7.2)$$

where  $\alpha_1 = (k_z^2 - \varepsilon \omega^2 / c^2)^{1/2}$ ;  $\alpha_2 = (k_z^2 - \omega^2 / c^2)^{1/2}$ . Applying the boundary conditions of continuity of  $E_z$  and  $\varepsilon' E_r$  at  $r = a$ , we obtain

$$A_1 I_0(\alpha_1 a) = A_2 K_0(\alpha_2 a), \quad (7.3)$$

$$\varepsilon A_1 \left( \frac{i k_z}{\alpha_1} \right) I_0'(\alpha_1 a) = A_2 \left( \frac{i k_z}{\alpha_2} \right) K_0'(\alpha_2 a). \quad (7.4)$$

From Eq. (7.3) and (7.4), we get the SPW dispersion relation,

$$\frac{K_0(\alpha_2 a)}{I_0(\alpha_1 a)} = \frac{1}{\varepsilon} \frac{\alpha_1}{\alpha_2} \frac{K_0'(\alpha_2 a)}{I_0'(\alpha_1 a)}. \quad (7.5)$$

We have plotted normalized frequency  $\omega / \omega_p$  as a function of normalized wave number  $k_z c / \omega_p$  in fig. 7.2 for different radii of plasma cylinder taking  $\omega_p = 1.8 \times 10^{12}$  rad/s. The frequency of the SPW initially increases monotonically with wave number and then saturates. An increase in plasma radius results in increased phase velocity. For  $a \omega_p / c \gg 1$  dispersion relation reduces to  $k_z = (\omega / c) (\varepsilon / (1 + \varepsilon))^{1/2}$ .

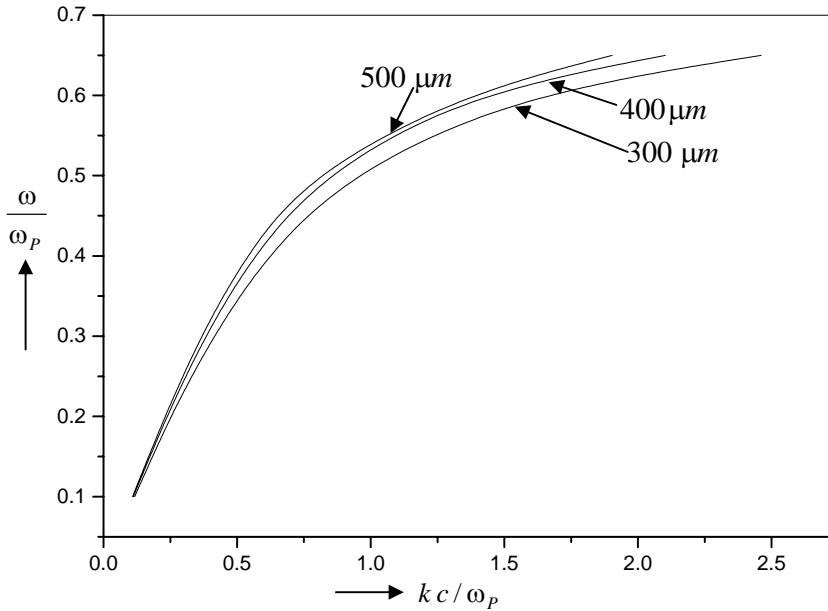


Fig. 7.2 Variation of normalized frequency  $\omega/\omega_p$  versus normalized wavenumber  $k_z c/\omega_p$  of the surface plasma wave in a plasma cylinder of three different radii  $a = 300 \mu m$ ,  $a = 400 \mu m$  and  $a = 500 \mu m$  respectively taking  $\omega_p = 1.8 \times 10^{12} \text{ rad/s}$ .

### 7.3 SPW excitation by a solid beam

Now we incorporate the role of the electron beam. We consider a solid beam propagating inside the plasma with velocity  $v_{ob} \hat{z}$  and density  $n_{ob}$ . The beam acquires an oscillatory velocity due to the SPW. The governing equation is

$$m \frac{d(\gamma \vec{v})}{dt} = -e \vec{E} - \frac{e}{c} (\vec{v} \times \vec{B}), \quad (7.6)$$

where  $\gamma = (1 - v^2/c^2)^{-1/2}$  is the relativistic gamma factor,  $-e$  and  $m$  are the electronic charge and mass, and the magnetic field of the wave is

$$\vec{B} = (c/i\omega)(\nabla \times \vec{E}) = -\hat{\theta} \left( \frac{\alpha_1 A_1 c}{i\omega} \right) \left( 1 - \frac{k_z^2}{\alpha_1^2} \right) I_0'(\alpha_1 r) e^{-i(\omega t - k_z z)}.$$

We write  $\vec{v} = \vec{v}_{0b} \hat{z} + \vec{v}_{1b}$ ,  $\gamma = \gamma_0 + \gamma_0^3 v_{0b} v_{1z} / c^2$ , and  $n = n_{0b} + n_{1b}$ , where  $\gamma_0 = (1 - v_{0b}^2 / c^2)^{-1/2}$ ,  $v_{1b}$  and  $n_{1b}$  are the perturbed beam velocity and density, have  $t, z$  variations as  $\exp[-i(\omega t - k_z z)]$ . The perturbed electron velocities in  $r$  and  $z$  directions, after linearization are obtained as

$$v_{1br} = \frac{e E_r + ((e \alpha_1^2 v_{0b}) / (k_z \omega))(1 - k_z^2 / \alpha_1^2) E_r}{m i \gamma_0 (\omega - k_z v_{0b})}, \quad (7.7)$$

$$v_{1bz} = \frac{e E_z}{m i \gamma_0^3 (\omega - k_z v_{0b})}. \quad (7.8)$$

From the equation of continuity  $\partial n / \partial t + \nabla \cdot (n \vec{v}) = 0$ , one obtains the perturbed electron density associated with the beam,

$$n_{1b} = \frac{n_{0b} (\nabla \cdot \vec{v}_{1b})}{i (\omega - k_z v_{0b})}. \quad (7.9)$$

The perturbed current density can be written as

$$\vec{J}_1 = -e(n_{1b} \vec{v}_{0b} + n_{0b} \vec{v}_{1b})$$

$$J_{1z} = \frac{-e n_{0b}}{i (\omega - k_z v_{0b})} \left( \frac{\partial v_{1bz}}{\partial z} + \frac{1}{r} \frac{\partial}{\partial r} (r v_{1br}) \right) v_{0b} - e n_{0b} v_{1bz}, \quad (7.10)$$

$$J_{1r} = \frac{-n_{0b} e^2}{m i \gamma_0 (\omega - k_z v_{0b})} \left[ E_r + ((\alpha_1^2 v_{0b}) / (k_z \omega))(1 - k_z^2 / \alpha_1^2) E_r \right] \quad (7.11)$$

We retain only the terms that goes as  $(\omega - k_z v_{0b})^{-2}$ . Thus

$$\vec{J}_1 = \frac{e^2}{m \gamma_0 (\omega - k_z v_{0b})^2} \left( \frac{i k_z n_{0b} E_z}{\gamma_0^2} + n_{0b} \left( 1 + \frac{\alpha_1^2 v_{0b}}{k_z \omega} \left( 1 - \frac{k_z^2}{\alpha_1^2} \right) \right) \left( E_r + \frac{E_r}{r} \right) \right) v_{0b} \hat{z}. \quad (7.12)$$

We define  $\vec{E}_S$  and  $\vec{H}_S$  as the mode structures of the SPW field in the absence of the beam, satisfying the Maxwell's equations [7]

$$\nabla \times \vec{E}_S = \frac{i \omega}{c} \vec{H}_S, \quad \nabla \times \vec{H}_S = -\frac{i \omega}{c} \epsilon' \vec{E}_S \quad (7.13)$$

with appropriate boundary conditions at the interface. Let  $E_{sz}$  and  $E_{sr}$  be the field components of the SPW given by Eq. (7.2) when  $A_1 = A_2 = 1$ . In the presence of beam current, let the fields be

$$\vec{E} = A(t)\vec{E}_s, \quad \vec{H} = B(t)\vec{H}_s. \quad (7.14)$$

$\vec{E}$  and  $\vec{H}$  satisfy the Maxwell's equations

$$\begin{aligned} \nabla \times \vec{E} &= -(1/c)(\partial \vec{H} / \partial t), \\ \nabla \times \vec{H} &= \frac{4\pi}{c} \vec{J}_{lb} + \frac{\epsilon'}{c} \frac{\partial \vec{E}}{\partial t}. \end{aligned} \quad (7.15)$$

Using Eq. (7.13) and (7.14) in Eq. (7.15), we obtain

$$\frac{\partial B}{\partial t} = -i\omega(A - B), \quad (7.16)$$

$$\left[ \epsilon' \frac{\partial A}{\partial t} - i\omega \epsilon' (A - B) \right] \vec{E}_s = -4\pi \vec{J}_{lb}. \quad (7.17)$$

Solving Eq. (7.16) and (7.17), assuming  $\partial B / \partial t \approx \partial A / \partial t$ , we obtain

$$-2i\epsilon'\omega(A - B)\vec{E}_s = -4\pi \vec{J}_{lb}. \quad (7.18)$$

Multiplying Eq. (7.18) by  $\vec{E}_s^* r dr$  and integrating over  $r$  from 0 to  $\infty$ , we obtain

$$\frac{\partial A}{\partial t} = -\frac{2\pi \int_0^\infty J_{lbz} \vec{E}_{sz}^* r dr}{\epsilon' \int_0^\infty \vec{E}_s \cdot \vec{E}_s^* r dr} = \frac{P}{i(\omega - k_z v_0)^2} A, \quad (7.19)$$

$$\text{where } P = \left[ \frac{2\pi e^2 v_{0b} n_{0b}}{mi\gamma_0 \epsilon} \left( \frac{ik_z}{(1 + \gamma_0^2 v_{0b}^2 / c^2)} I_1 + \left( 1 + \frac{\alpha_1^2 v_{0b}}{k_z \omega} \left( 1 - \frac{k_z^2}{\alpha_1^2} \right) \right) (I_2 + I_3) \right) \right] / I_4;$$

$$I_1 = \int_0^\infty E_{sz} E_{sz}^* r dr, \quad I_2 = \int_0^\infty E_{sr}' E_{sz}^* r dr; \quad I_3 = \int_0^\infty E_{sr} E_{sz}^* r dr; \quad I_4 = \int_0^\infty \vec{E}_s \cdot \vec{E}_s^* r dr.$$

Writing  $\omega = k_z v_b + \delta$ ,  $\partial A / \partial t = -i\delta$ , we obtain

$$\delta^3 = P e^{i2l\pi}, \quad l = 0, 1, 2. \quad (7.20)$$

Eq. (7.20) gives the growth rate

$$\omega_i = \text{Im}\delta = (\sqrt{3}/2)P_2^{1/3}. \quad (7.21)$$

In fig. 7.3, we have plotted the variation of growth rate with frequency  $\omega/\omega_p$  for three different radii of plasma cylinders using the following parameters:  $\omega_p = 1.8 \times 10^{12} \text{ rad/s}$ ,  $n_{0b} = 10^{12} \text{ cm}^{-3}$ . The growth rate initially increases with frequency and then decreases after attaining a maximum value. The maximum growth rate for the plasma of radius  $a = 300 \mu\text{m}$ , turns out to be  $1.02 \times 10^{10} \text{ sec}^{-1}$  at  $\omega/\omega_p = 0.36$ . With the increase in the radius of plasma, the maximum growth rate increases. For the plasma of radius  $a = 400 \mu\text{m}$  and  $a = 500 \mu\text{m}$ , it turns out  $1.08 \times 10^{10} \text{ sec}^{-1}$  and  $1.11 \times 10^{10} \text{ sec}^{-1}$  at  $\omega/\omega_p = 0.40$  and  $\omega/\omega_p = 0.43$  respectively.

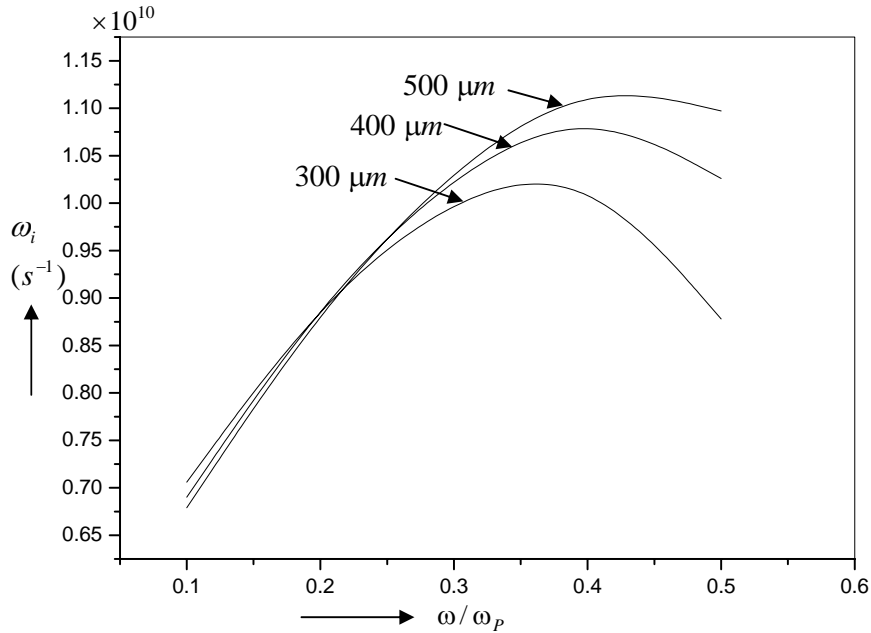


Fig. 7.3 The growth rate  $\omega_i (s^{-1})$  of the surface plasma wave as a function of normalized frequency  $\omega/\omega_p$  for plasma cylinder of radius  $a = 300 \mu\text{m}$ ,  $a = 400 \mu\text{m}$  and  $a = 500 \mu\text{m}$ . The other parameters are:  $\omega_p = 1.8 \times 10^{12} \text{ rad/s}$ ,  $n_{0b} = 10^{12} \text{ cm}^{-3}$ .

In fig. 7.4, we have plotted normalized wave frequency  $\omega/\omega_p$  as a function of normalized beam velocity  $v_{ob}/c$  for the parameters:  $\omega_p = 1.8 \times 10^{12} \text{ rad/s}$ ,  $n_{ob} = 10^{12} \text{ cm}^{-3}$ . The wave frequency decreases with beam velocity depending upon the radius of plasma cylinder. With the increase in the radius of plasma, the SPW frequency is higher in magnitude corresponding to a specific value of beam velocity.

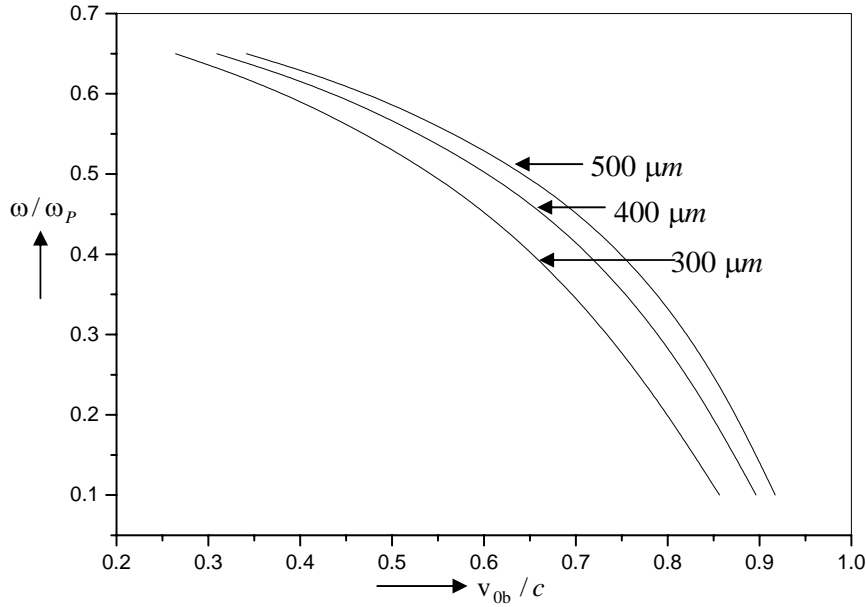


Fig. 4 The wave frequency  $\omega/\omega_p$  as a function of beam velocity  $v_{ob}/c$  for plasma cylinder of radius  $a = 300 \mu m$ ,  $a = 400 \mu m$  and  $a = 500 \mu m$ . The other parameters are:  $\omega_p = 1.8 \times 10^{12} \text{ rad/s}$ ,  $n_{ob} = 10^{12} \text{ cm}^{-3}$ .

#### 7.4 SPW excitation by an annular beam outside the cylinder

In case plasma cylinder is small one may employ an annular electron beam propagating outside the cylinder with velocity  $v_{ob} \hat{z}$  and density  $n_{ob} = \frac{n_{ob}^o}{r} \delta(r - r_b)$  where  $r_b$  is the beam radius,  $n_{ob}^o = I_b / e v_{ob}$  and  $I_b$  is the beam current. In the presence of SPW, the beam acquires an oscillatory velocity and density, which is

governed by Eq. (7.6) and (7.9). Solving for oscillatory velocity and electron density, one may obtain current density as discussed in previous section. The corresponding growth rate for the SPW is given by

$$\omega_i = \text{Im } \delta = (\sqrt{3}/2) P_2^{1/3}.$$

$$\text{where } P_2^{1/3} = \left[ \frac{2\pi e^2 v_{0b} n_{0b}}{mi\gamma_0 \varepsilon} \left( \frac{ik_z}{(1+\gamma_0^2 v_{0b}^2/c^2)} R_1 + \left( 1 + \frac{\alpha_1^2 v_{0b}}{k_z \omega} \left( 1 - \frac{k_z^2}{\alpha_1^2} \right) \right) (R_2 + R_3) \right) \right] / R_4;$$

$$R_1 = [I_0(\alpha_1 r_b)]^2; R_2 = -\frac{ik_z}{2} [I_0(\alpha_1 r_b) + I_2(\alpha_1 r_b)] I(\alpha_1 r_b); R_3 = -\frac{ik_z}{\alpha_1 r_b} [I_0'(\alpha_1 r_b) I_0(\alpha_1 r_b)];$$

$$R_4 = \left[ [I_0(\alpha_1 r_b)]^2 + (k_z / \alpha_1)^2 [I_1(\alpha_1 r_b)]^2 \right].$$

We have plotted growth rate as a function of normalized frequency  $\omega/\omega_p$  of the SPW for the plasma of radius  $a = 300 \mu m$  in fig. 7.5 for the parameters:  $n_{0b}^o = n_{0b} \pi a^2 = 2.83 \times 10^7 \text{ cm}^{-1}$ ,  $r_b = 305 \mu m$ ,  $\omega_p = 1.8 \times 10^{12} \text{ rad/s}$ . The maximum growth rate in the case turns out to be  $1.90 \times 10^9 \text{ sec}^{-1}$  at frequency  $\omega/\omega_p = 0.43$ .

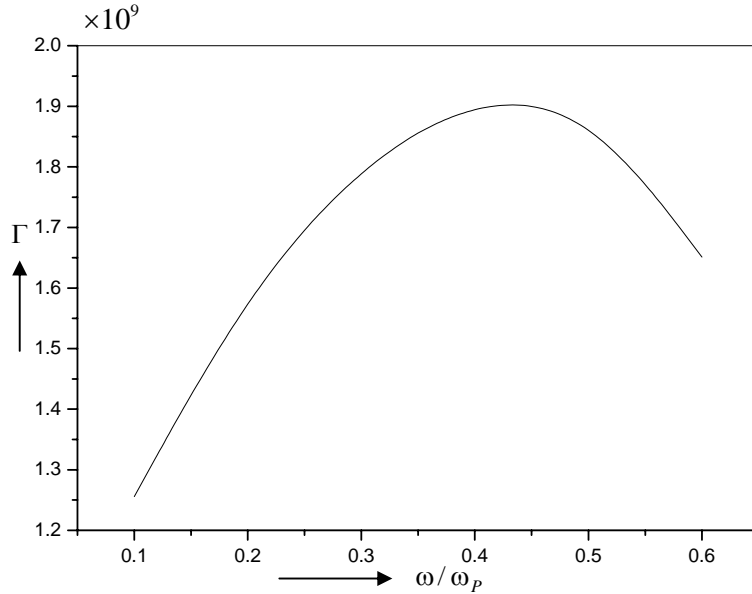


Fig. 7.5 The growth rate  $\omega_i (s^{-1})$  as a function of normalized frequency  $\omega/\omega_p$  for plasma cylinder of radius  $a = 300 \mu m$  when SPW excitation is carried out by annular beam propagating outside cylinder.

## 7.5 Discussion

A relativistic electron beam excites a surface plasma wave over a plasma cylinder via Cerenkov interaction. The frequency of surface plasma wave initially increases monotonically with the wave number and then saturates depending upon the radius of plasma cylinder. With the increase in radius, phase velocity increases. The frequency of the maximally growing SPW decreases with the beam velocity. The growth rate increases with frequency, attains a maximum and then decreases. For a plasma of radius  $a = 300 \mu m$ , the growth time turns out to be in the sub-nanosecond range at  $\omega/\omega_p = 0.36$ . The increase in the radius of the plasma, increases the optimum growth rate. The annular beam propagating outside the plasma cylinder also facilitates the SPW excitation on the cylinder. In this case the optimum growth rate is slower.

The present study should be relevant to capillary plasma created by an intense short pulse laser. The energetic electrons accelerated by the laser wake fields can drive the surface plasma waves.

## Reference

1. H. Raether, Surface plasmons on smooth and rough surfaces and on gratings, in Springer Tracts in Modern Physics, vol. 111( Springer-Verlag, New York, 1988).
2. C. S. Liu, Gagan Kumar, and V. K. Tripathi, J. Appl. Phys. **100**, 013304 (2006).
3. C. Denton, J. L. Gervasoni, R. O. Barrachina, and N. R. Arista, Phys. Rev. A **57**, 4498 (1998).
4. C. S. Liu and V. K. Tripathi, IEEE Trans. Plasma Science **28**, 353 (2001).
5. A. W. Trivelpiece and R. W. Gould, J. Appl. Phys. **30**, 1784 (1959).
6. L. Tonks, Phys. Rev. **37**, 1458 (1931).
7. C. S. Liu and V. K. Tripathi, IEEE J. Quantum Electron. **34**, 1503 (1998).

## Chapter 8

# CONCLUSIONS AND DIRECTIONS FOR FUTURE WORK

In this thesis, we have studied various linear and non-linear consequences of surface plasma waves. The theory of fiber optic sensor is consistent with the experimental observations. The resonant coupling of free electrons of nanoparticles attached to metal surface with the SPW leads to great enhancement in the sensitivity of the sensor.

The scheme of resonant electron acceleration by a SPW in a double metal surface configuration is advantageous for electron acceleration with the control in their trajectory. One may accelerate electrons to tens of keV energy using modest level of SPW. For a single surface SPW, our model of ponderomotive acceleration of electrons explains the experimental results by Zawadzka et al. [1] at laser intensity of  $10^{13}$  W/cm<sup>2</sup>.

The metallic particles adsorbed over the metal surface are found to cause anomalous absorption of the SPW via resonant plasmon oscillations inside the particles. The resonant plasmon oscillations occur for a specific frequency  $\omega$  of the incident wave for which plasma frequency of the particle becomes  $\sqrt{3}$  times the incident laser frequency in case of spherical particle. At resonant frequency strong dissipation of the surface wave energy by nanoparticles occurs.

The surface plasma wave over a compensated semi-conductor vacuum interface is susceptible to filamentation instability at modest powers. The nonlinearity arises through the ponderomotive force driven electron and hole density redistribution inside the semiconductor.

The excitation of surface plasma wave can be facilitated by a solid electron beam propagating inside or an annular electron beam propagating just outside the cylinder. The excitation of SPW by solid beam is found to be more efficient than the annular beam. The electron beam interacts with the plasma via Cerenkov resonance.

The present work can be extended to develop theoretical formulism for the negative refraction of visible light. The negative refraction has been demonstrated for microwaves and infrared waves [2], however for visible light it has always been a challenge as the component of the materials needs to be comparable to the wavelength of visible light which is quite difficult. Dionne and Lezec recently proposed a device consisting of an insulator silicon nitride sandwiched between two sheets of silver [3]. Light entering the device, mode converted into a surface plasma wave. When the SPW is passed through the gap of about 50 nm between gold-coated prism and silver plate, it gets totally refracted. Dionne achieved it for light with 480-530 nm.

Terahertz radiation generation has been gaining wide attention because of their application is the detection of explosive materials. The excitation of surface plasma waves by a pico-second laser on the metal surface provides the possibility of generating terahertz-pulse radiation. When a grating of suitable wave number is placed on the plasma surface, then incident laser excites a surface plasma wave at the interface. For large amplitude surface plasma wave, emission of electrons takes place from the surface resulting in current density wave. When the incident laser is of picosecond, then current density drives terahertz pulse radiation. Welsh et al. [4] have demonstrated the terahertz pulse generation via the excitation of surface plasma waves on metal surface with a

grating. One may develop the theoretical formalism for it based on the understanding of surface plasma wave work present in the thesis work.

The present work is very relevant to the emerging field of plasmonics [5]. The field of plasmonics is based on exploiting the coupling between light and surface plasma waves. In order to realize the ultracompact optical components and ultrasensitive detectors poor light-SPW coupling should be improved. The next step could be the improvement of light-SPW coupling. This requires careful designing the plasmonic structures with reduced losses at visible and infrared frequencies keeping in mind the laser power for the SPW excitation. The theoretical work discussed in the thesis may help in the development of plasmonic structures.

If we could design creatively the metal-dielectric interfaces such that plasmons with same frequency but of much shorter wavelength than the incident wave can be generated, then one may think of plasmons to travel along nanowires. This can be helpful in carrying information across chips at much faster rate. Therefore the present work can be extended to the excitation of surface plasma waves along nanowires and their propagation along them with reduced absorption losses. Hence there is a need to develop soliton plasmonic so as to realize plasmonics devices.

## References

1. J. Zawadzka, D. Jaroszynski, J. J. Carey, and K. Wynne, *Appl. Phys. Lett.* **79**, 2130 (2001).
2. C. G. Parazzoli, R. B. Gregor, K. Li, B. E. C. Koltenbah, and M. Tanielian, *Phys. Rev. Lett.* **90**, 107401 (2003).
3. J. Dionne and H. Lezec, “How to drive light round the wrong bend”, *Nature* **445**, 346 (2007).
4. G. H. Welsh, N. T. Hunt, and K. Wynne, *Phys. Rev. Lett.* **98**, 026803 (2007).
5. H. Atwater, “Promises of plasmonic”, *Sci. Am.*, March 2007.

## APPENDIX-1

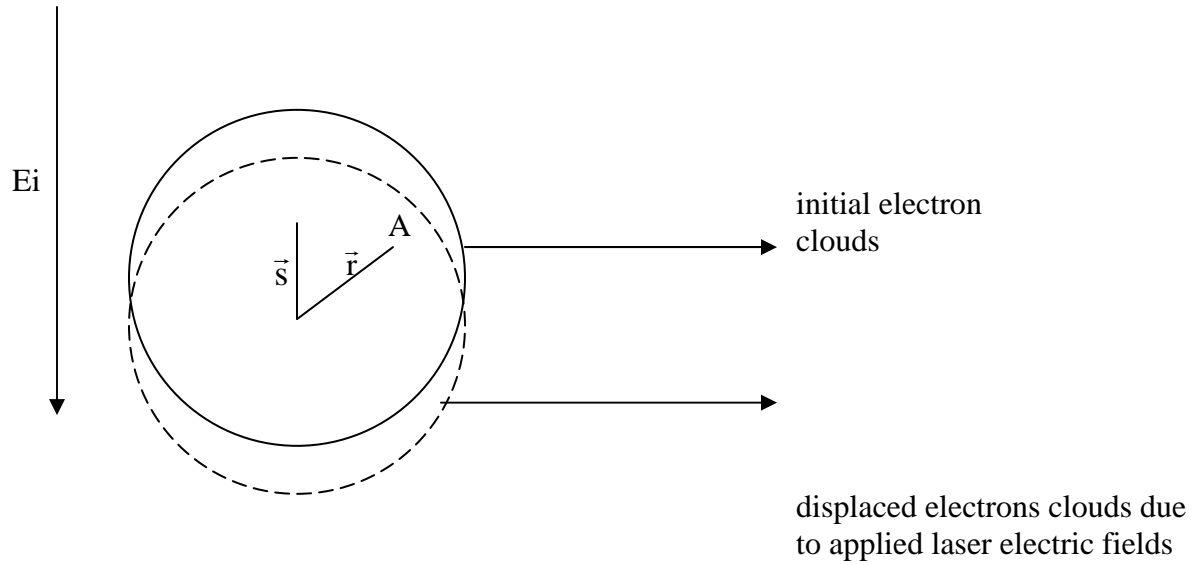


Fig. A-1 Electrons clouds in nanoparticle under laser electric field.

Electrons get displaced due to laser electric field, while displacement of ions is negligible. Ion density is taken to be the same as electron density  $n_e$ .

From figure A-1 electric field at point A using Gauss theorem,

$$\epsilon_0 \int \vec{E} \cdot d\vec{S} = 4\pi\rho r^3/3.$$

where  $\rho = -en_e$  is the density of electrons,

$$\epsilon_0 \vec{E} 4\pi r^2 = 4\pi\rho r^3/3.$$

$$\vec{E} = \rho \vec{r}/3\epsilon_0.$$

The electric field induced in the overlapping region if the displacement due to electric field is  $s$ ,

$$\vec{E} = \rho \vec{r} / 3\epsilon_0 - \rho(\vec{r} - \vec{s}) / 3\epsilon_0.$$

$$\vec{E} = \rho \vec{s} / 3\epsilon_0.$$

That total force on an electron due to induced field,

$$\vec{F} = -e\vec{E}.$$

$$= - (n_e e^2 / 3\epsilon_0) \vec{s}.$$

$$= -m n_e e^2 \vec{s} / 3m\epsilon_0.$$

$$= (-m(\omega_{pe})^2) \vec{s} / 3$$

where  $\omega_{pe} = (n_e e^2 / m\epsilon_0)^{1/2}$ .

## Bio-data of the Author

### GAGAN KUMAR

Plasma Group  
Physics Department  
Indian Institute of Technology Delhi  
Hauz Khas, New Delhi 110016, India  
Contact No.: +919899522772,  
E-mail: [gagankminocha@yahoo.co.in](mailto:gagankminocha@yahoo.co.in)

---

### EDUCATIONAL QUALIFICATIONS

---

- **Bachelor of Science (B. Sc.):**  
Dayanand College Hisar, Haryana, India (1998-2001).  
Marks: 75.8%
- **Master of Science (M. Sc.) in Physics:**  
Kurukshetra University, Kurukshetra (2001-03)  
Marks: 74.2%
- **Doctor of philosophy (Ph.D.):**  
Indian Institute of Technology Delhi (April 2004 to February 2008)  
C.G.P.A.: 9.0 /10.0

### RESEARCH EXPERIENCE

---

The interest has been the interaction of high power lasers and surface plasma waves (SPW) with solid state plasmas. Various aspects such as surface enhanced Raman scattering (SERS) in relevance to sensors, electron acceleration, anomalous absorption, filamentation instability and electron emission using different numerical and computational methods have been studied.

### SCHOLASTIC ACHIEVEMENTS

---

- Qualified National Eligibility Test (NET)-Junior Research Fellowship (JRF), Council of Scientific and Industrial Research (CSIR) in 2003 organized by ministry of Human Resource and Development, Govt. of India.
- Qualified Graduate Aptitude Test in Engineering (GATE) in Physics, 2002 organized by ministry of Human Resource and Development, Govt. of India.
- Qualified State Level Eligibility Test (SLET) in 2004.
- Awarded by DST-ICTP fellowship in 2007 by Department of Science and Technology to attend Summer College on Plasma Physics-New Developments 2007.
- 2<sup>nd</sup> position in M. Sc. (Physics) in Kurukshetra University, Kurukshetra.
- 1<sup>st</sup> position in B. Sc. in D. N. Post Graduate College, Hisar.
- Awarded as meritorious student by State Government (HAR) in B. Sc.

## PUBLICATIONS

---

1. C. S. Liu, **Gagan Kumar**, V. K. Tripathi, “Laser mode conversion into a surface plasma wave in a metal coated optical fiber”, *J. Appl. Phys.* **100**, 013304 (2006).
2. **Gagan Kumar**, D. B. Singh, V. K. Tripathi, “Surface enhanced Raman scattering of a surface plasma wave”, *J. Phys. D: Appl. Phys.* **39** (2006) 4436–4439.  
The Corrigendum of this paper published in *J. Phys. D: Appl. Phys.* **39** (2006) 4738.
3. D. B. Singh, **Gagan Kumar**, and V K Tripathi, “Probing of a surface plasma wave by an obliquely incident laser on the metal surface”, *J. Appl. Phys.* **101**, 043306 (2007). (Selected in Virtual Journal of Ultrafast Science).
4. C. S. Liu, **Gagan Kumar**, D. B. Singh and V. K. Tripathi, “Electron acceleration by surface plasma waves in double metal surface structure,” *J. Appl. Phys* **102**, 113301 (2007).
5. **Gagan Kumar** and V. K. Tripathi, “Anomalous absorption of surface plasma wave by particles adsorbed on metal surface”, *Appl. Phys. Lett.* **91**, 161503 (2007).
6. **Gagan Kumar** and V. K. Tripathi, “Filamentation of a surface plasma wave over a semiconductor free space interface”, *J. Appl. Phys.* **102**, 123301 (2007).
7. D. B. Singh, **Gagan Kumar**, and V K Tripathi, “Surface plasmon induced heating and emission of electrons from metallic targets”, *Phys. Plasmas.* **14**, 102108 (2007).
8. **Gagan Kumar** and V. K. Tripathi, “Excitation of surface plasma wave over plasma cylinder by a relativistic electron beam”, Communicated to Phys. Plasmas.

## CONFERENCES/ SUMMER SCHOOL/ WORKSHOP

---

- a. **Gagan Kumar** and V. K. Tripathi, “Mode conversion of a TM mode laser into a surface plasma wave”, *Proc. 20<sup>th</sup> national Symposium on Plasma Science and Technology*, CUSAT, cochin, India, Dec. 5-7, 2005.
- b. **Gagan Kumar** and V. K. Tripathi, “Modeling of SERS Sensor in an ATR configuration”, *Proc. 21<sup>st</sup> national Symposium on Plasma Science and Technology*, MNIT Jaipur, India, Dec. 19-23, 2006.
- c. Participated in “*PSSI-IPR workshop on National Fusion Program-ITER and Beyond*” held at Ahmedabad, during November 8-10, 2006.
- d. Participated and presented a paper in poster session “*Summer College on Plasma Physics-New Developments 2007*” held on 30 July - 24 August 2007 in Abdus Salam ICTP – Trieste, Italy.

## EDUCATIONAL INVOLVEMENT

---

- Teaching assistantship in undergraduate (B. Tech) lab courses in last three years.
- Expertise in guiding B. Tech., M. Sc. and M. Tech. students at various level of their major, minor and summer projects.

## **TECHNICAL SKILL**

---

<b>Software Known</b>	:	MATLAB 7.0, MATHEMATICA 5.0 & MATHCAD 2000 PROFESSIONAL
<b>Languages</b>	:	C, FORTRAN 9.5, Basic knowledge of C++
<b>Operating Environment</b>	:	MS-DOS, Windows 98/ 2000/ XP/ Vista, Linux
<b>Package</b>	:	Latex, MS Office 2003/ 07

## **PERSONAL DETAILS**

---

The author was born on October 10, 1980 at Maham a town of Rohtak district (Haryana) in India. In 2003 he received M. Sc. degree in Physics from Kurukshetra University with specialization in Electronics and High Energy Physics. In 2003 he joined M. Tech in Computer Science and Engineering. Since April, 2004 he has been working at the Department of Physics, Indian Institute of Technology Delhi for Doctorate degree. The research concerns the interaction of surface plasma waves with electron beams and nanoparticles. His research interests are plasmonics, electron acceleration, surface enhanced Raman scattering, and parametric instabilities. In free time, he likes to spend time in reading books and articles related to current science and technology.